FE-1817-6
Distribution Category UC-90e

POLLUTANT CONTROL THROUGH STAGED COMBUSTION OF PULVERIZED COAL

Final Report
Covering Period May 1978 - October 1978

J.O.L. Wendt and J.W. Glass

Department of Chemical Engineering
College of Mines
University of Arizona
Tucson, Arizona 85721

May 1979

Prepared for the United States Department of Energy
Under Contract E49-18-1817

ACKNOWLEDGMENTS

The authors would like to thank P. De Pastena who helped obtain some of the measurements and D. W. Pershing and J. W. Lee, who provided guidance at the initial stages of this phase of the project. Thanks are due to Ms. Denise Butler who typed the manuscript, and to the California Institute of Technology, who provided facilities for the final completion of this report. Special acknowledgment is due to Mr. Henry C. Jacobsen of DOE, Fossil Energy, who was the Contract Monitor for this project.

ABSTRACT

Pulverized fuel was burned in a 2 kg/hr aerodynamically well-defined plane flame combustor, and the resulting time resolved profiles of CO_2, CO, O_2 and NO were measured. In this final report on Contract E 49-18-1817 the influence of pulverized fuel composition on NO formation mechanisms is emphasized, with particular stress on the role of coal volatile content. The latter quantity was varied by burning first an FMC char with 3.6% Volatile Matter, then an IGT char with 13.6% Volatile Matter and lastly a series of various coals comprising a lignite, a sub-bituminous coal, and three bituminous coals. These fuels were investigated under fuel rich and staged combustion conditions.

Under staged combustion, second stage NO was found to be strongly influenced by the amount of first stage volatile nitrogen carryover. The latter quantity depended on the first stage fuel richness and on the amount of volatiles in the coal. Under fuel rich conditions the NO profile was controlled by the fuel nitrogen volatility relative to the volatility of the non-nitrogeneous combustibles in the coal.

A series of tests on one coal showed that the observed decay of NO in the first fuel rich stage could be simply correlated with temperature. This latter result implies that a high heat removal rate in the first stage of a staged combustion process will lead to minimum NO emissions after staging.

TABLE OF CONTENTS

TABLE OF CONTENTS--Continued

1.0 OBJECTIVES AND SCOPE

The objectives of this research contract are to:

1) Establish quantitatively the dependence of total and fuel NO_x emissions on combustion zone temperature, coal composition and local oxygen level in swirling, turbulent pulverized coal flames.

2) Define the optimum application of classical staged combustion as a means of lowering pollutant emissions from pulverized coal firing.

3) Estimate the relative importance of thermal NO, volatile NO and char NO under a variety of normal and staged combustion conditions.

4) Analyze resulting data in order to obtain general insight into fuel nitrogen conversion during pulverized coal combustion with a view of developing scale up criteria to be used for NO_x abatement from practical combustion units.

In order to meet these objectives the program work scope was divided into three identifiable tasks shown in Table 1. Task 1, NO_x Formation in Swirling Turbulent Pulverized Coal Flames has been completed and results reported elsewhere in reports FE1817-1 and FE1817-2. Task 2, NO_x Formation in Staged Combustion Systems is reported in DOE reports FE1817-4 and 5 and is concluded in this report. Task 3, Analysis, is reported in this report, as well as in all preceding reports. In general, Reports FE1817-1 through FE 1817-3 are concerned with NO_x formation in swirling, turbulent diffusion flames, while Reports FE1817-4 through FE1817-6 focus on the optimum application of staged combustion. In FE1817-4 the limitations to NO_x abatement through Classical Staging were delineated, and a new combustion modification, denoted as Advanced Staging, was introduced and tested. In this final report on Contract E 49-18-1817, the Focus in on mechanisms of NO_x formation under fuel rich conditions, and on the influence of coal composition thereon.

TABLE 1.1 TASK COMPLETION CHART FOR CONTRACT E(49-18)-1817

Technical Program Organization		Contract Task Numbers	Percent Completed	Results Reported
TASK 1.0	NO_x Formation-Swirling, Turbulent Pulverized Fuel Flames			
1.1	Combustor Characterization	Tasks 1 & 2	100%	FE1817-1 & 2
1.2	Fuel NO_x Definition	Task 9	100%	FE1817-1 & 2
1.3	Coal Composition Studies	Task 10	100%	FE1817-2
1.4	Temperature Investigation	Task 11	100%	FE1817-2
TASK 2.0	NO_x Formation-Staged Combustion Systems			
2.1	Staging Evaluation	Task 3	100%	FE1817-4
2.2	Mechanism Characterization	Task 4	100%	FE1817-5 and this report
2.3	Effect of Coal Composition	Task 6	100%	FE1817-5 and this report
TASK 3.0	Analysis			
3.1	Char and Volatile Nitrogen Definition	Task 12	100%	FE1817-3
3.2	Local O_2 Dependence	Task 13	100%	FE1817-1, 2 & 3
3.3	Correlation Development	Task 5	100%	FE1817-3 & 5 and this report

Results reported herein constitute, therefore, a continuation of the staged combustion experiments of Wendt, Lee, and Pershing (1978) using pulverized Western Kentucky coal. The previous work delineated the effectiveness of staged combusiton as a function of first stage stoichiometry, residence time and flame temperature. The relative rates of NO formation and destruction in rich flames and the significance of fuel NO to total NO were determined both for fuel-rich and fuel-lean staged combustion.

This work deals primarily with the effects of coal composition on staging effectiveness and on NO formation and reduction in fuel-rich flames. The effect of temperature on NO reduction was also examined. Two coal chars and four coals of varying composition were burned at fuel-rich stoichiometric ratios of 0.8 and 0.4 to define the baseline combustion and NO formation and reduction phenomena for each. Each coal was then burned at an overall second stage stoichiometric ratio of 1.2 and first stage rich SR = 0.8 and 0.4 to delineate the effects of coal composition on staging effectiveness. General guidelines for the application of staged combustion with regard to composition can be formulated from the experimental results.

It is premature, at this time, to formulate detailed mechanistic models of NO formation and reduction in staged combustion of pulverized coal although this work has provided some insight. Future work will focus on a more detailed understanding of the phenomenological mechanisms governing NO formation and reduction and staging effectiveness in pulverized coal flames. In this work empirical correlations of certain portions of the data (such as on the effect of temperature on NO decay ratio) were developed as warranted.

Particular attention was given to inferred evidence of the state of the volatile nitrogen (VN) and char nitrogen pools and of the distribution of nitrogenous species within volatiles evolved in the fuel-rich first stage. Although direct evaluation of the nitrogen balance was not made, circumstantial evidence allowed for a phenomenological description of the NO formation and destruction mechanisms to be developed and provided guidelines for future work.

Since species and temperature data reported herein are presented in time-resolved form, this work may provide a data base for the future evaluation of kinetic models of fuel nitrogen conversion during the staged combustion of pulverized coal.

2.0 SUMMARY AND CONCLUSIONS

Much of the data presented herein is still undergoing analysis, in the light of new information presently being generated on the effect of coal composition on volatile nitrogen and volatile combustible yields. Therefore it may be premature to draw definitive conclusions at this stage. However, the experiments performed do point to the following conclusions and implications.

1) The behavior of coal nitrogen under staged conditions is a strong function of coal composition. Some coals appear to produce volatile nitrogen which is destroyed, others produce volatile nitrogen which persists until it is oxidized in the second stage. Others still produce volatile nitrogen which destroys NO after staging.

2) The presence of volatile matter in char increases the rate of NO reduction under fuel rich conditions.

3) The peak NO under fuel rich conditions is strongly dependent on the relative rate of volatile and XN evolution. The key parameters are the rate of O_2 consumption relative to XN evolution, and this strongly depends on coal composition.

4) Temperature plays a key role in the decline of NO, (and, presumably, XN) in the first fuel rich stage. Our data suggests that a rapid temperature quench in the first stage is a desirable combustion modification. This conclusion is not valid for the FMC char where homogeneous reactions are less important. It does indicate the practical importance of wall cooling in the first stage.

3.0 EXPERIMENTAL FACILITY

3.1 Combustion and Analytical System

The combustion and analytical systems used in this experiment were identical, with the exception of the premixed burner, to that used and described by Wendt, Lee and Pershing (1978).

The furnace used in this experiment consisted of a downfired, premixed burner atop a 15 cm I.D. X 200 cm fire tube with 25 cm refractory walls. Two air injection ports placed opposite each other and spaced 38 cm apart gave the ability of introducing second stage air as combustion proceeded in the fire tube.

Sampling of the gas was done *in situ* with a 5 cm diameter insulated water-cooled and quenched probe described in a previous report, FE 1817-4. The probe was mounted on an elevator which permitted it to be positioned on the combustor axis at any desired position to within 20 cm of the furnace top. Appendix C describes results of a study undertaken to recheck the proper operation of the water quenched probe. In this work all measurements were made using sample and water flow rates leading to an assymptotic maximum level of NO measured. It is assumed that there was little NO reduction in the probe under these sampling conditions.

The analytical system consisted of a Beckman paramagnetic oxygen analyzer, a Beckman polaragraphic oxygen analyzer, Beckman NDIR CO and CO_2 analyzers and a Thermo-Electron chemiluminescent NO/NO_x analyzer. All data reported herein were made with the chemiluminescent analyzer in the NO mode.

Air rates were measured with calibrated rotameters and a laminar flow element. The coal was supplied by a screw feeder. The reader is referred to Wendt, Lee, and Pershing (1978) for further details.

3.2 Mixing Chamber

The mixing chamber used in this experiment is shown in Figure 3.1. It is essentially similar to the mixing chamber that Howard (1965) used in his experiments to determine the mechanism of coal combustion. The primary air and coal suspension are mixed with the heated secondary air in the line leading to the mixing chamber. The total fuel and air mixture is impacted against the top plate, flow is reversed and the mixture is transported to the combustor cone. This burner provided intense mixing of the air and fuel in both the lines leading to the chamber and in the chamber. Radial composition profiles taken with Western Kentucky coal as the fuel showed that a radial tolerance in the combustor of ±30 ppm NO could be achieved with this chamber and that the baseline NO profile matched that determined previously (Figure 3.2).

In addition, the viewport used in previous experiments was blocked with the exception of a 5 cm diameter hole for viewing the flame. This was done to minimize the possiblity that the port could lead to the formation of a recirculation zone which might bias the one-dimensional flow in the combustor. However, the trials of the new mixing chamber with and without the plug in place showed that recirculation, if any, had no effect on the combustor performance.

3.3 Suction Pyrometer and Thermocouples

A double-shielded and water cooled suction pyrometer was constructed for measuring the flame temperature in the combustor. The pyrometer is described schematically in Figure 3.3 and, in principle, followed established designs (Land, 1956).

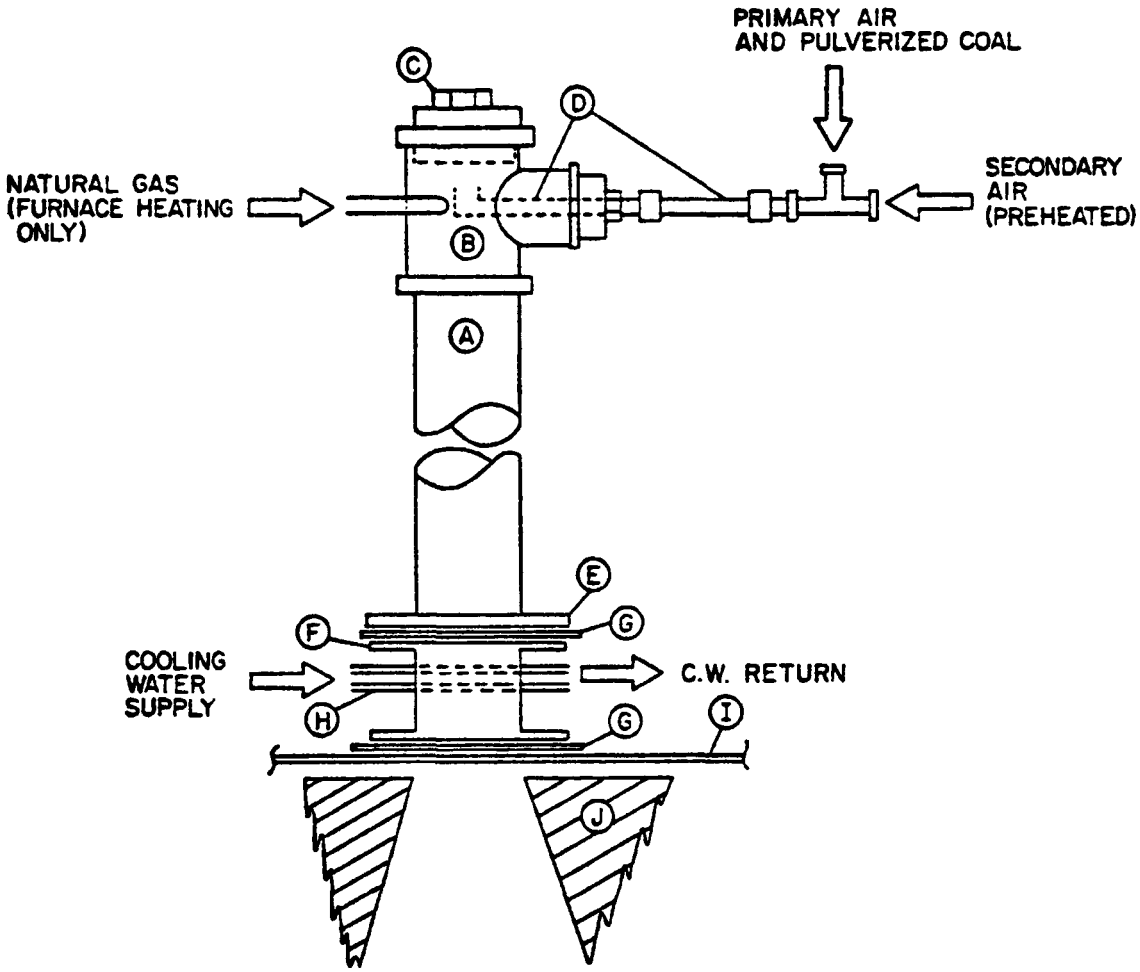

A - 2in x 10in 316 S.S. Pipe
B - 2in x 11/2in 304 S.S. Tee
C - 2in Flatface Plug, 316 S.S.
D - 1/2in 316 S.S. Supply tubing
E - 2in x 6in C.S. 150lb flange
F - Cooling tube assembly
G - Fibrefrax gasket
H - 316 S.S. Cooling tubes
I - C.S. Furnace top plate
J - Refractory quarl

Figure 3.1. Premixed Burner Mixing Chamber.

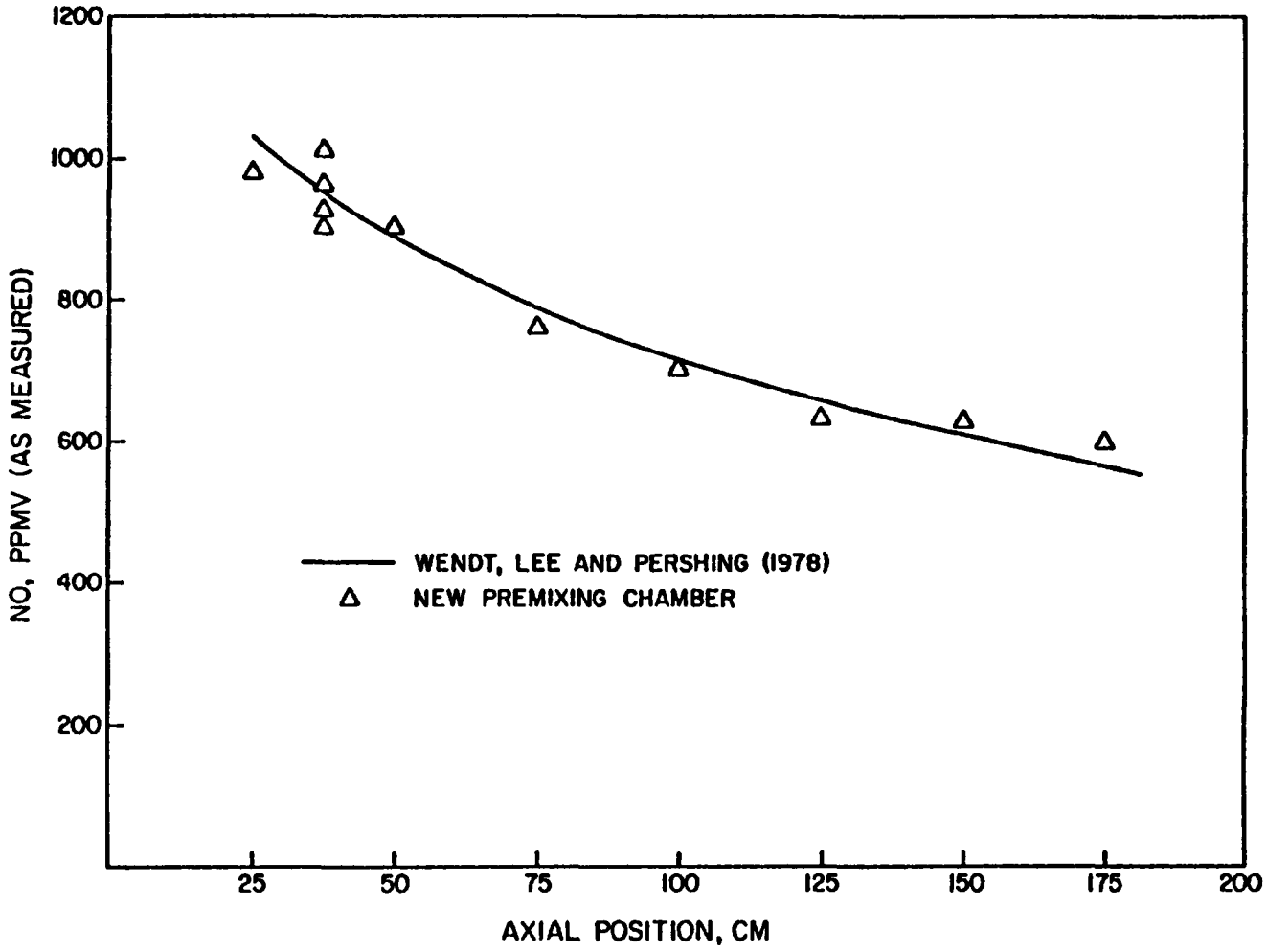

Figure 3.2. Validation of Mixing Chamber Performance.

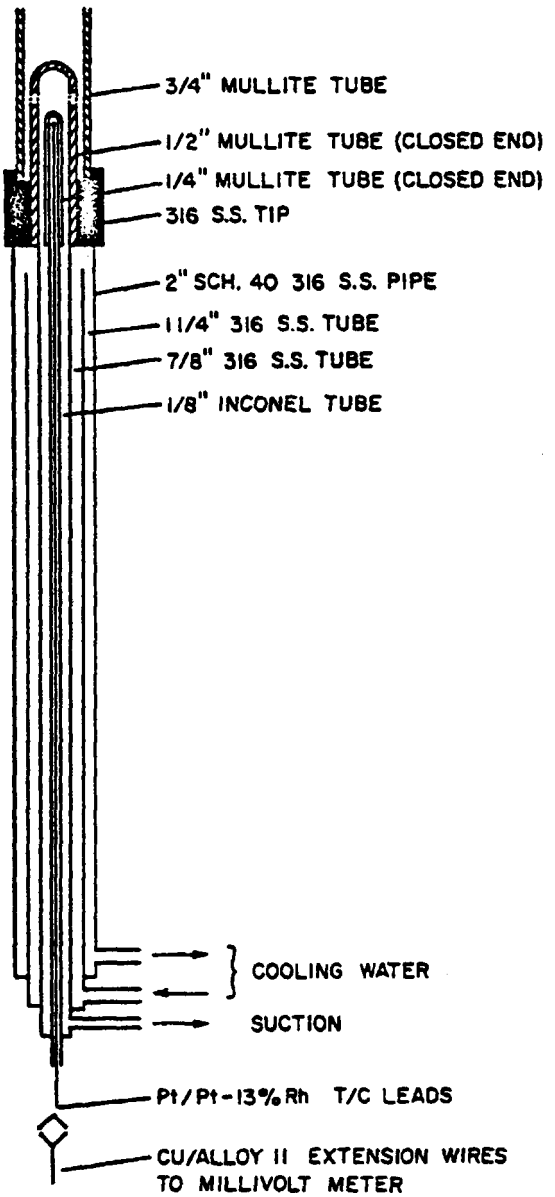

Figure 3.3. Suction Pyrometer.

The shields were of McDanel MV-30 ceramic tubes. The sensing junction was 0.008 in Pt/Pt-13% Rh wires insulated with 0.125 in. double-hole ceramic tubes. The thermocouple leads were connected to a millivoltmeter with copper/copper alloy 11 extension wires. The millivoltmeter was not temperature compensated but tests conducted with an ice-bath showed that a constant additive bias of 0.15 millivolts in the system should be applied to the raw temperature measurements.

Suction was provided by a 4.5 SCFM rated vacuum pump, which gave about 3.2 SCFM actual pumping rate and a linear gas velocity of about 380 ft/sec. (965 cm/S) at 1400° K gas temperature across the measuring junction.

In operation in a coal flame, the pyrometer was purged with nitrogen to prevent slag and ash plugging the annulus until a measurement was taken. After purging ceased and suction was applied, the pyrometer required 60-90 sec. to equilibrate before purging could be resumed.

The suction pyrometer worked admirably in gas flames but suffered from a severely short life in coal flames, especially in high temperature regions in which molten slag existed, in spite of the nitrogen purging. The instrument was removed from service as soon as the equilibration time exceeded 90 seconds, about every other measurement, to unplug the tip and piping and replace the fragile ceramic tubing. Owing to the high cost of the ceramic tubes (about $10.00 per replacement) and the time required for measuring each of the estimated 300 desired points (upwards of 20 min.), the pyrometer was abandoned in favor of type K thermocouples. Section 4.10 shows that the latter gave essentially identical temperature readings as the pyrometer.

The type K Inconel shielded and magnesia insulated thermocouples (Omega Engineering CAIN-186-18) could be inserted to the centerline through the side of the combustor and placed in holes drilled to 1/4" of the side for wall temperature measurements. In rich coal flames the thermocouples gave about 10 hours continuous service before the Inconel shielding corroded and the junction deteriorated. The thermocouples were used for all of the temperature measurements reported herein.

3.4 Coal Compositions

The compositions of the coals and chars used in this experiment are given in Table 3.1. This table also includes the firing rates, heat release and firing densities (heat released per unit furnace volume and per unit area) for each of the fuels.

3.5 Experimental Procedure

The experimental procedures consisted of several distinct parts. Overnight operation with natural gas as the fuel was defined to match as closely as possible the heat release conditions expected in the experimental runs. An overnight heat release of about 60 MBTU/hr was found to satisfactorily heat the furnace and provided for minimal temperature drift during an experimental run.

An experimental run consisted of three distinct parts. First, the stoichiometric air requirement at excess air conditions was checked to provide a basis for substoichiometric operation. A nominal check point of SR = 1.2 was used for all runs. In a few instances, notably the IGT char, the checkpoint value could not be obtained. This is not critical to the furnace performance as long as the stoichiometry is acceptably lean, say SR = 1.10 (Wendt, Lee and Pershing, 1978).

TABLE 3.1

COAL COMPOSITION

Ultimate Analysis (% Dry)	Colorado	Pittsburgh #8	Western[1] Kentucky	Montana Powder River	Texas Lignite	FMC Char (Low Volatile)	IGT Char (High Volatile)
C	73.1	77.2	73.0	67.2	60.44	72.8	66.3
H	5.1	5.2	5.0	4.4	4.61	0.9	1.75
N	1.16	1.19	1.4	1.1	1.21	0.99	0.72
S	1.1	2.6	3.1	0.9	1.75	3.5	1.78
O	9.7	5.9	9.3	14.0	14.38	0.7	6.57
Ash	9.8	7.9	8.2	11.7	17.61	21.2	22.88
Heating Value Btu/lb wet	12,400	13,700	12,450	8,900	6,677	12,200 (est)	11,900 (est)
Char values by the dulong formula (Perry and Chilton, 1973, p. 9-4)							
Proximate Analysis %							
Volatile Matter	38.9	37.0	36.1	30.5	28.68	3.6	13.6
Fixed Carbon	52.6	54.0	51.2	39.0	24.08	73.8	57.5
Moisture	3.3	1.2	4.8	21.2	35.96	1.8	7.8
Ash	8.9	7.8	7.8	9.2	11.28	20.8	21.1
VM/FC	0.74	0.69	0.71	0.78	1.20	0.05	0.24
Experimental Conditions							
Firing Rate, lb/hr	5.2	4.0	5.0	5.3	7.6	5.9	7.4
BN/hr	64,500	53,100	61,800	47,000	50,600	71,600	37,700
Firing Density BN/hr ft^3	56,300	46,400	53,900	40,800	44,200	62,500	76,000
BN/hr ft^2	7,040	3,800	6,750	5,100	5,500	7,800	9,600

Following the stoichiometric air check, the furnace was set at SR = 0.8 or 0.4 (based on the stoichiometric air rate) for evaluation of the baseline profile. The reduced heat release at more fuel-rich stoichiometrics resulted in some temperature drift as the furnace walls cooled so that sufficient time for reducing transient effects had to be given prior to sampling or temperature measurements. Thirty to forty minutes proved sufficient. Temperature measurements were made prior to introducing the sampling probe to minimize the cooling effects of the probe.

Air staging was always made from the lowest to the highest position to minimize hot spots and other temperature abnormalities which could have an effect on the results. Gas sampling was also form the lowest to highest positions to minimize similar potential abnormalities.

For all runs reported herein, the secondary air preheater was set at 550° to give a total air supply temperature of about 500° F.

These conditions and procedures are essentially those used by Wendt, Lee and Pershing (1978) to which the reader is referred for more detail.

3.6 Wall Reactions under Fuel Rich Combustion Conditions

De Soete (1978) has recently presented data which showed that NO can be reduced on hot char and/or silica surfaces in the presence of CO and/or H_2 and in the absence of O_2. It was therefore important to determine whether the NO profiles and NO decay rates reported in previous reports on this contract resulted from wall reactions in our combustor, under our experimental conditions.

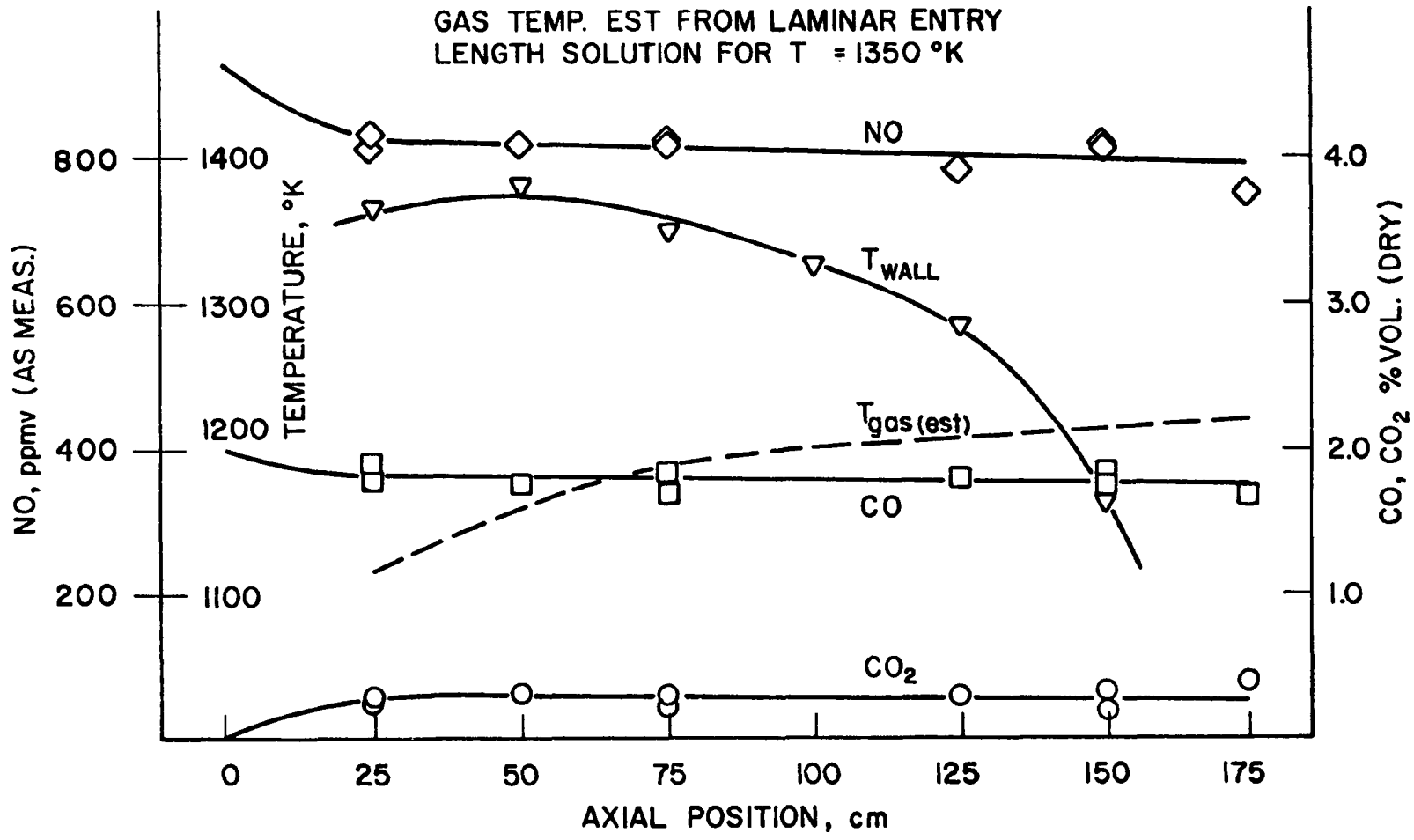

Figure 3.4: NO Reduction by CO in N_2 Atmosphere. Inlet Conditions: CO-1.95%, NO-860 ppm, CO_2-0.0%, N_2-balance.

The combustor walls were heated by firing with gas for over twelve hours. Wall temperatures were measured. Simulated combustion conditions are shown in Table 3.2. Flow rates were similar to those arising in the course of normal experimentation. The inlet mixture contained 1.95% CO, 860 ppm NO and the balance N_2.

Figure 3.4 shows the wall temperature and the gas concentration profiles. Ther latter were obtained with the water spray probe. With the exception of a small (50 ppmV) reduction in the NO concentration near the combustor inlet, No reduction is minimal. Wall effects can therefore be neglected in the analysis of the experimental data reported herein.

The initial reduction of NO and rise in CO_2 may be due to the presence of oxygen from a small air leak.

Since the ports which give access to the gas for centerline temperature measurements were plugged with slag, the gas temperature, reported in Figure 3.4, is estimated from the laminar thermal entry length solution for pipe flow with a constant wall temperature of 1330° K. On this basis, it can be seen that the gas temperature lags the measured wall temperature throughout most of the combustor.

From these data, it is concluded that under flow rate and wall temperature conditions experienced in this work, heterogeneous reactions destroying NO at the combustor wall are not of first order.

TABLE 3.2

Experimental Conditions: Wall Reaction Test

N_2 flow, cm^3/sec at STP	
SCFM	8.0
Inlet gas temperature, °K	533.0
Inlet gas composition, % vol.	
O_2	0.0
CO_2	0.0
CO	1.95
NO_1 ppmV	860.0
N_2	Balance

4.0 ESTIMATION OF THE TRUE GAS TEMPERATURE FROM THERMOCOUPLE AND SUCTION PYROMETER-MEASURED GAS TEMPERATURES

4.1 Introduction

One objective of this work is the presentation of the experimentally determined gas phase concentrations in time-resolved form. Accurate temperature measurements are required to meet this objective.

The measurement of high temperatures is not a simple matter. Radiant heat transfer becomes dominant and its effects on a body in a high temperature environment cannot be ignored. A thermocouple placed in such an environment will not indicate a true temperature if portions of the surroundings, such as furnace walls, are at a significantly different temperature. The effects of radiative cooling of a thermocouple to the furnace walls must be accounted for if accurate temperature measurement is desired. The coupled problems of estimating surface properties, such as emissivities, and gas phase properties such as the concentrations of emitting species and the surface areas of suspended solids and soot make the solution of the radiant heat transfer problem rather formidable.

In this chapter, the theory of heat transfer involving a thermocouple in a high temperature coal flame is considered. The theory is first applied to the case of a coal flame in which the surface area of the coal and, as a result, the emissivity of the gas volume can be specified *a priori*. Since the emissivity of the gas is also a function of unmeasured soot and hydrocarbon concentrations as well as the unknown coal surface area, the calculation of the volume emissivity is then coupled with an overall furnace heat balance based on experimentally-determined temperature profiles to improve the accuracy of the estimate. This latter procedure gives a final temperature correction formula which can be applied to temperatures measured with a thermocouple.

4.2 Temperature Correction

An estimate of the true gas temperature can be obtained by considering the heat balance for a body in thermal equilibrium with its surroundings (West and Westwater, 1953; Warshawsky, 1957). The system under consideration is shown in Figure 4.1.

$$\dot{q}_{\substack{rad \\ gt}} + \dot{q}_{\substack{conv \\ gt}} = \dot{q}_{\substack{rad \\ tw}} + \dot{q}_{\substack{cond \\ tb}} \qquad 4.1$$

The left hand side represents energy transferred to the thermocouple by thermal radiation and convection from the gas. The right hand side represents the heat losses from the thermocouple by thermal radiation to the walls of the enclosure and by conductive transfer to the base of the thermocouple.

From the Stephan-Boltzmann law

$$\dot{q}_{rad} = \sigma A_T \left\{ \frac{1}{\frac{1}{\varepsilon_1} + \frac{1}{\varepsilon_2} - 1} \right\} \left[T_1^4 - T_2^4 \right] \qquad 4.2$$

which can be arranged in the form

$$\dot{q}_{rad} = h_r A_T (T_1 - T_2) \qquad 4.3$$

where the "radiative transfer coefficient" is defined

$$h_r = \sigma \left\{ \frac{1}{\frac{1}{\varepsilon_1} + \frac{1}{\varepsilon_2} - 1} \right\} \frac{(T_1^4 - T_2^4)}{(T_1 - T_2)} \qquad 4.4$$

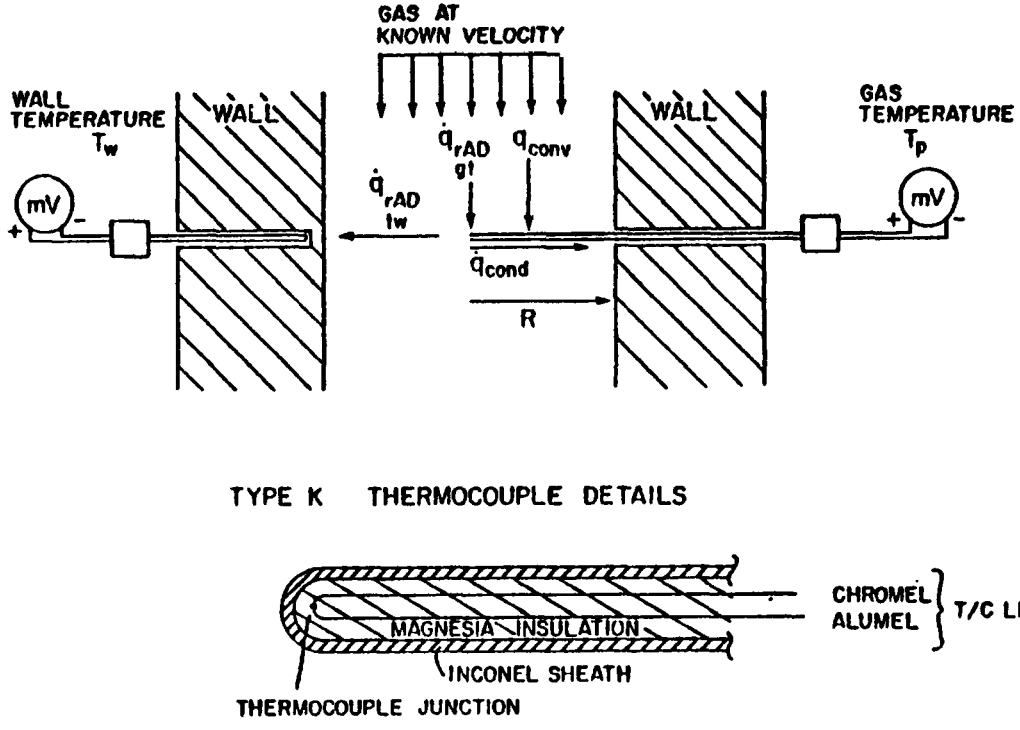

Figure 4.1. Thermocouple Heat Balance.

This definition leads to an easier understanding of the performance of a suction pyrometer and a thermocouple and follows West and Westwater (1953). A further benefit is that in many systems, the radiant transfer actually follows a first order temperature dependence with h_r relatively constant (West and Westwater, 1953; Hottel and Sarofim, 1967, p. 464).

The conductive and convective transfer relations follow the usual forms and the heat balance becomes

$$h_{r_{gt}} A_T (T_g - T_t) + h_{c_{gt}} A_T (T_g - T_t) = \tau_g \, hr_{tw} A_T (T_T - T_W) - K_t A_{cs} \frac{dT_t}{dz} \quad 4.5$$

The coefficient τ_g in equation (5) is the transmissivity of the gas. As τ_g approaches 0.0, the gas becomes opaque to the transmission of radiant energy from the thermocouple to the walls.

Equation (5) cannot be solved analytically for the unknown true gas temperature Tg if the conductive term is included. Since only an estimate of the gas temperature is required, it will be shown that the conductive cooing term is negligible and can be eliminated.

Dropping the conductive term and solving for the gas temperature gives

$$T_g = T_T + \frac{hr_{tw} \, \tau g}{h_{r_{gt}} + h_{c_{gt}}} (T_T - T_W) \quad 4.6$$

This relationship can bee applied to any system which meets the criterion of negligible conduction error. The accuracy is limited by the accuracy of the estimates of the gas and solid emissivities and of the convective heat transfer coefficient. This relationship shows that

measurement errors can be decreased by increasing the radiative and convective heat transfer to the thermocouple and decreasing the radiant cooling losses to cold walls which is the basis for suction pyrometry.

4.3 Emissivities

Estimates of the surface emissivities of the thermocouple and walls of the enclosure can be obtained from the literature (Hottel and Sarofim, 1967, p. 159). Normally the emissivity of the gas can be neglected, but in a coal combustion system which contains suspended solids, the solids contribution, as well as the contributions of water and carbon dioxide, to the gas emissivity must be taken into account.

For any volume emitter containing n emitting species (Hottel and Sarofim, 1967, p. 201; Gray, Kilham and Müller, 1976, p. 73)

$$1 - \varepsilon_g = \prod_{i=1}^{n} (1 - \varepsilon_i) \qquad 4.7$$

$$\varepsilon_i = 1 = e^{-k_i L} \qquad 4.8$$

where the i^{th} species emissivity, ε_i, is measured at the unknown gas temperature. At low partial pressures and over a suitably narrow temperature range, the emissivities of the gaseous components are small and constant (Perry and Chilton, 1973, p. 10-40). For the coal, the attenuative factor is given by (Hottel and Sarofim, 1967, p. 378)

$$K = \frac{a_T}{4V} \qquad 4.9$$

The total surface area, a_T, is determined by direct measurement of solid samples, if available.

The volume of gas can be determined from (Appendix A)

$$V = (\gamma)(SA)\ (P/F)_{wet}\ (Tg/To) \qquad 4.10$$

The path length, L, is a function of the geometry of the enclosure. For gas radiating to the center of a cylinder (radiation to the thermocouple) (Hottel and Sarofim, 1967, p. 467)

$$L = R \qquad 4.11$$

Combining equations (8-11)

$$\varepsilon_g = 1 - \exp\left(-\frac{a_T R}{4V}\right) \prod_{i=1}^{n} (1 - \varepsilon_{gas\ i}) = 1 - a_1 \exp\frac{-a_2}{T_g} \qquad 4.12$$

The gas transmission coefficient τg can be taken as $1-\alpha g$ where αg is the absorptive coefficient. At thermal equilibrium (for a black body) $\alpha g = \varepsilon g$. Assuming that this will give a satisfactory first approximation for the gas phase

$$\tau_g = 1 - \varepsilon_g$$

In the form of Equation (12)

$$\tau_g = a_1 \exp\left(\frac{-a_2}{Tg}\right) \qquad 4.13$$

For Western Kentucky coal, Table 4.1 shows the gas emissivity calculated from component emissivites at 2200° F (1478° K). The effect of CO has been neglected since it is typically at low concentrations and A_T is taken as 1000 cm^2/g based on the particle size distribution given by Pershing (1976). The H_2O and CO_2 concentrations are those reported by Wendt, Lee, and Pershing (1978).

TABLE 4.1

GAS VOLUME EMISSIVITY FOR WESTERN KENTUCKY COAL

Stoichiometric Ratio	ϵ_{H_2O}	ϵ_{CO_2}	ϵ gas	ϵ gas (1400°K)
1.2	0.012	0.045	$1-0.944 \exp\left(\frac{-216}{Tg}\right)$	0.13
0.95	0.014	0.051	$1-0.936 \exp\left(\frac{-273}{Tg}\right)$	0.16
0.80	0.016	0.051	$1-0.934 \exp\left(\frac{-319}{Tg}\right)$	0.17
0.40	0.033	0.053	$1-0.916 \exp\left(\frac{-615}{Tg}\right)$	0.27

It must be emphasized that the gas emissivities shown in Table 4.1 are only estimates. The gaseous component properties taken at 1400° K limit the range of these equations to the neighborhood of this temperature. However, the possible error at extremes in temperature are compensated by the relatively small contributions of H_2O, CO_2 and temperature to the overall result. The major source of error will be the value of A_T used in the equations. It is decreased as coal burnout increases if the ash agglomerates, etc. (Field, et al., 1967, p. 291; Essenhigh, 1977) so that a constant value is not necessarily appropriate.

4.4 Furnace Heat Balance

The value of the surface area for Western Kentucky coal of 1000 cm^2/g used in the emissivity of the combusting mixture was found to give unreasonably high true gas temperatures. Since the surface area must change during the course of combustion and the solid phase was not sampled, the temperature correction was coupled to an overall furnace heat balance in which the surface area is used as adjustable parameter.

The furnace centerline and wall temperatures were measured as shown in Figure 4.2. Assuming a value of A_T, the "corrected" gas temperature can be determined at each zone boundary from the radiative balance on the thermocouple. From an overall heat balance on the combustion products at a given stoichiometric ratio

$$\dot{q}_{net} = \sum_{i=1}^{n} (\dot{q}_{gw}^{rad} + \dot{q}_{gw}^{conv}) \text{ zone } i \qquad 4.14$$

For a zone

$$\dot{q}_{gw}^{rad_i} = \sigma K A_i \left(\frac{1}{1/\epsilon_{gi}+1/\epsilon_w-1}\right) (T_{gi}^4 - T_{wi}^4) \qquad 4.15$$

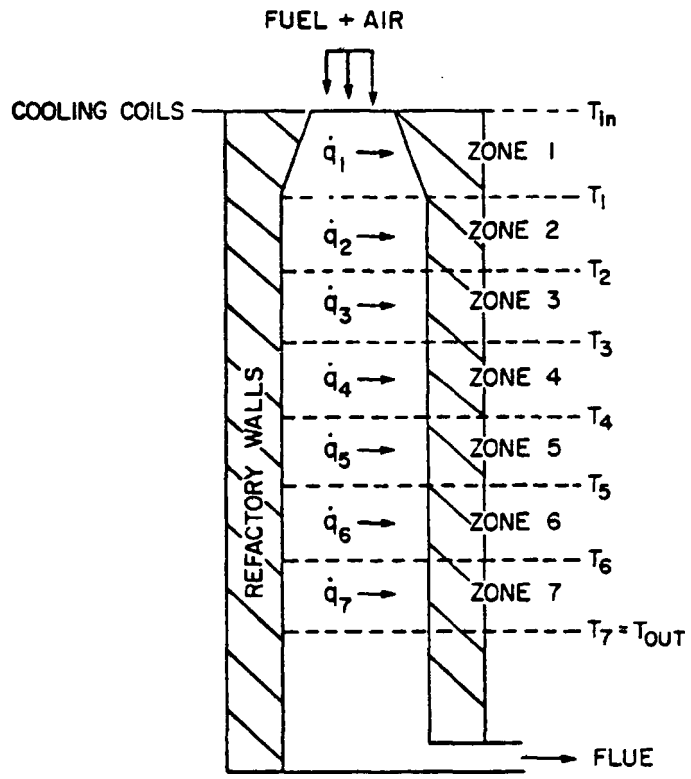

Figure 4.2. Furnace Radiative Heat Balance.

Where ε_{gi} is calculated from Equation (12) with L = 0.73D for radiative transfer from a cylinder of gas to the bounding walls. Note that axial radiative transfer is neglected. The zone gas temperature, T_{gi}, is taken as the arithmetic average of the corrected gas temperatures at the zone boundaries.

K in Equation (4.15) is an adjustment factor recommended by Hottel and Sarofim (1967, p. 464) to account for departures from clear gas radiative heat transfer.

$$K = \frac{1 - t^3}{1 - t^4} \quad \text{where } t = Tw/Tg$$

The heat loss through the furnace walls, q_{net}, is calculated from the heating value of the coal, the measured compositions and temperature at the flue and the flue gas flow, assuming that the flue temperature is low enough that it needs no correction. (Subsequently shown to be valid.)

The heat release for Western Kentucky coal is calculated with ideal gas heat capacities as a function of experimental conditions by the method in Appendix A.

$\gamma = 1.0$ 4.16

$$q_T = -123755 + 43.70\ T_o + 3.576 \times 10^{-3}\ T_o^2 + 2.583 \times 10^5\ T_o^{-1} - (27.92\ T_i + 1.8 \times 10^{-3}\ T_i^2 + 7.28 \times 10^4\ T_i^{-1}) \text{ cal/g mole } ^oC$$

$\gamma \leq 1.0$ 4.17

$$q_r = q_T(\gamma) + B\gamma\ (70093 - 3.60\ T_o - 0.56 \times 10^{-3}\ T_o^2 - \frac{1.95 \times 10^5}{T_o} + (1-\gamma)\ (3.78 + 0.336\ T_o + 5.69 \times 10^5\ T_o^2)$$

$\gamma \geq 1.0$ 4.18

$$\dot{q}_L = \dot{q}_T + (\gamma-1)\ (38.07)\ (T_o - T_i) + 2.48 \times 10^{-3}\ (T_o^2 - T_i^2) + 0.99 \times 10^5\ \left(\frac{1}{T_o} - \frac{1}{T_i}\right)$$

The Western Kentucky coal test case heat balances used to determine the true gas temperatures are shown in Table 4.2. The temperature profiles for the test cases, determined by Lee (1977) are plotted in Figure 4.3.

These heat releases are used to constrain the possible value of A_T, the total surface area of the coal used in determining the emissivities in the thermocouple heat balances.

4.5 Physical Properties of the Gas Phase

It is convenient for approximation purposes to use nitrogen properties for the viscosity and thermal conductivity of the gas phase. Using the monatomic single component form of the Chapman-Enskog theory (Bird , Stewart, and Lightfoot, 1960, p. 23) for determining the viscosity of nitrogen at high temperatures and the Euken polyatomic formula for the thermal conductivity (Bird, Stewart and Lightfoot, 1960, p. 257) and fitting the results to exponential functions.

$$\mu\ (\text{poise}) = 2.66 \times 10^{-4} \exp\ (4.49 \times 10^{-4}\ T_g)\ r^2=0.998 \qquad 4.19$$

$$k\ (^{cal}/_{cm\text{-}s}) = 8.62 \times 10^{-5} \exp\ (5.43 \times 10^{-4}\ T_g)\ r^2=0.998 \qquad 4.20$$

These are valid in the range 1000K-2000K.

4.6 Nusselt Number

The convective transfer coefficients are most easily determined from Nusselt number correlations. For cylinders in crossflow, the Nusselt number (Perry and Chilton, 1973, p. 10-13) is

TABLE 4.2

TEST CASES FOR GAS TEMPERATURE CORRECTIONS

S.R.	T_{in}, °K	T_{out}, °K	Coal Rate g/sec.	$\dot{q}_{net}$, kcal/hr
1.20	588	1117	0.63	10900
0.95	588	1089	0.63	10900
0.80	588	1117	0.63	8700
0.40	370	1114	0.63	2700

$$Nu = 0.911\ Re^{0.385} \qquad 4.21$$

The Reynold's number is based on the cylinder diameter.

From the physical properties of the gas and the test case, stoichiometric air flows of 10.0 SCFM (4.72 1/s, furnace diameter of 0.5 ft (15.24 cm), and a product/feed ratio of 1.03, for the thermocouple

$$h_c\ (^{cal}/_{hrcm^2}) = 28.8\ \gamma^{0.385}\ \exp\ (3.70 \times 10^{-4}\ Tg) \qquad 4.22$$

For the suction pyrometer (Perry and Chilton, 1973, p. 10-24)

$$Nu = 0.020\ Re^{0.8}\ Pr^{0.33}\ (\frac{Ds}{DL})^{0.53} \qquad 4.23$$

and

$$h_c\ (^{cal}/_{hrcm^2}) = 64.1\ \exp\ (1.85 \times 10^{-4}\ T_g) \qquad 4.24$$

$(^{Ds}/DL)$ is the ratio of the inner to outer diameters of the pyrometer annulus.

The Reynold's number for the suction pyrometer is based on the operating conditions in Table 4.2 with the characteristic length taken as the width of the pyrometer annulus and Pr = 0.75.

4.7 Thermocouple Temperature Correction Algorithm

Combining Equations (6), (12), (14), and (15) gives

$$Tg = T_T + \left\{\frac{hr_{tw}\ A_2\ \exp\ (-\frac{A_1}{Tg})}{hr_{gt} + h_{c_{gt}}}\right\}(T_T - T_w)$$

$$q_{net} = \sigma \sum_{i=1}^{n} A_i \left[\frac{1}{\frac{1}{\varepsilon_{gi}} + \frac{1}{\varepsilon_w} - 1}\right] (T_{gi}^4 - T_{wi}^4) \qquad 4.25$$

where q net is defined from the overall gas phase enthalpy balance. As previously mentioned, A_1, is specified (Table 4.2) and A_2 is adjusted to satisfy the heat balance and temperature correction simultaneously.

The measured temperature profiles for the Western Kentucky coal test cases are shown in Figure 4.3. The wall temperatures used in Equation (14) are determined from the correlation shown in Figure 4.6. The wall emissivity was taken as 0.5 and the thermocouple emissivity as 0.85 (Hottel and Sarofim, 1967, p. 159). Since the cone temperature was not measured, the temperature was assumed to be equal to the first measured temperature at 25 cm.

The resulting corrected gas temperature is plotted as a function of stoichiometric ratio in Figure 4.4. The results of satisfying the furnace heat balance and temperature correction simultaneously using the surface area, A_T, as an adjustable parameter are shown in Table 4.3.

These values of the gas phase emissivities are not unreasonable considering that axial radiative transfer has been neglected and given the uncertainty in the surface emissivities used in the heat balances.

Further, the emissivities calculated by the method give overall extinction coefficients of 0.75 - 1.15 m^{-1} which is in the range of the 1 m^{-1} usually given for industrial scale fuel-lean pulverized coal flames (Gray, Kilham and Muller, 1976, p. 77; Field, et al., 1967, p. 459).

The corrected gas temperatures in Figure 4.4 are correlated with the measured temperatures and stoichiometric ratios by

$$Tg = 481 + 5.788 \times 10^{-4}\ T_t^2 - 6.146 \times 10^{1}\ \gamma^2,\ r^2 = 0.96 \qquad 4.26$$

where $0.4 \leq \gamma \leq 1.2$

$1080K \leq T_T \leq 1500K$

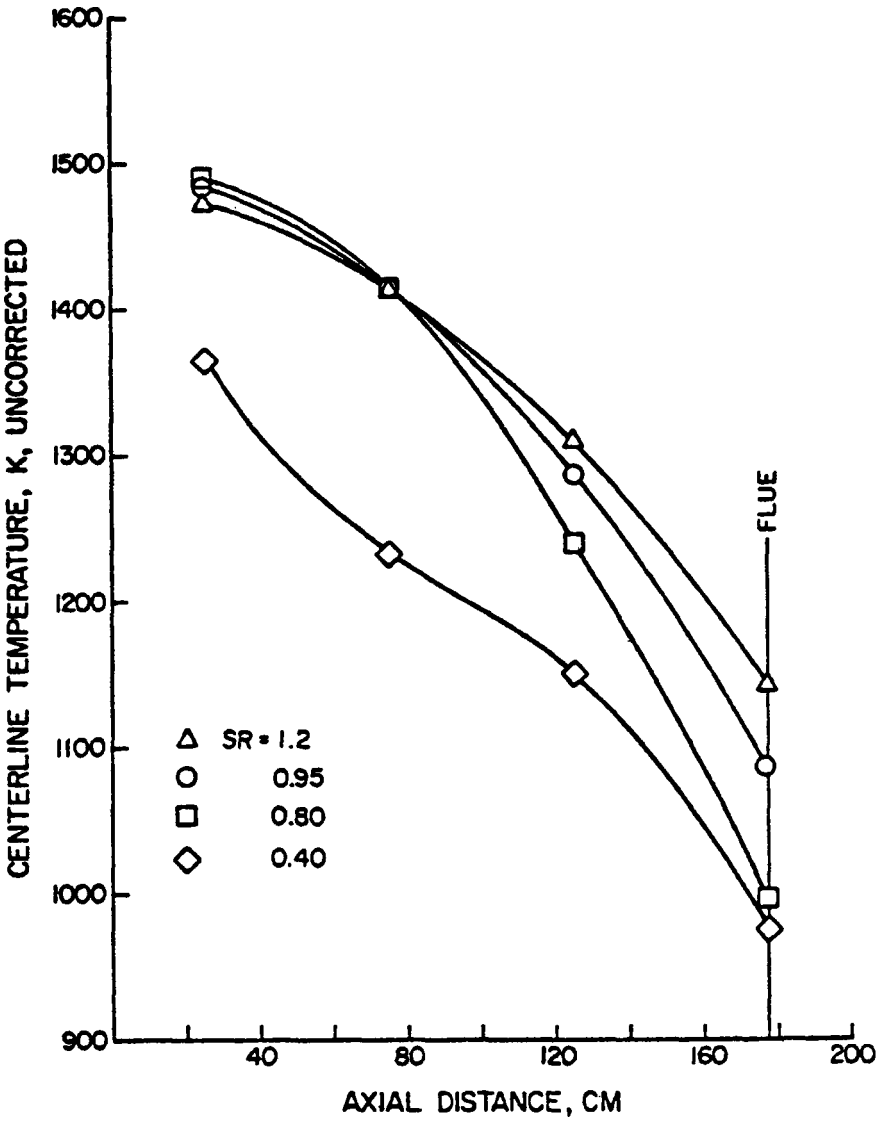

Figure 4.3. Western Kentucky Coal Test Case Temperature Profiles.

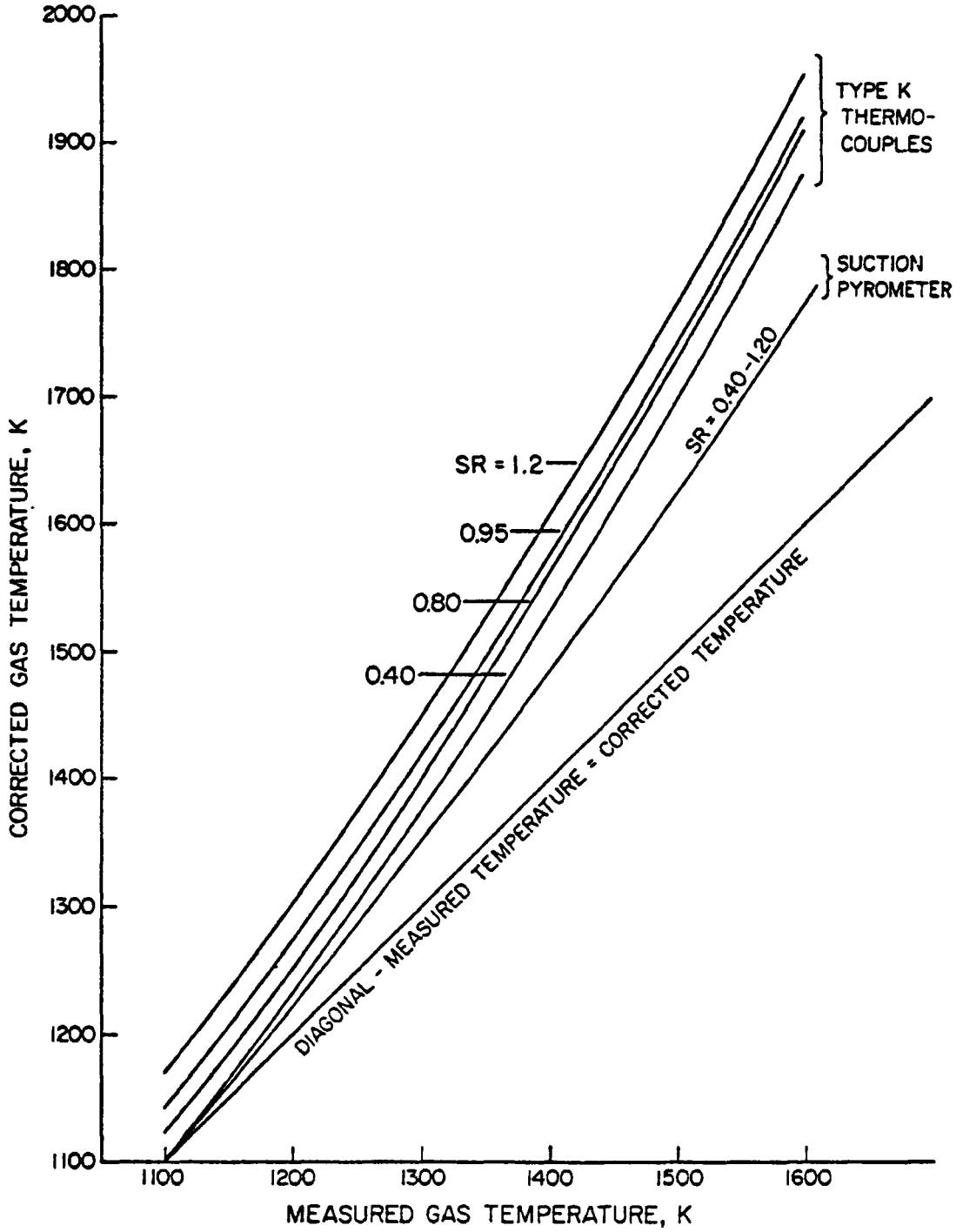

Figure 4.4. Corrected Gas Temperatures.

TABLE 4.3

EMISSIVITIES OF THE PULVERIZED COAL FLAME

SR	A_2	A_T cm^2/g	ε_g @ 1400°K*	τ_σ @ 1400°K
1.20	183	157%	0.12	0.88
0.95	127	868	0.11	0.89
0.80	40	233	0.08	0.92
0.40	10	30	0.68	0.92

Equation (26) is plotted in Figure 4.4. For reasons discussed subsequently, one-half of these corrections were applied to the measured temperatures for all of the coal and char experiments to calculate the residence time in the furnace (Appendix B).

4.8 Suction Pyrometer Temperature Correction

Equation 4.6 is modified in the case of a suction pyrometer as a result of the shielding to eliminate (or greatly reduce) the thermocouple-to-wall radiative heat transfer to give (Figure 4.5)

$$Tg = Tp + \left\{ \frac{\left(\frac{1}{N+1}\right) hr_{pw}}{hc_{gp}} \right\} (Tp - T_w) \qquad 4.27$$

The transmission of the gas has been eliminated from this equation since there is a large uncertainty in the value of the emissivity of the ceramic shields used in the pyrometer. A nalue of 0.26 was chosen for the McDanel MV-30 tubes used for shielding. Hottel and Sarofim (1967, p. 159) give values of the emissivity ranging from 0.18 to 0.40 depending on the grain size of the material. The chosen value is that of 10 μ mean grain size at 1500° K.

The pyrometer-wall radiative coefficient is modified by the factor (1/N+1) to account for the number of shields, N, used to reduce the radiative cooling of the thermocouple bead. The convective transfer coefficient, hc_{gp}, is given by Equation 4.24.

The resulting corrected temperature is given in Figure 4.4. Since the convective coefficient is not a function of the stoichiometric ratio, given that the transmission coefficient for pyrometer-to-wall radiative exchange can be neglected, there is only a single correction.

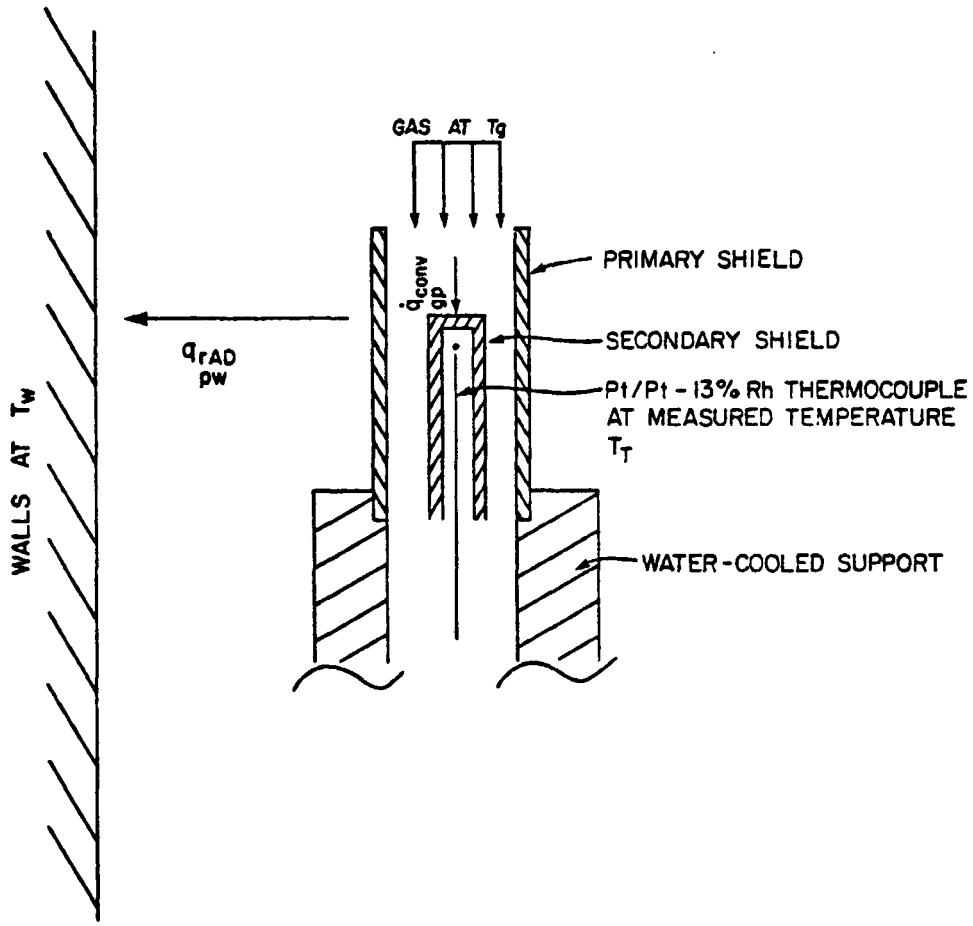

Figure 4.5. Suction Pyrometer Heat Balance.

For the suction pyrometer, the true gas temperature is given by

$$Tg = Tp + 9.65 \times 10^{-11} \exp(-1.84 \times 10^{-4} Tp)(Tp^4 - Tw^4) \; T[=] \; ^\circ K \qquad 4.28$$

where Tw is given by the previously mentioned wall temperature, vs. centerline temperature correlation. Equation 4.28 is plotted in Figure 4.4.

4.9 Wall Temperature vs. Measured Centerline Temperatures

The measurement of the furnace wall temperature is more easily accomplished than measuring the gas temperature since fixed thermowells can be used. Since the furnace is operated according to a fixed procedure prior to an experimental run, the wall temperature should correslate with the measured centerline temperature if run-to-run experimental conditions are the same.

Figure 4.5 shows the suction pyrometer-measured temperature as a function of measured wall temperature. The pyrometer temperature is given by

$$Tp = -12283 + 1913 \ln T_w r^2 = 0.84 \; T \; [=] \; ^\circ K \qquad 4.29$$

4.10 Comparison of Thermocouple and Suction Pyrometer Measured Temperatures

Several comparisons were made between the thermocouple and pyrometer-measured temperatures on gas and coal flames. Owing to the inherent difficulties attendent to operating the suction pyrometer in the coal flame (see comments in Section 3), these tests were minimized. Figure 4.7 shows that there is no significant difference between the two. In fact, the pyrometer temperature at long axial distances in the furnace are consistently lower than those measured with thermocouples. This is presumed to be a result of misalignment of the pyrometer when it could

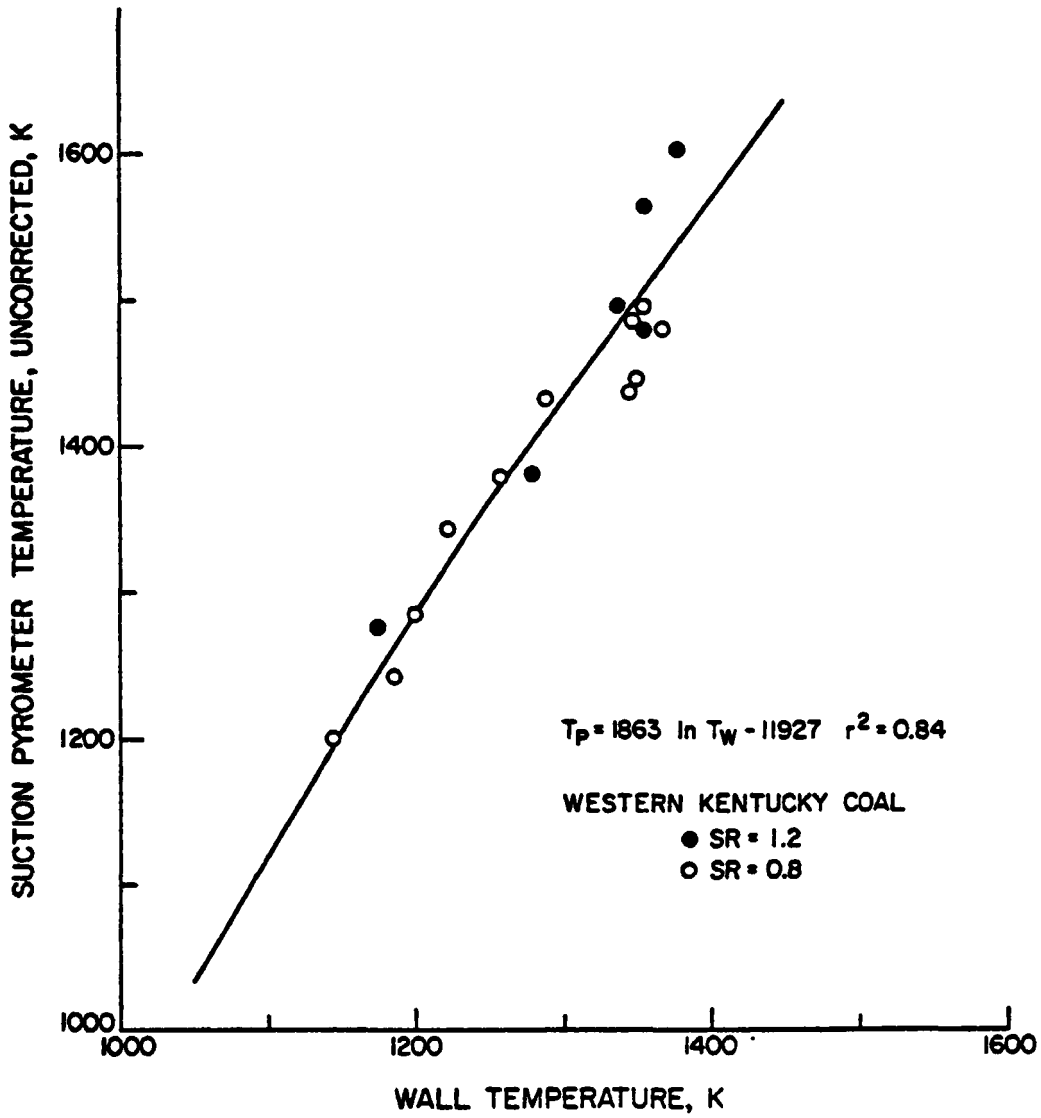

Figure 4.6. Uncorrected Suction Pyrometer Temperature vs. Wall Temperature, Western Kentucky Coal.

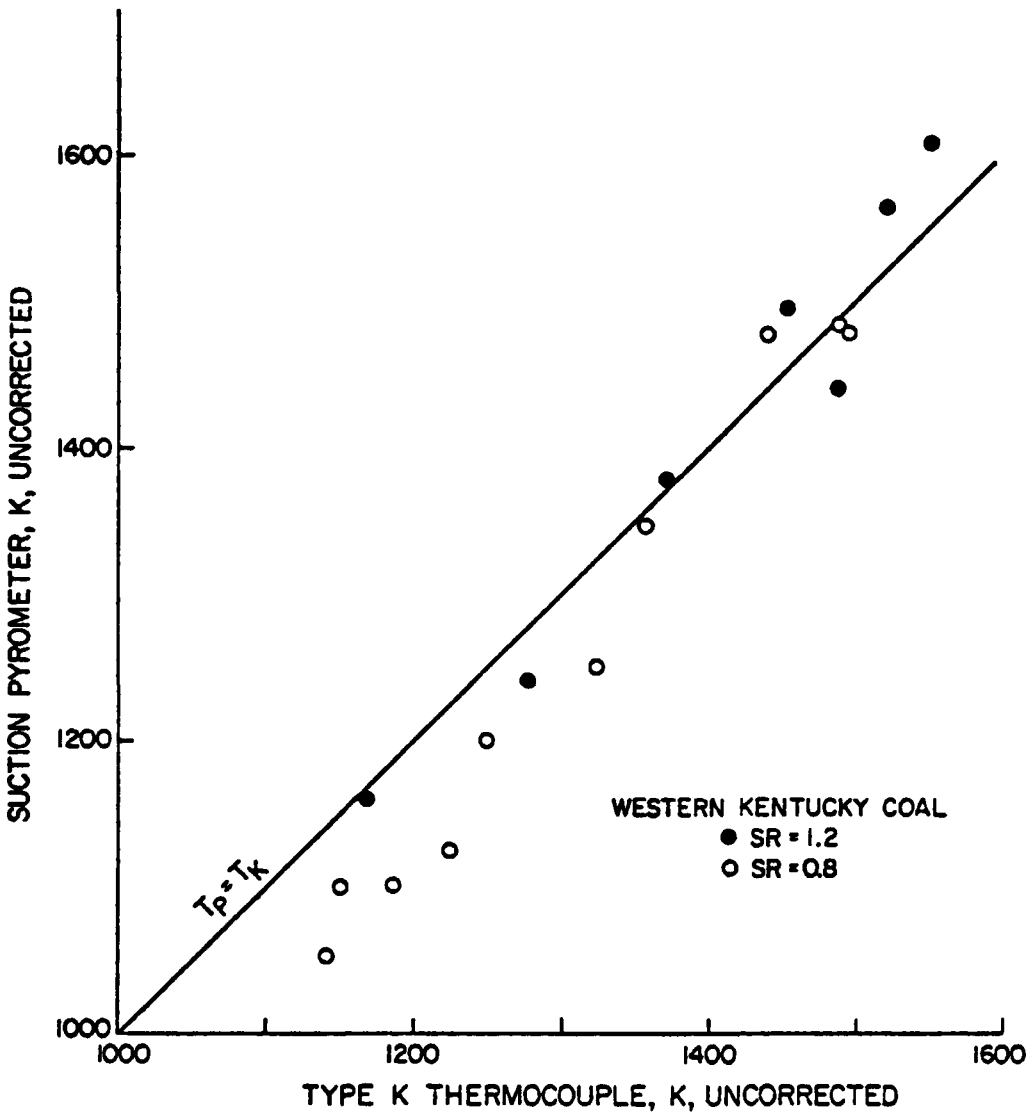

Figure 4.7. Suction Pyrometer vs. Type K Thermocouple Temperatures.

not be visually centered. If the pyrometer is near the cold walls, it will indicate a lower temperature than if properly centered.

According to the temperature correction equations developed previously, the thermocouples and pyrometer give a corrected gas temperature as a function of measured temperatures given by Equations (26) and (28). Since the corrected pyrometer temperature is roughly one-half of the corrected thermocouple temperature, the actual correction applied to the measured temperature was chosen as exactly half of the thermocouple correction.

4.11 Conductive Cooling of a Thermocouple

Following the treatment of fin cooling by conduction given in Bird, Stewart and Lightfoot (1960, p. 288)

$$\Theta = \frac{\cosh[N(1-Z)]}{\cosh[N]}$$

where $\Theta = \frac{T-Tg}{T_w-Tg}$ dimensionless temperature

$Z = \frac{x}{L}$ dimensionless axial distance

$N^2 = \frac{4h_cL^2}{kB}$

L = thermocouple length

h_c = convective heat transfer coefficient

k = thermocouple thermal conductivity

B = thermocouple diameter

For the thermocouple under consideration

$h_c = 7.68 \exp (2.06 \times 10^{-4} T_j)$

L = 3 in.

k = 18 BTU/hr ft° R for cooling of the nickel sheath

B = 0.125 in.

Given a measured temperature of 2250° F = 2710° R at Z = 1.0 for example, and a corresponding wall temperature of 2467° R (Equation 4.29)

$$\theta = \frac{1}{\cosh 4.48} = 0.023$$

or the conductive cooling amounts to 6° R which is negligible given a measured temperature of 2710° R.

4.12 Convective Heat Transfer to Furnace Walls

Convective heat transfer to the combustor walls can be neglected in the overall furnace gas heat balance. For laminar flow in a vertical tube (Bird, Stewart and Lightfoot, 1960, p. 399).

$$Nu_{ln} = 1.86\ (Re\ Pr\ D/L)^{1/3}\left(\frac{\mu b}{\mu o}\right)^{0.14}$$

The Reynolds and Prandt numbers are based on the bulk fluid temperature and flow rate.

From Equations (4.19) and (4.20)

$$h_{ln} = 0.77 \exp\left[2.54 \times 10^{-4} T_b - 3.49 \times 10^{-5} T_o\right],\ SR = 1.2$$

where T_b and T_o are the bulk and furnace wall temperatures. For SR = 1.2, at which the flow in the furnace is a maximum, say 12 SCFM (a typical value), assuming, over one zone

T_{b_1} = 2250 F T_{b_2} = 2000 F

T_{w_1} = 1977 F T_{w_2} = 1800 F

A = 1.31 ft^2

ΔT_{ln} = 235° F

$Q_{zone} = h_{ln} A \Delta T_{ln} = 431$ BTU/hr. Over 7 zones, $Q \approx 3000$ BTU/hr which is of the order of 4-6% of the total heat losses in the furnace and may be neglected in an approximate heat balance.

5.0 EXPERIMENTAL RESULTS

5.1 Presentation of Results

The results are presented in subsequent sections according to increasing volatilities of the coals studied. The low volatile FMC char is presented first with particular attention to the phenomena associated with low coal and fuel nitrogen volatility. The balance of the coals (except Western Kentucky, the results of which are described in DOE report FE 1817-4) are presented and arguments are developed to support the hypothesis that both the volatile nitrogen (VN) pool (the nitrogenous coal volatiles and NO precursors) and the NO formed during the substoichiometric first stage of staged combustion must be accounted for to predict the phenomena resulting from staged combustion.

Each coal was burned in three modes and the results are presented accordingly. First, baseline substoichiometric time-resolved composition profiles are presented for stoichiometric ratios (SR) of 0.8 and 0.4. The salient features of these profiles are discussed. The second and third modes of combustion studied are staged combustion at first stage stoichiometries, SR1, of 0.8 and 0.4 and second stage SR2 of 1.2. For each coal, at least two staging positions were used. The third (longest residence time) position was not emphasized except for the lignite and high volatile IGT char since the reduced carbon burnout associated with the cooler parts of the furnace was not expected to provide meaningful data. Since no intermediate nitrogenous volatiles were measured for the baseline conditions, the state of the VN pool at the staging point is inferred from the staged combustion profiles.

5.2 Coal Chars

The combustion of coal chars from which most of the volatile matter has been previously removed is important insofar as the behavior of nonvolatile fuel nitrogen is concerned. Since neither the VN pool nor the residual nitrogen content of the coals as combustion proceeds were measured, inferences from the char data provide the only means at present of evaluating the effects of char nitrogen on staging effectiveness.

The chars contain little total volatiles. Consequently, the entire combustion sequence could be followed analytically since the delayed ignition shifted the profiles within the low residence time range (0.25 sec) of the sampling probe.

The baseline profile for the FMC char at SR = 0.8, Figure 5.1, is typical of the profiles for all of the coals and chars and also of the Western Kentucky coal profiles of Wendt, Lee and Pershing (1978). NO formation is rapid, and terminates in a peak value. The peak NO occurs in the presence of oxygen indicating that NO reduction and NO precursor reduction reactions begin to dominate the NO formation reactions prior to oxygen depletion. Subsequently, the reduction of NO following the peak is strongly dependent on residence time.

This profile shows that NO undergoes a secondary increase and CO, a decrease, at long residence times. The fact that the furnace is operated super-atmospheric (0.5 in H_2O) leads to the circumstantial conclusion that this is not a result of an air leak. The mechanisms for this unusual behavior still require to be elucidated.

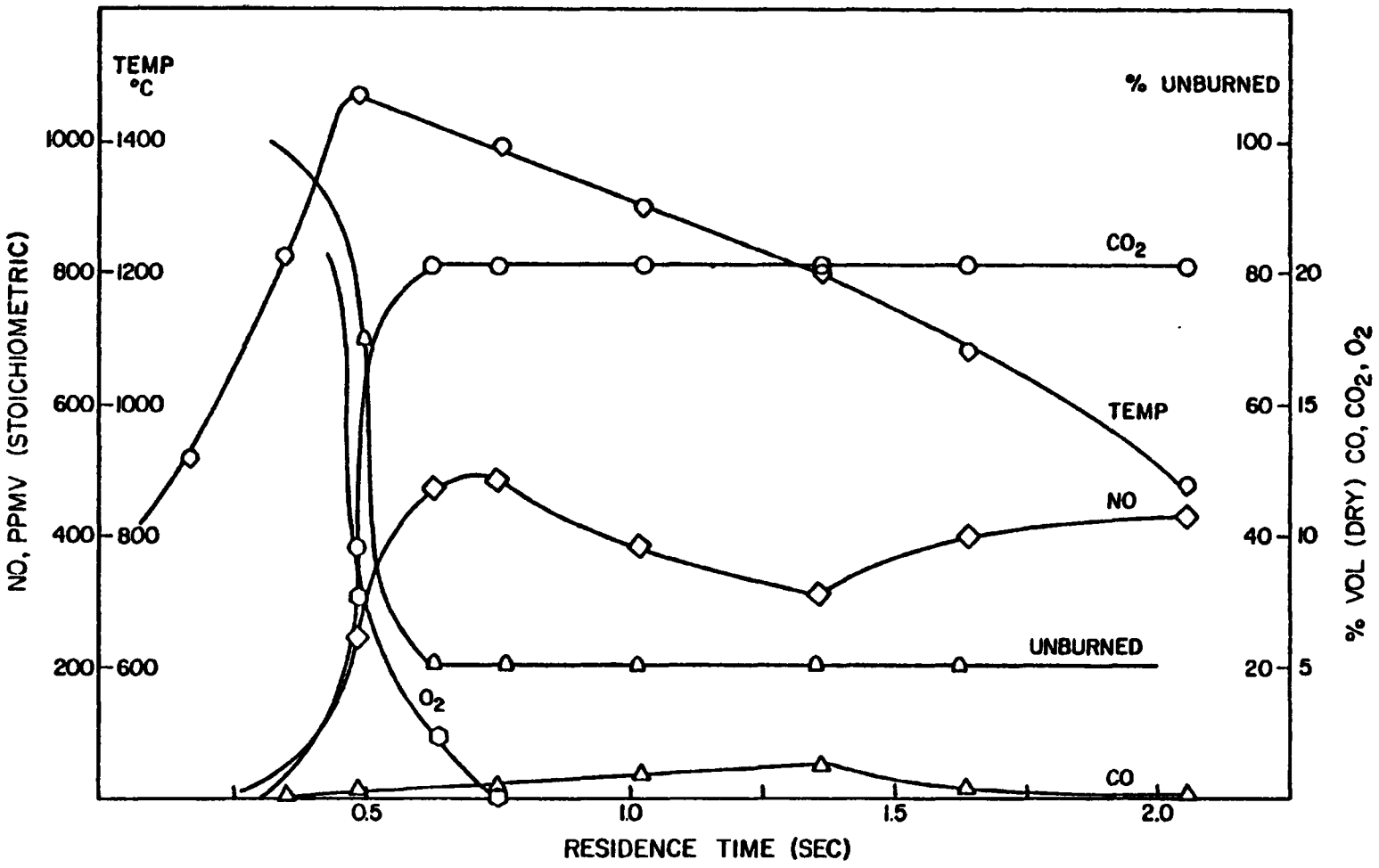

Figure 5.1. Baseline Substoichiometric Composition Profiles FMC Char, SR = 0.8.

The base FMC char profile at SR = 0.4, Figure 5.2 is similar to that at less fuel-rich conditions except that the increased fuel richness causes faster oxygen depletion and a suppressed peak NO value. NO formation within the constraint of low oxygen is still rapid, and the peak value occurs within the first second. NO reduction is slower and an asymptotic low value of about 60 ppm exists.

The FMC char profiles under staging conditions provide some indirect information about the state of the VN and char nitrogen pools at the staging point. At SR1 of 0.4, Figure 5.3, the second stage air was introduced before the first stage peak, the terminal second stage NO is approximately the first stage peak value. This could indicate that char nitrogen reactions leading to NO are occurring heterogeneously since the rise in second stage NO is rather slow.

When second stage air is introduced after the first stage peak has formed and has been reduced, the second stage NO reaches about the same value after a slow rise. If this is heterogeneously formed, there is some intrinsic limiting factor which gives rise to the same terminal values shown in this graph. The NO which has been destroyed in the first stage presumably forms nitrogen, not VN, since the second stage air consistently gives a sharp step increase in NO formed from VN as seen in subsequent sections.

The corrected temperatures for the FMC char under staged conditions are shown in Figure 5.4. The temperature profiles are much steeper following the staging point as a result of the additional gas volume in the combustor.

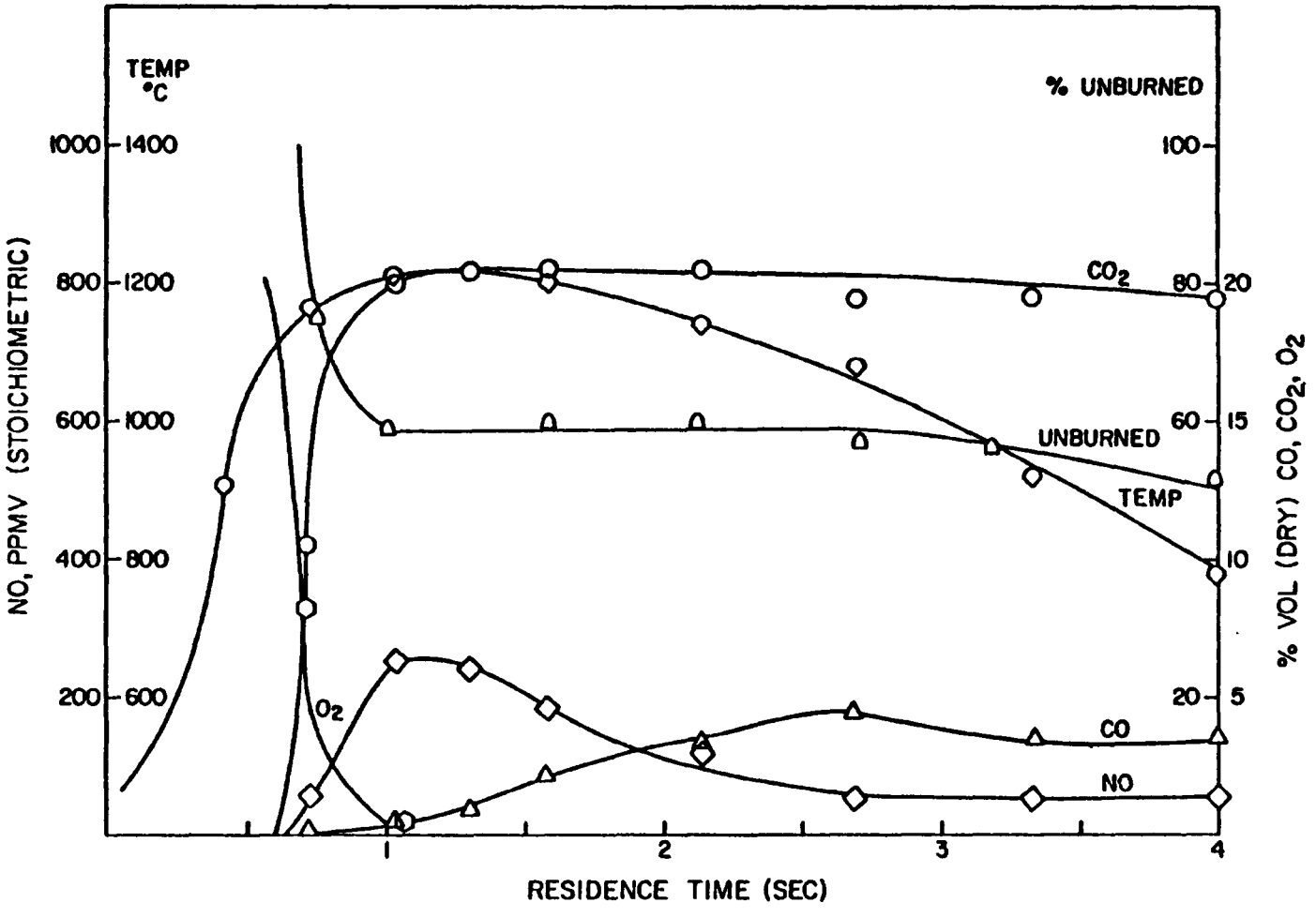

Figure 5.2. Baseline Substoichiometric Composition Profiles FMC Char SR = 0.4.

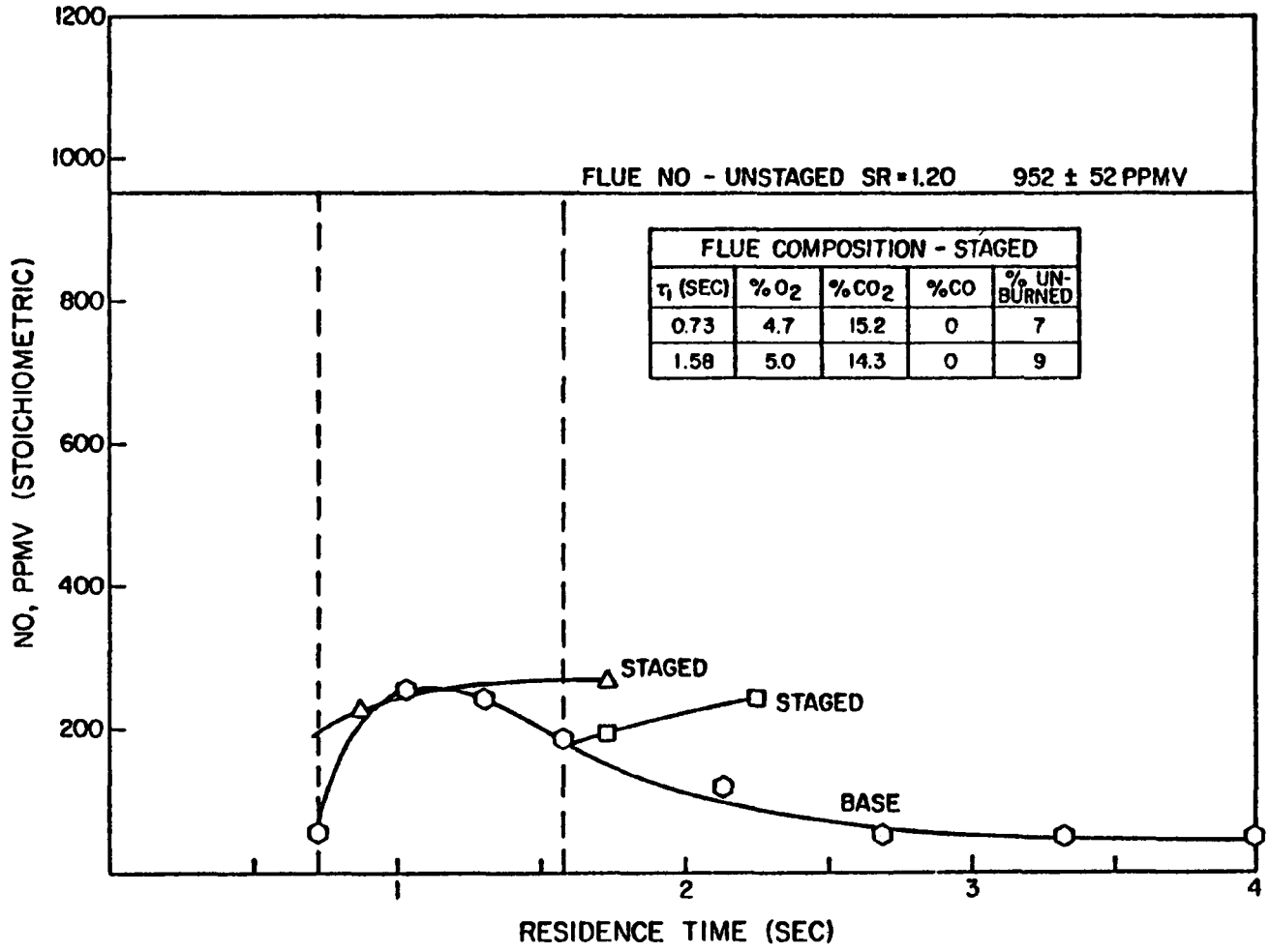

Figure 5.3. Staged Combustion Compositions
FMC Char; Base SR = 0.4, SR1 = 0.4, SR2 = 1.2.

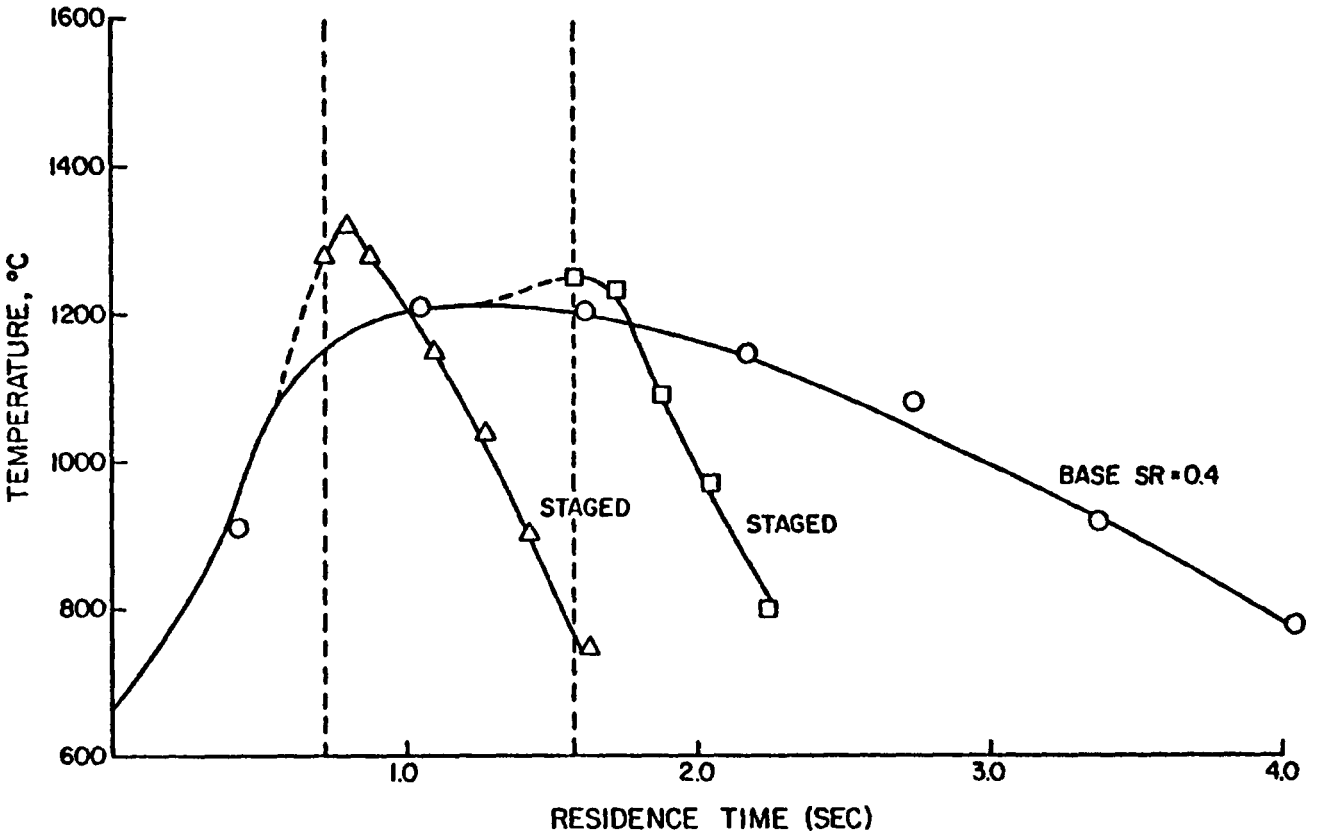

Figure 5.4. Baseline and Staged Temperature Profiles
FMC Char; Base SR = 0.4, Staged SR1 = 0.4, SR2 = 1.2.

The fuel nitrogen conversion in the second stage and the percentage reduction in NO emissions, compared to unstaged fuel-lean combustion at SR = 1.2, the staging effectiveness, in the second stage are given in Table 5.1 for the FMC char. The unstaged flue NO at SR = 1.2 of 952 ppm is equivalent to 77% of total fuel nitrogen conversion. This is the greatest fuel N conversion in unstaged fuel-lean combustion determined for all of the coals studied in this experiment and undoubtably reflects the low amount of volatile material in the char which can compete for oxygen and act as a fuel N reducing agent in lean pyrolysis and combution. That 23% of the fuel N is not converted is perhaps indicative of poor micromixing or poor diffusion.

The baseline profiles for the IGT char are similar to those for the FMC char. In Figure 5.5, the peak NO for SR = 0.8 occurs prior to the disappearance of oxygen. In this case, probably as a result of increasing total volatiles and VN content of the IGT char, the NO formation is more rapid than with the FM char. The reduction of NO is more rapid also, since additional fuel fragments increases the rate. Since the char is devolatilized, the hydrocarbon fragments are assumed to be heavier than simple -CH as a result of deep pyrolysis of the ring structure. These fragments may be an important reactant in NO reduction, especially at long residence times. Once again, there is a secondary increase in NO at long residence times along with dip in CO_2 and a decrease in CO contents of the gas.

The baseline profile at SR = 0.4, Figure 5.6, is again suppressed as a result of early oxygen depletion, although the NO peak occurs in the presence of oxygen. This profile is characterized by very fast formation and reduction of NO.

TABLE 5.1

FUEL N CONVERSION AND STAGING EFFECTIVENESS

SR1 (SR2 = 1.2)	τ_1, Sec	Fuel N Conversion	Staging Effectiveness
0.8	N.A	---	---
0.4	0.73	22%	53%
	1.58	20	58

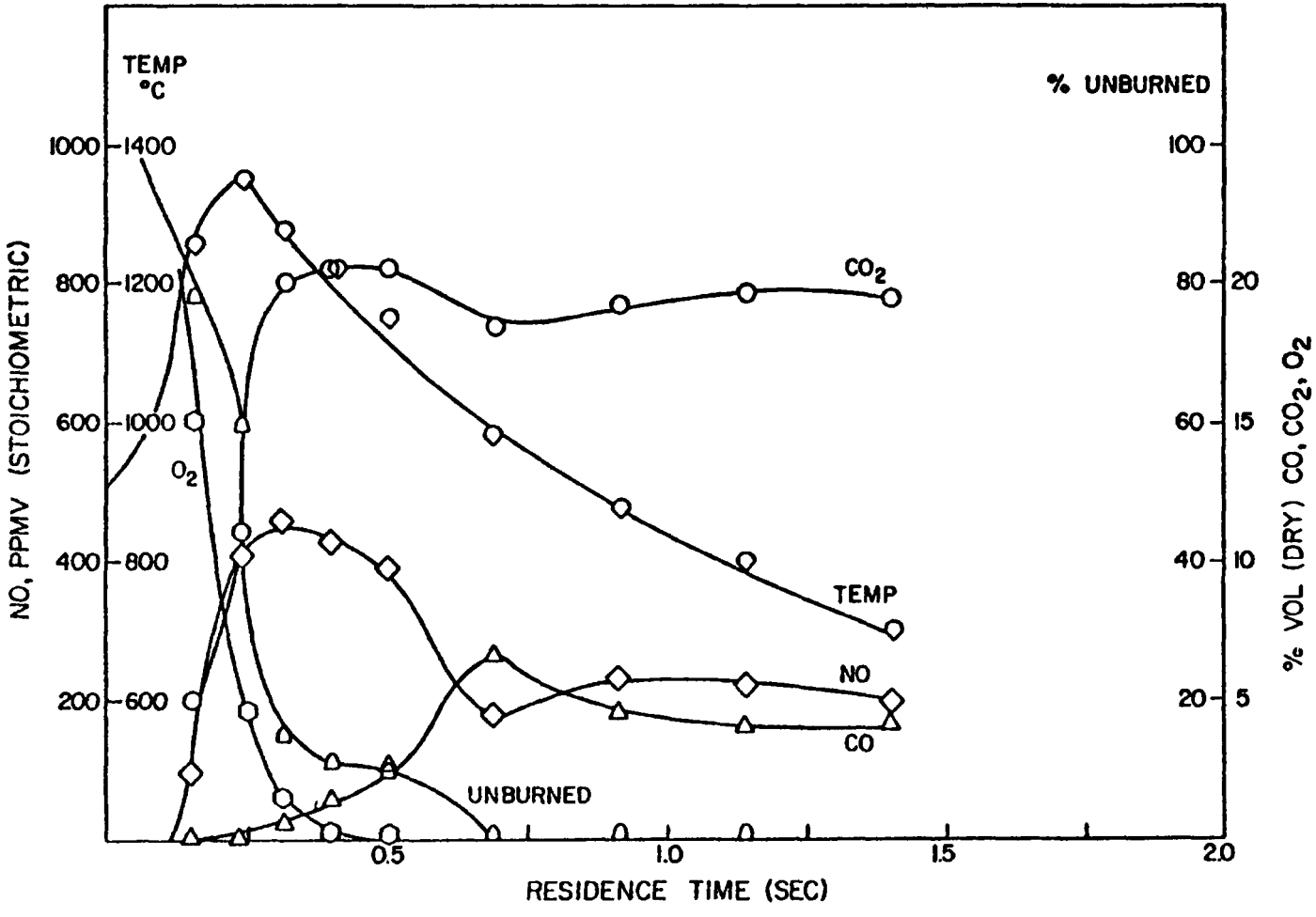

Figure 5.5. Baseline Substoichiometric Composition Profiles IGT Char, SR = 0.8.

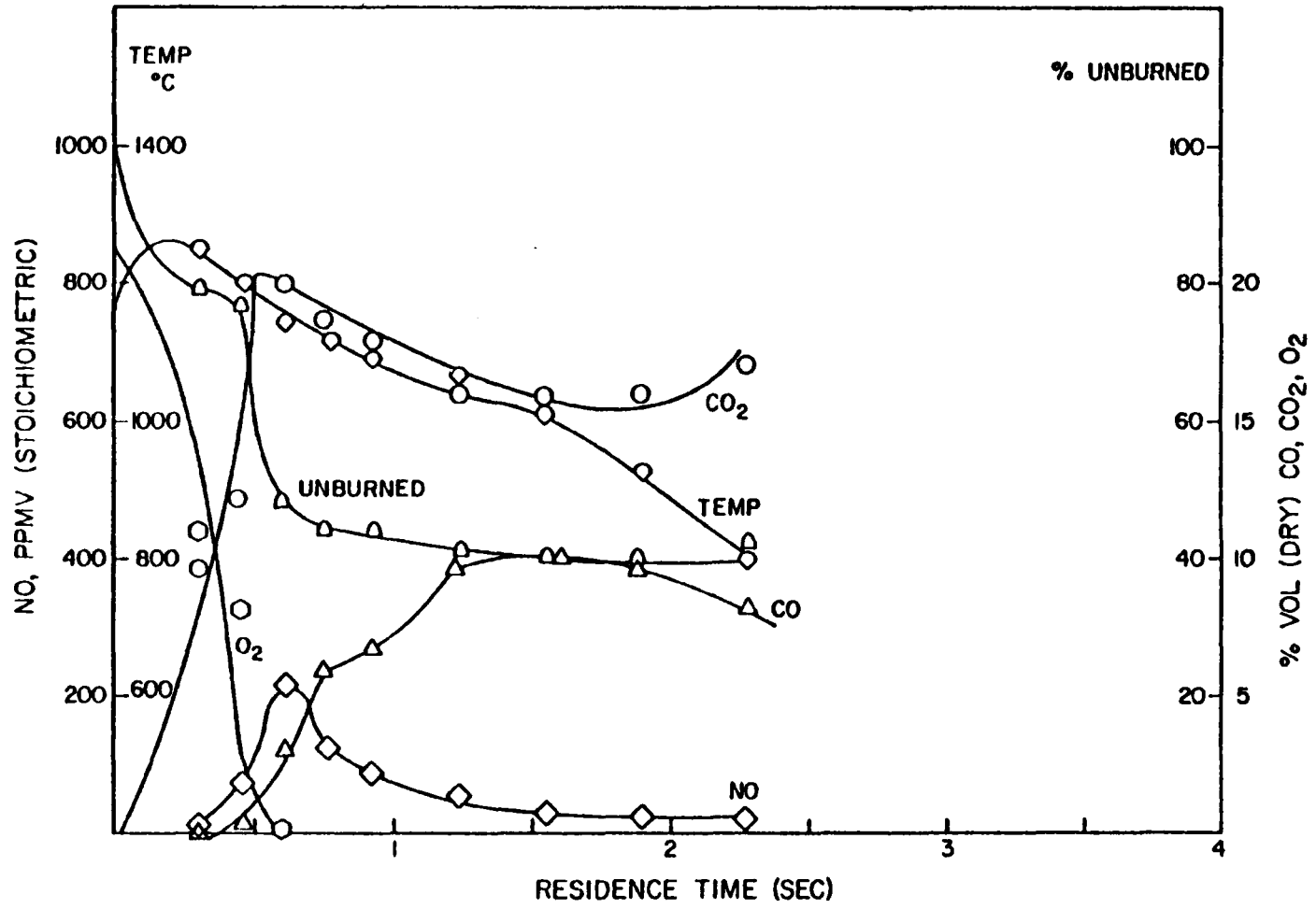

Figure 5.6. Baseline Substoichiometric Composition Profiles IGT Char, SR = 0.4.

At SR1 = 0.8, Figure 5.7 staging results in a second stage flue NO value roughly that of the first stage peak when the staging point is just prior to the peak NO value. At longer first stage residence times, the second stage flue NO is about that of the baseline NO at the staging point after a slow rise. It should be noted that the unburned carbon, carbon dioxide, and oxygen values reported on these graphs are very nearly constant over the entire second stage. The temperature profiles associated with these staged runs are shown in Figure 5.8.

The IGT char at SR1 = 0.4, Figure 5.9, shows the same qualitative behavior as the FMC char at the same conditions. When second stage air is introduced prior to attainment of the baseline peak NO, there is a rapid increase in NO which is then constant over the entire second stage. When air is introduced after the first stage NO peak, there is a slow increase following a small step increase at the staging point possibly a result of some VN conversion to NO as oxygen becomes available. The temperatures associated with these runs are shown in Figure 5.10.

These results do not include any analytical information about the type and amount of volatile nitrogen present or the amount of fuel nitrogen remaining in the coal. It can be conjectued that the small step increases in NO at the staging point, at SR1 = 0.4, is due to rapid conversion of volatile nitrogen under fuel-lean conditions. The subsequent slow rise in NO could be an artifact of mixing or of fuel nitrogen burnout at long residence times. The former is much more attractive than the latter since it permits the assumption that very little volatile nitrogen is left at SR1 = 0.8 and that the first stage baseline profile is indicative of the NO reduction achievable when staged air is introduced at that point.

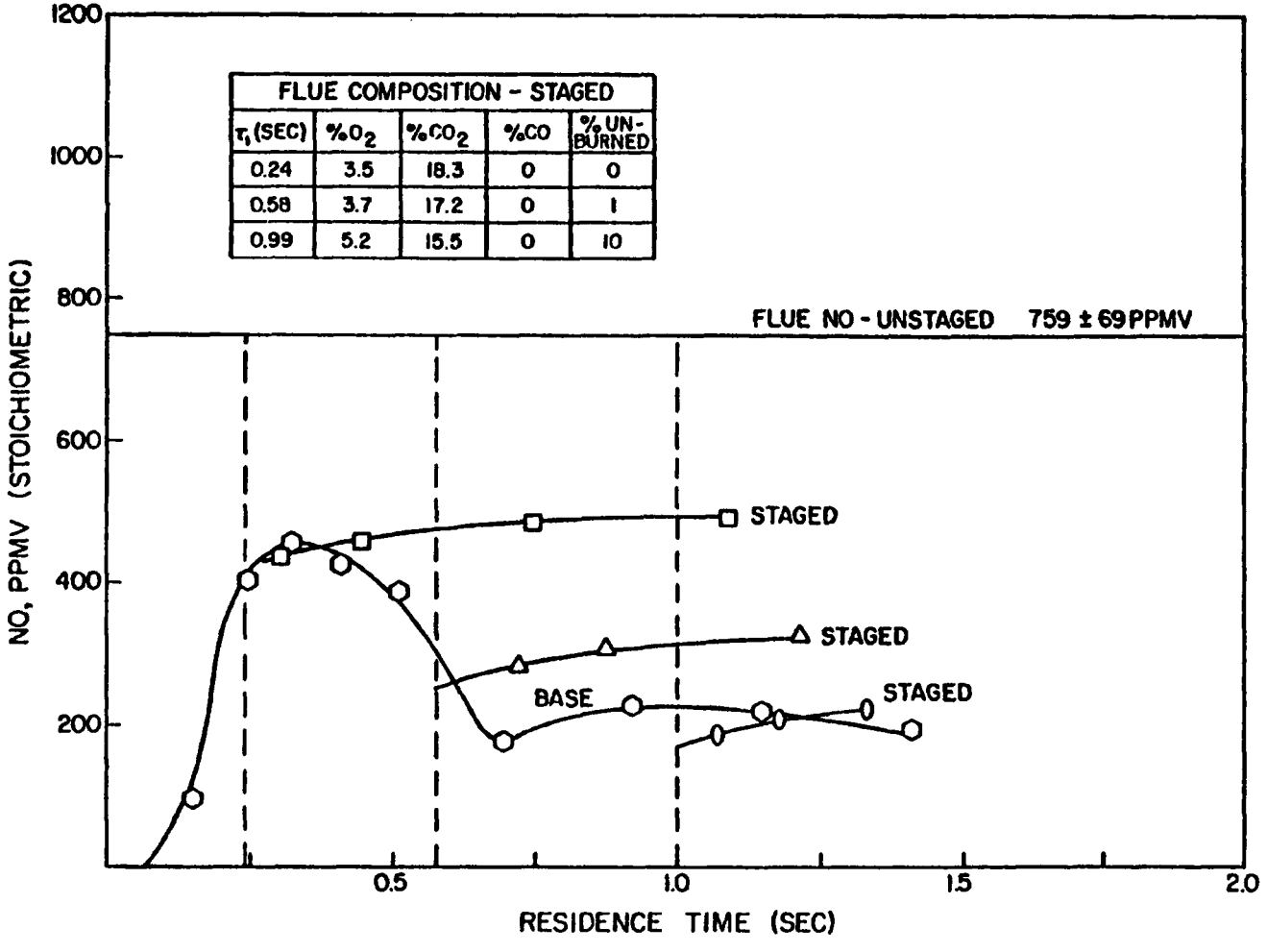

Figure 5.7. Staged Combustion Compositions
IGT Char, SR1 = 0.8, SR2 = 1.2.

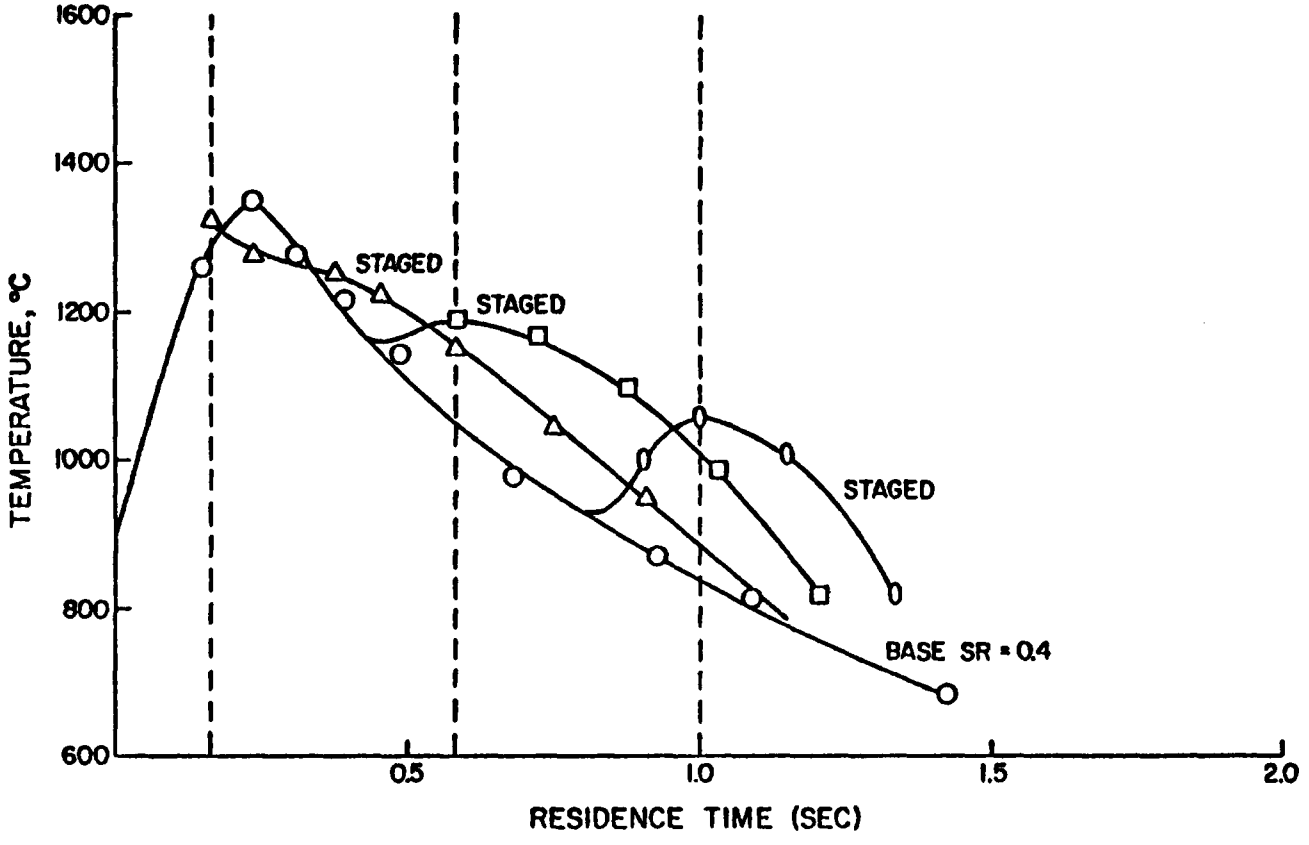

Figure 5.8. Baseline and Staged Temperature Profiles
IGT Char; Base SR = 0.8, Staged SR1 = 0.8, SR2 = 1.20.

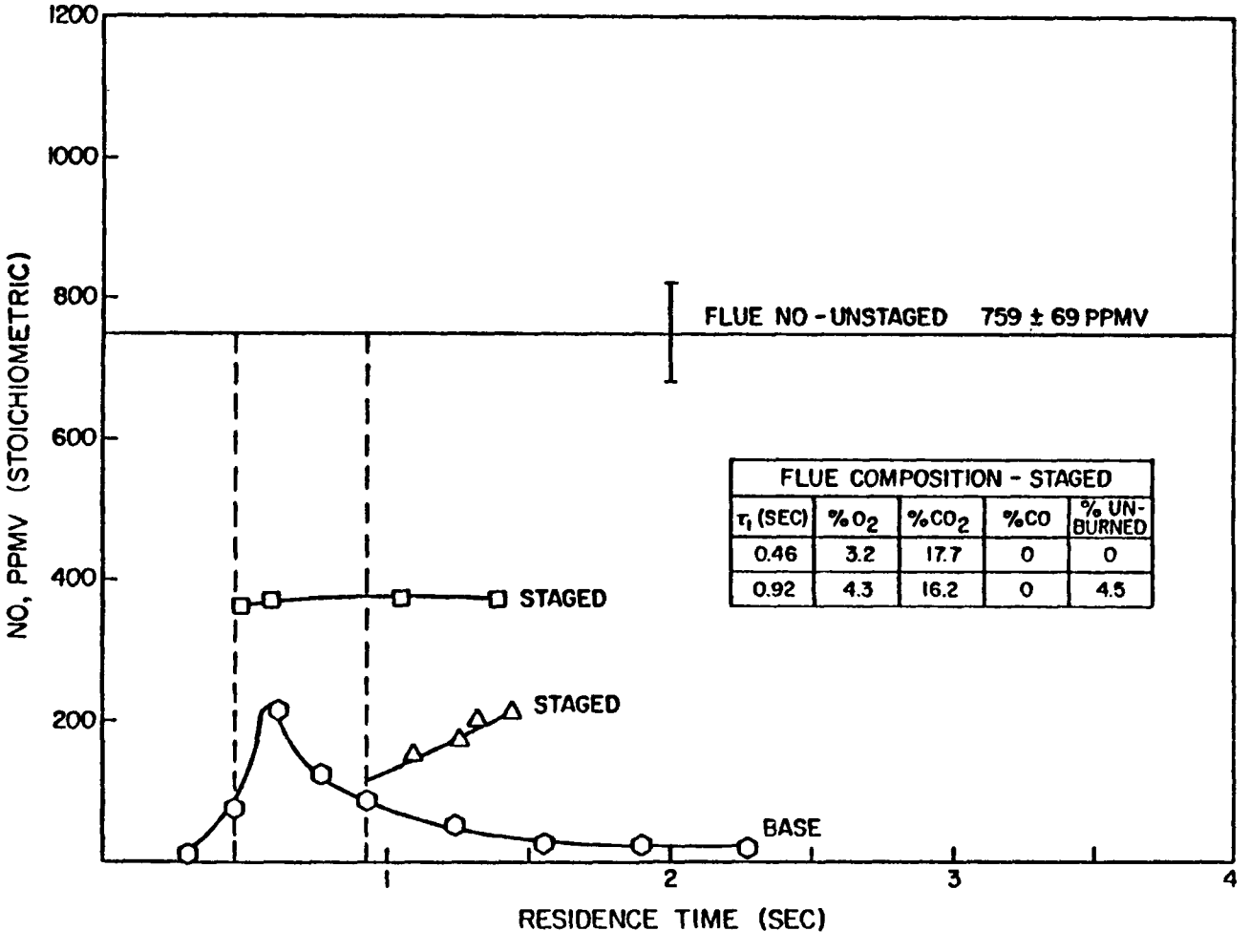

FLUE COMPOSITION - STAGED				
τ_1 (SEC)	$\%O_2$	$\%CO_2$	%CO	% UN-BURNED
0.46	3.2	17.7	0	0
0.92	4.3	16.2	0	4.5

Figure 5.9. Staged Combustion Compositions
IGT Char SR1 = 0.4, SR2 = 1.2.

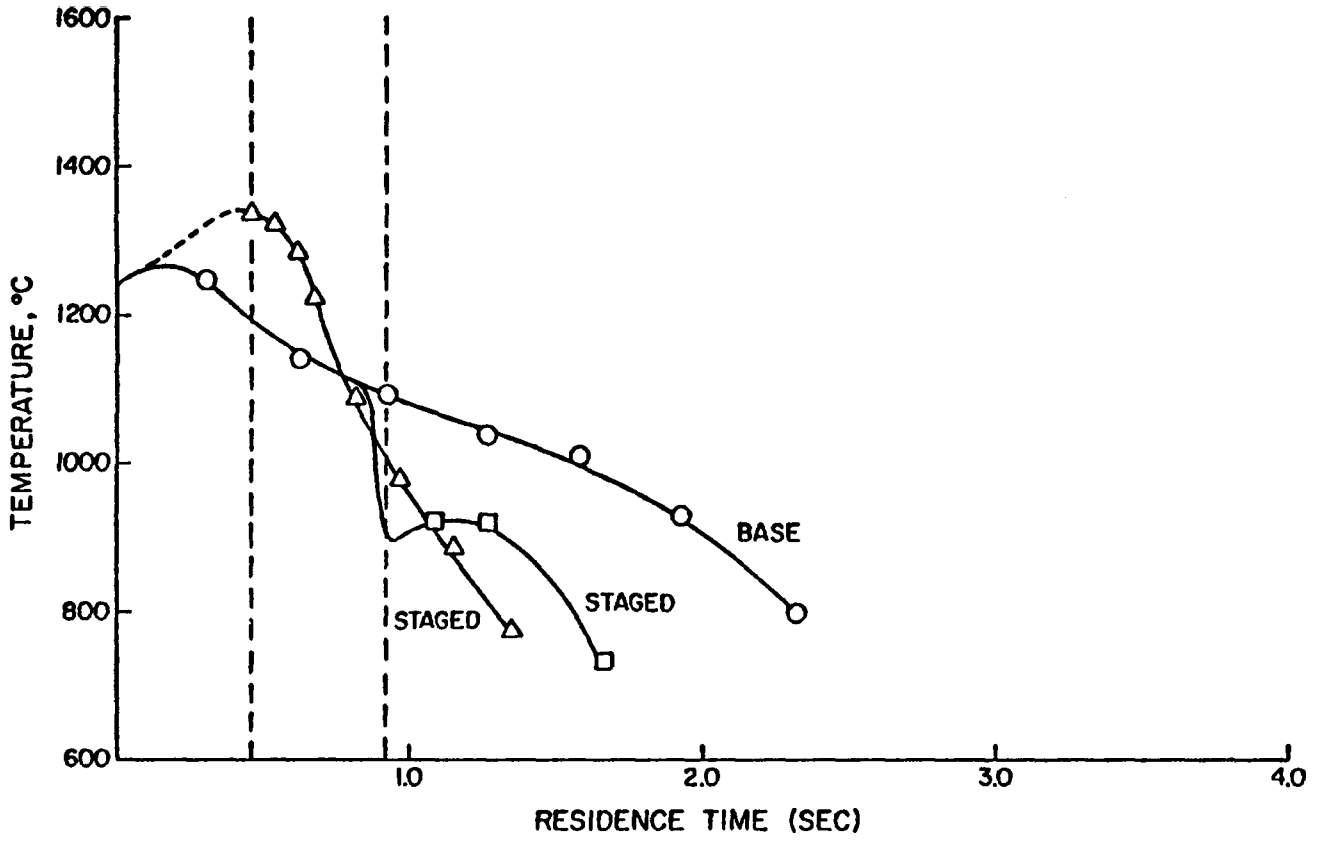

Figure 5.10. Baseline and Staged Temperature Profiles
IGT Char; Base SR = 0.4, Staged SR1 = 0.4, SR2 = 1.2.

The FMC char runs at SR = 0.4 show that in the absence of significant amounts of volatile combustibles, the peak first stage NO is a result of the slow net conversion, possibly locally limited by oxygen, of the char nitrogen prior to the depletion of oxygen. If second stage air is introduced before the peak baseline NO, the char nitrogen is oxidized to about the peak NO value. This is also the case with IGT char at SR1 = 0.8, where staging at the peak baseline NO point resulted in very little net additional second stage NO. Air addition at longer residence times simply dilutes the NO already formed (if the assumption of imperfect micromixing is assumed). When the data are reduced to stoichiometric conditions, the NO remains constant. At SR1 = 0.4, however, the IGT char with a higher volatile content than the FMC char, is oxygen depleted prior to the baseline peak so that additional air oxidizes the volatile nitrogen to NO. At longer residence times at SR1 = 0.4 and 0.8, the NO is depleted primarily to N_2 since additional air gives only a small net increase in NO at the staging point in the case of the IGT char.

Unstaged combustion of IGT char at SR = 1.2 gives 759 ppm of NO emitted or 47% of total fuel N conversion to NO. This is substantially less than the 77% of fuel N converted under the same conditions of unstaged combustion of FMC char and is within the 33-50% conversion range of the coals. This circumstantially indicates the importance of volatiles in suppressing NO formation in fuel-lean combustion as well as in fuel-rich combustion. Fuel N conversion and staging effectiveness for the IGT char runs are reported in Table 5.2.

TABLE 5.2

FUEL N CONVERSION AND STAGING EFFECTIVENESS

IGT CHAR

SR1 (SR2 = 1.2)	τ_1, sec	Fuel N Conversion	Staging Effectiveness
0.8	0.24	30%	35%
	0.51	20	57
	1.00	14	70
0.4	0.46	19	59
	0.93	13	72

5.3 West Texas Lignite

The baseline profile for the lignite at SR = 0.8 is shown in Figure 5.11. Compared to the char profiles which are complete as a result of delayed ignition, the high volatiles content of the lignite causes earlier ignition which shifts the initial portions of the carbon combustion and NO formation reactions out of range of the sampling probe. As shown in Figure 5.11, combustion is nearly complete at 0.25 seconds. The unburned carbon is zero at all measured points indicating that complete gasification has occurred. This is due to the high water content of this coal which probably initiates the water gas reaction.

NO formation is quite rapid, within the first 0.25 seconds, and the reduction is also quite rapid. The peak NO has occurred again in the presence of oxygen although the true peak value is indeterminate from the data at hand. The NO is reduced to a more-or-less asymptotic level and a slight rise is indicated at long residence times.

At SR = 0.4, Figure 5.12, NO formation is suppressed, again as a result of oxygen depletion. Reduction begins in the presence of oxygen although the peak NO point is outside the range of the sampling probe. NO is reduced at the flue to about 7 ppm which is the lowest found for any coal. The water in the coal might be responsible, since it will form significant H_2 at the temperature of this run (Appendix B). Hydrogen is known to reduce NO under fuel-rich conditions (Myerson, 1975).

Both profiles indicate, circumstantially, that large amounts (compared to the chars) of VN are released early, in the presence of oxygen, and oxidized since the NO levels are much higher and occur much faster.

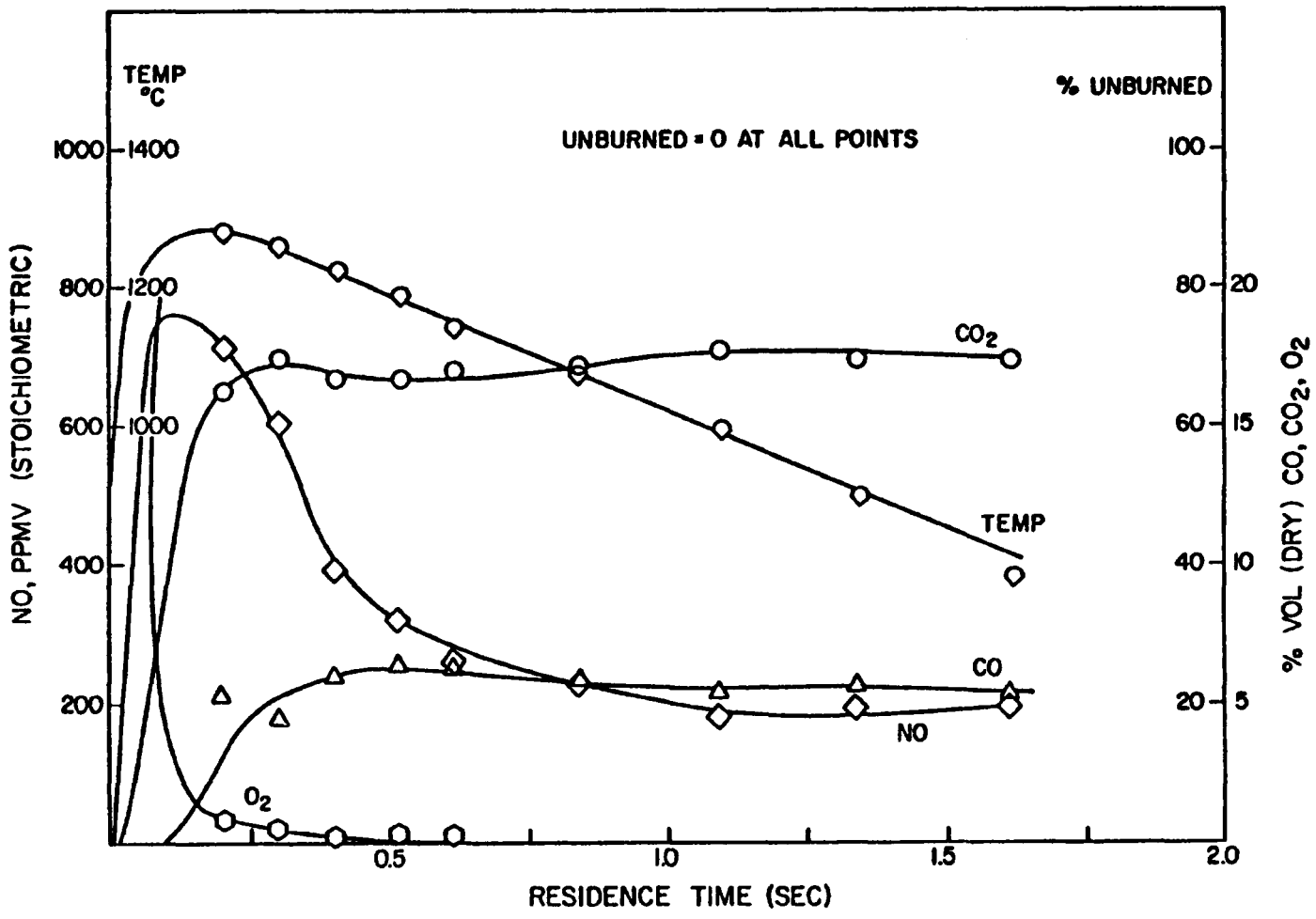

Figure 5.11. Baseline Substoichiometric Composition Profiles
West Texas Lignite, SR = 0.8

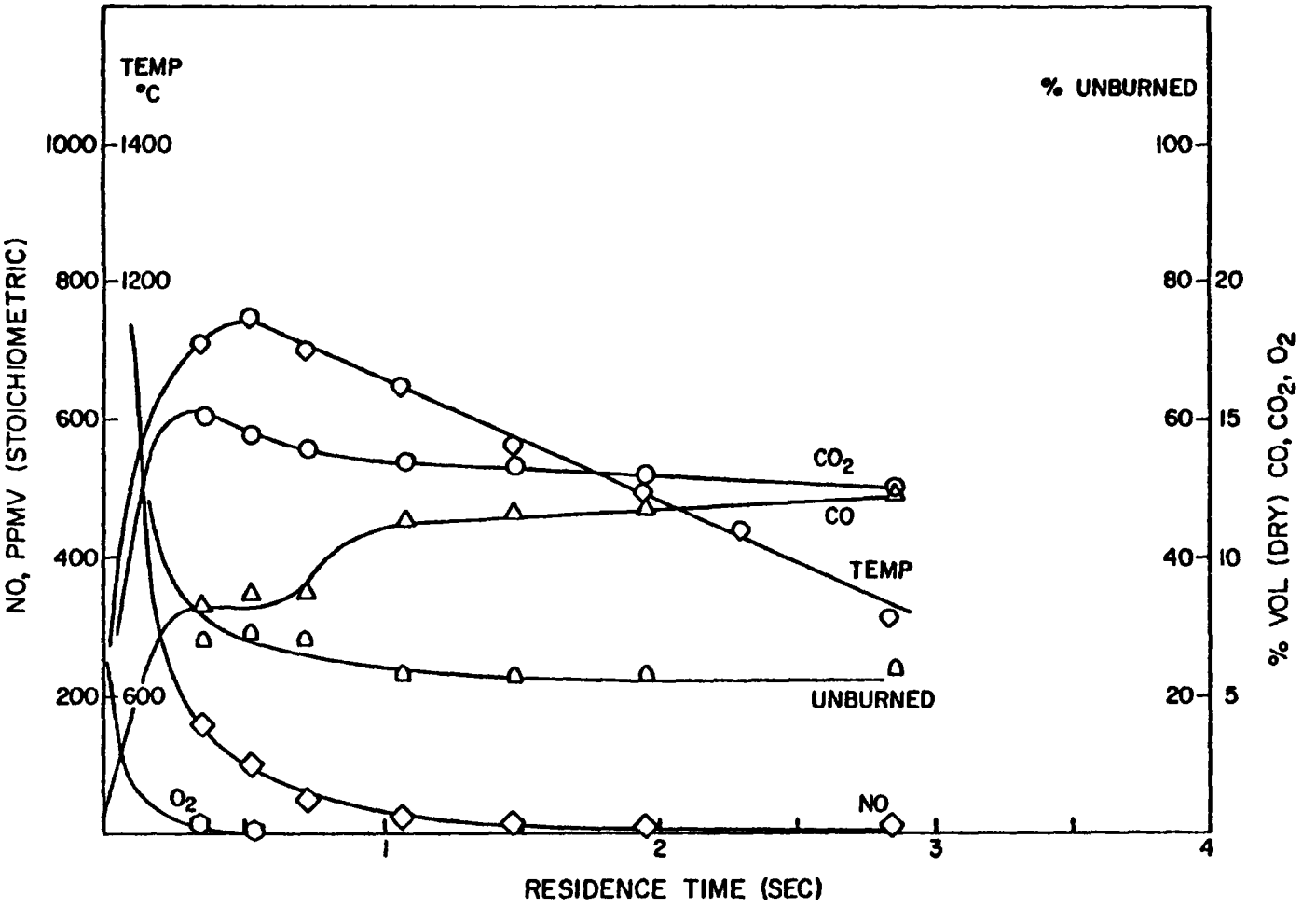

Figure 5.12. Baseline Substoichiometric Composition Profiles West Texas Lignite, SR = 0.4.

The staged combustion runs at SR1 of 0.8 are shown in Figure 5.13. The associated temperature profiles are shown in Figure 5.14. At SR1 = 0.8, Figure 5.13, injection of second stage air near the NO peak, on the declining portion of the baseline curve, gives only a small increase in NO compared to the baseline value at the staging point. At later injection points after substantial first stage NO reduction, the NO is seen to suddenly increase with only a small subsequent change at the flue. More volatile nitrogen is present at longer residence times than at shorter times as indicated by the step increase. Some of the baseline NO reduction is at the expense of an increase in the VN pool which is subsequently oxidized in the second stage giving the sudden rise in NO at the staging point. As the baseline NO decline rate decreases at SR1 = 0.8, the VN pool remains relatively constant as shown by the identical 140 ppm net increases in second stage NO at long residence times.

First stage residence time is extremely important insofar as baseline NO is reduced with time. It becomes less important at longer residence times where the second stage NO is controlled by a constant baseline NO and constant (or nearly constant) VN pool which can be oxidized once sufficient oxygen is present.

The staged lignite runs at SR1 = 0.4 (Figure 5.5) further supports the importance of volatile nitrogen. In this case, the VN pool appears to have been predominantly passed through the first stage rather than having been formed from the destruction of first stage NO as at SR1 = 0.8. With very fuel-rich conditions, much of the volatile material, including nitrogenous species, are evolved after most of the oxygen has been depleted. This material is passed through to the second stage where it can be oxidized to NO.

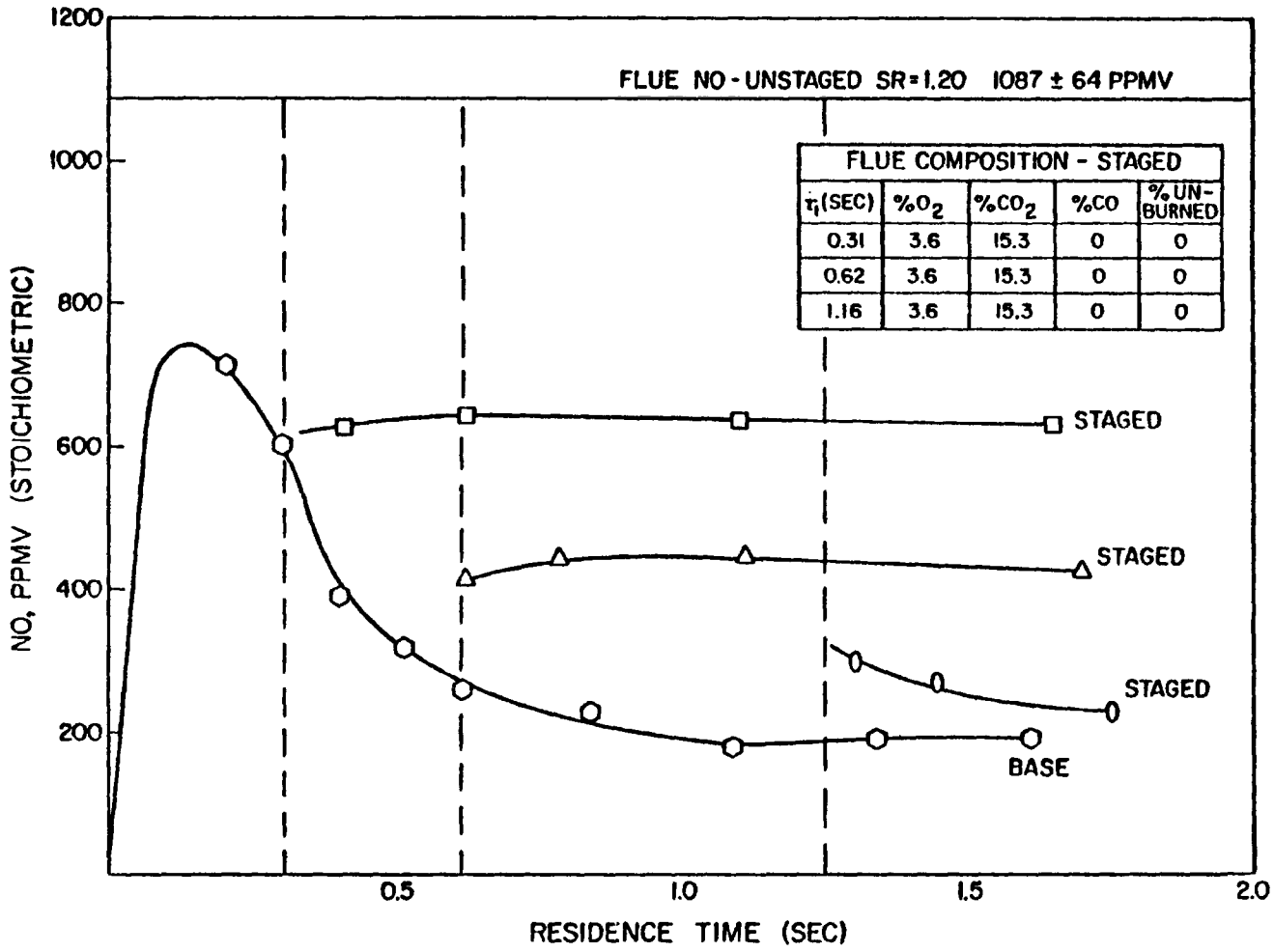

Figure 5.13. Staged Combustion Compositions
West Texas Lignite; SR1 = 0.8, SR2 = 1.2.

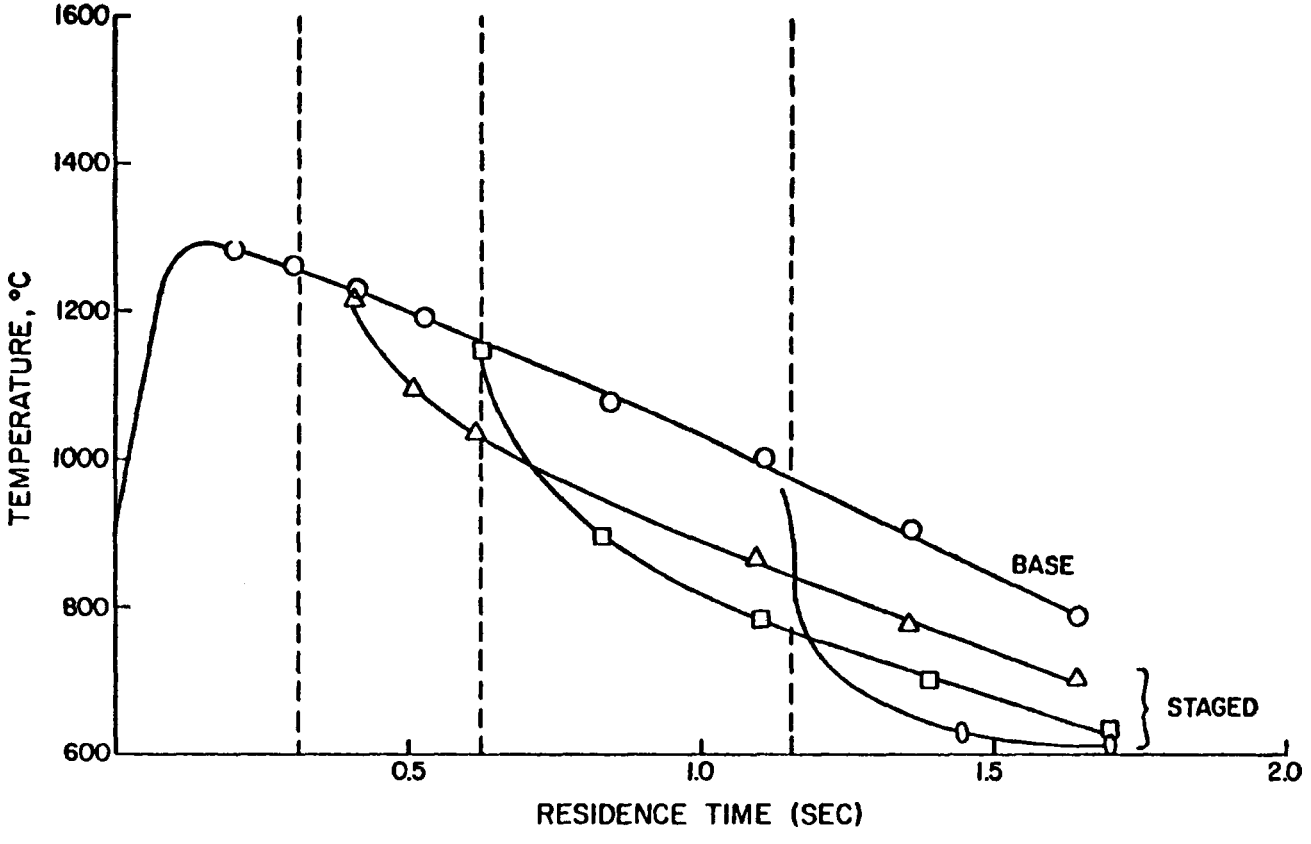

Figure 5.14. Baseline and Staged Temperature Profiles
West Texas Lignite; Base SR = 0.8, Staged SR1 = 0.8, SR2 = 1.2.

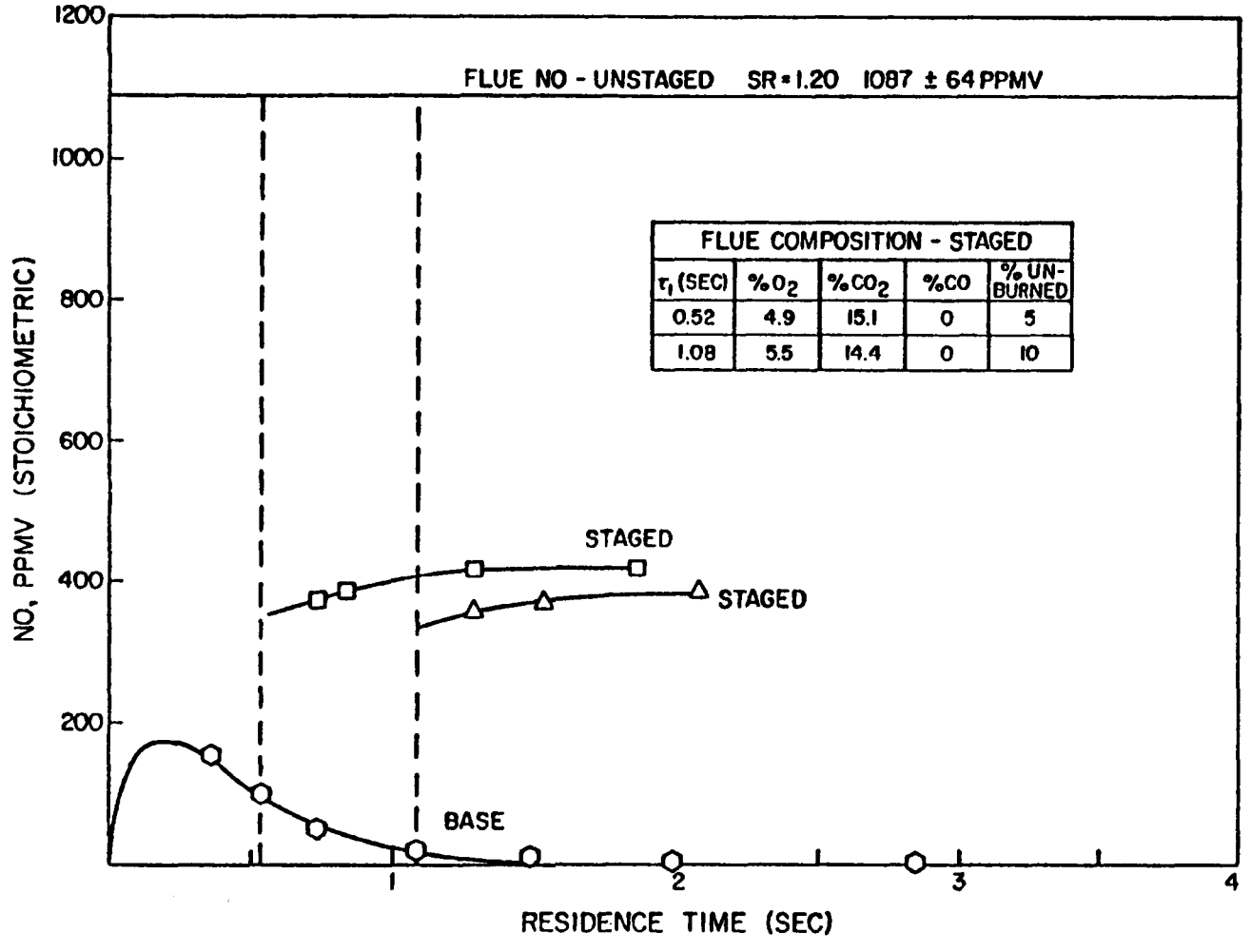

Figure 5.15. Staged Combustion Compositions
West Texas Lignite; SR1 = 0.4, SR2 = 1.2.

The lignite VN pool at SR1 = 0.4 is relatively constant with time. The decrease of 80 ppm of baseline NO between staging points is reflected by a 40 ppm decrease in second stage flue NO. Most of the second stage flue NO is passed through VN plus some contribution from NO reduction to VN. Residen-e time is ineffective as a control parameter at this first stage stoichiometry. The 40 ppm emissions improvement at SR1 = 0.4 is negligible compared to SR1 = 0.8 at 0.6 seconds of first stage residence time owing to the presence of unconverted VN at the very fuel-rich conditions.

The temperature profiles for the staged lignite runs at SR1 = 0.4 are shown in Figure 5.16.

In the case of the chars, second stage NO is controlled by the baseline NO and unconverted char nitrogen at all stoichiometrics since little VN is available in the second stage. The lignite forms some VN at SR1 = 0.8 from NO reduction in the first stage. At SR1 = 0.4, much VN is passed through the first stage. Both processes give additional secondstage NO compared to the baseline value at the staging point. Further, it appears that at a first approximation the rate of reduction of the VN pool to N_2 is much slower in the first stage than is the rate of NO reduction.

Unstaged fuel-lean combustion of the lignite gives 1087 ppm NO emissions at SR = 1.2. This represents 33% conversion of fuel nitrogen which is the lowest of all the coals and chars tested. Fuel nitrogen conversion and staging effectiveness for the lignite are reported in Table 5.3.

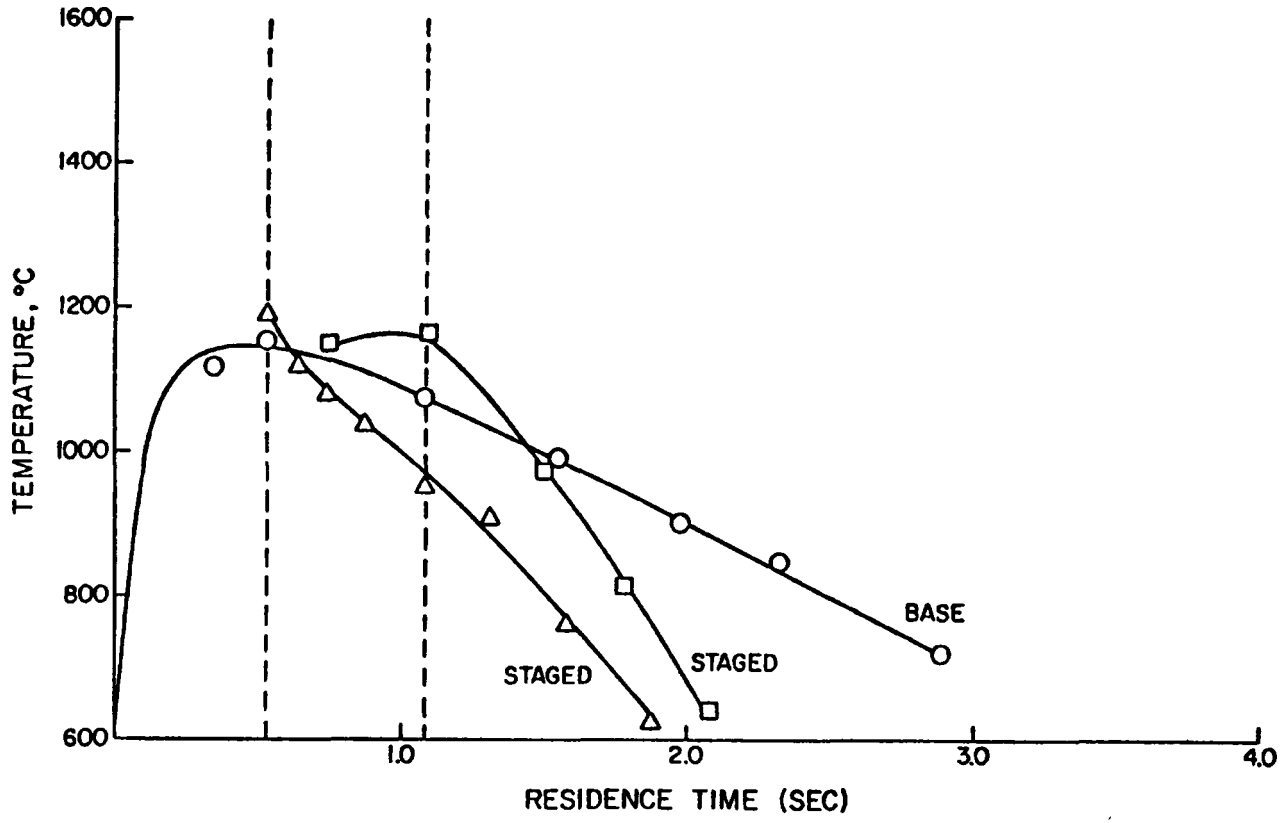

Figure 5.16. Baseline and Staged Temperature Profiles
West Texas Lignite; Base, SR = 0.4, Staged SR1 = 0.4, SR2 = 1.2.

TABLE 5.3

FUEL N CONVERSION AND STAGING EFFECTIVENESS

WEST TEXAS LIGNITE

SR1 (SR2 = 1.2)	τ_1, sec	Fuel N Conversion	Staging Effectiveness
0.8	0.30	19%	43%
	0.61	13	60
	1.24	7	79
0.4	0.54	13	62
	1.09	12	65

5.4 Montana-Powder River Coal

The Montana coal bears closer chemical similarity to the lignite than to the more volatile Pittsburgh #8 (Table 3.1). Compared to the lignite, it has somewhat more ASTM volatile matter, less water as moisture but substantially more fixed carbon. It should as a result, burn under fuel-rich and staged conditions similarly to the lignite.

Reference to the baseline profile at SR = 0.8, Figure 5.17, demonstrates the similarity to the lignite. Ignition is fast, occurring outside the range of the sampling probe. Complete gasification is indicated by the absence of unburned carbon.

NO formation is quite fast and the peak NO, although not measured directly, is in the presence of oxygen. An increase in NO near the flue was found, but at a farther axial distance in the furnace than in the case of the chars.

At SR = 0.4, Figure 5.18, the Montana coal behaves similarly to the lignite. It is not conclusive that the peak NO occurs in the presence of oxygen although it is suspected. The NO peak is much suppressed in this case and, as the ligntie, is reduced to a negligible level at the flue.

The NO formation in the staged combustion runs with Montana coal is described in Figure 5.19 for SR1 = 0.8. The temperatures for these runs are shown in Figure 5.20. At SR1 = 0.8, introduction of staged air produces second stage flue NO which is very nearly the value of the first stage baseline at the staging point. The 100 ppm - 75 ppm dips in NO near the staging points is presumed to be an artifact of mixing although chemical affects cannot be neglected arbitrarily. If so, at SR = 0.8, the second stage flue NO indicates that very little volatile nitrogen

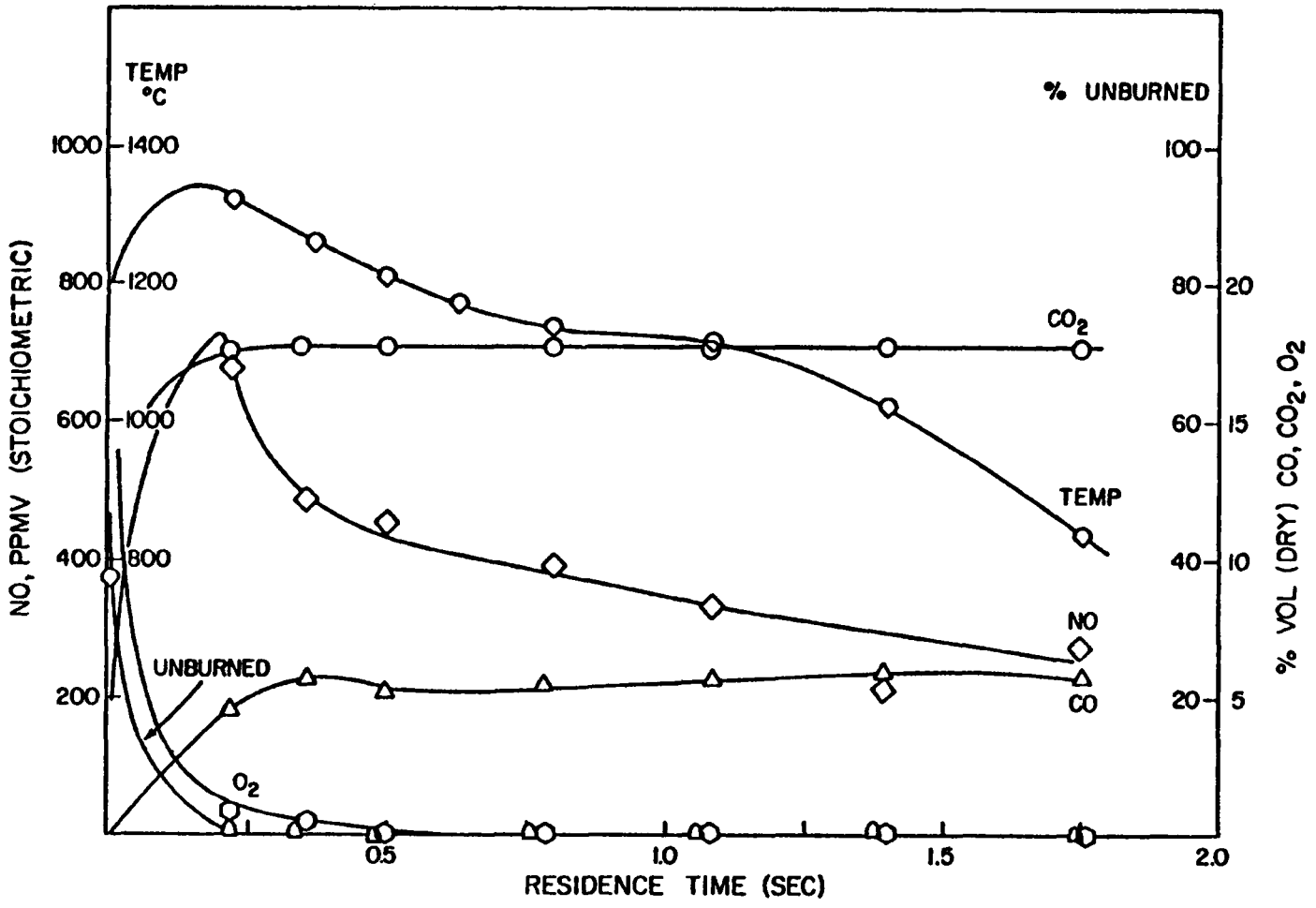

Figure 5.17. Baseline Substoichiometric Composition Profiles Montana-Powder River Coal, SR = 0.8.

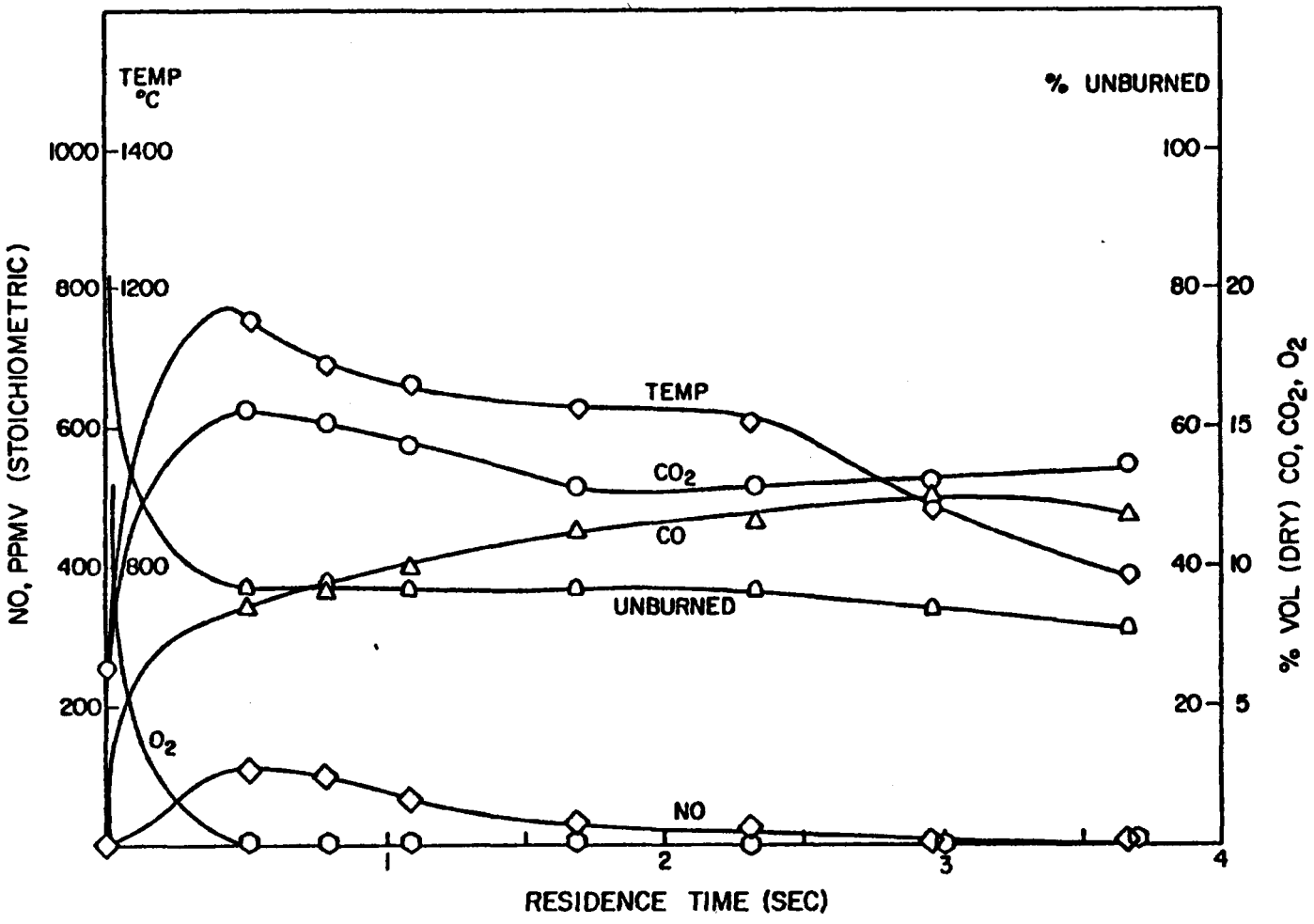

Figure 5.18. Baseline Substoichiometric Composition Profiles Montana-Powder River Coal, SR = 0.4.

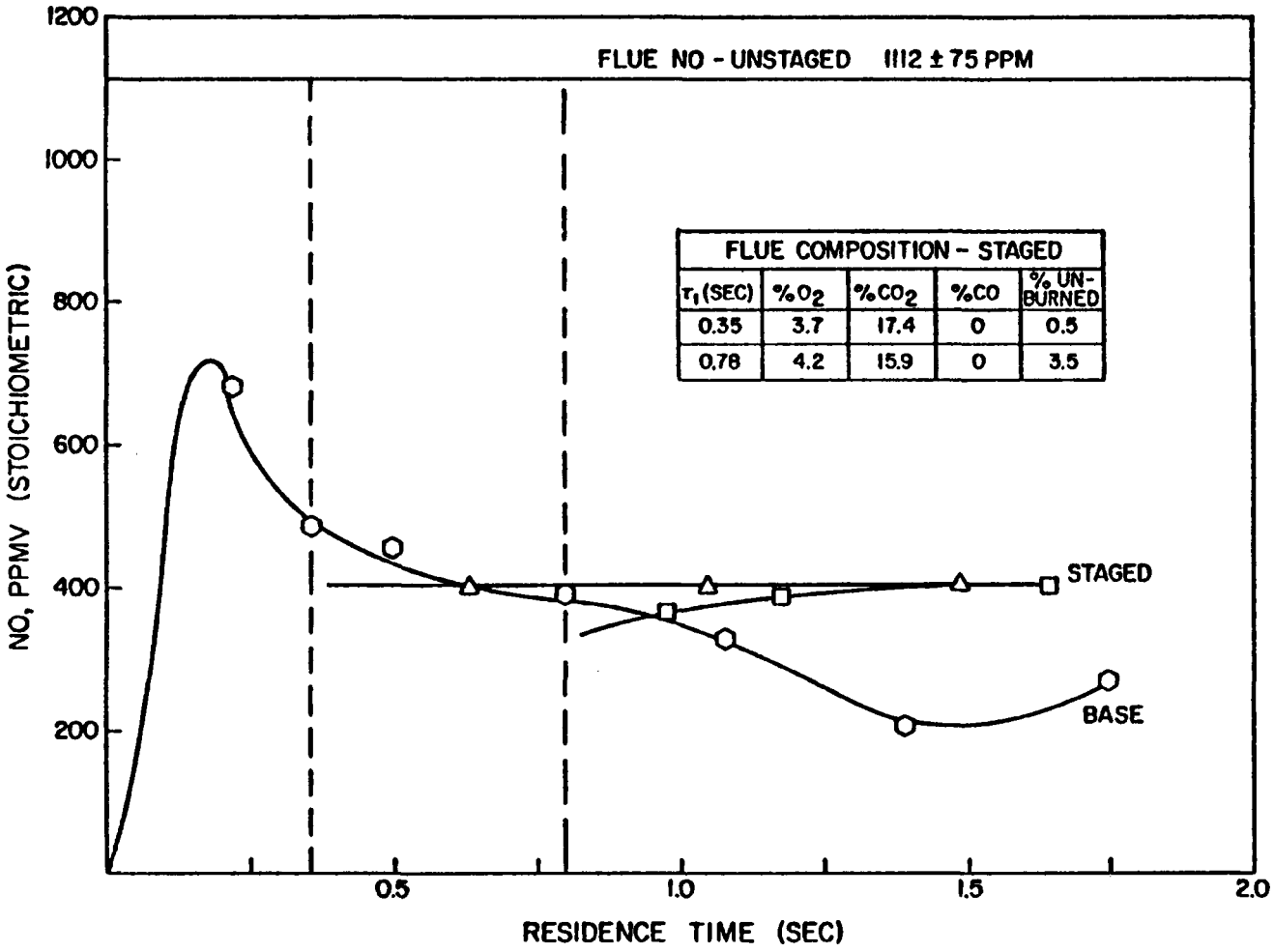

Figure 5.19. Staged Combustion Compositions
Montana-Powder River Coal, SR1 = 0.8, SR2 = 1.2.

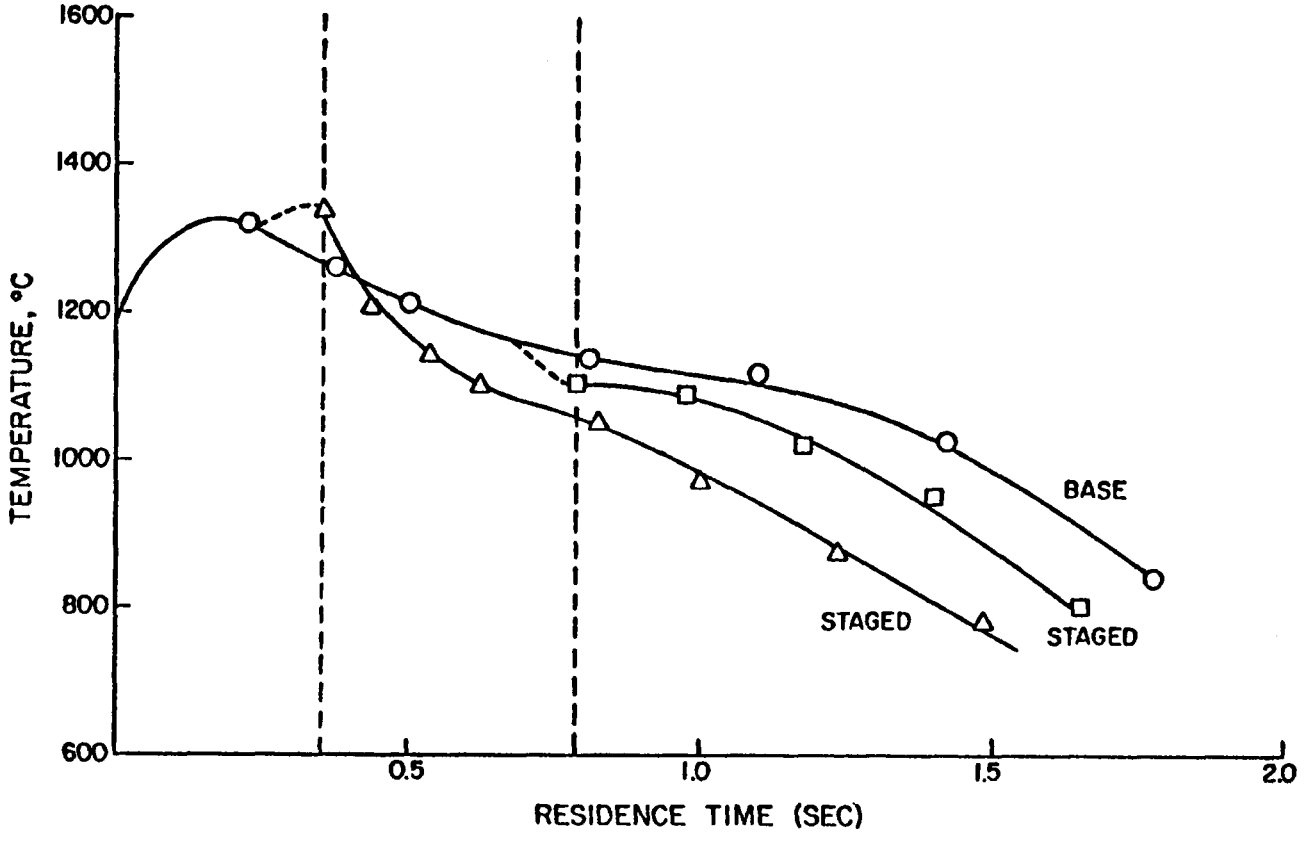

Figure 5.20. Baseline and Staged Temperature Profiles Montana-Powder River Coal, Base SR = 0.8, Staged SR1 = 0.8, SR2 = 1.2.

remains at the staging points and that first stage NO destruction is primarily to nitrogen. The baseline peak NO then reflects complete conversion of fuel nitrogen to nitrogen or to NO. Little, if any, VN remains to be oxidized to NO when second stage air is introduced.

Within the range of first stage residence times studied, residence time has no effect on second stage flue NO at SR1 = 0.8. Presumably, if second stage air were introduced say at 0.25 seconds, the second stage flue NO would be the same as the baseline value of 600 ppm since it is conjectured that no volatile nitrogen remains to form additional NO at this point. The mechanism of baseline NO reduction with this coal is toward VN elimination or directly to N_2, compared to the lignite in which some VN has been formed from NO at long residence times.

The NO formation from staged combustion of the Montana coal is shown in Figure 5.21 and the associated temperature profiles are shown in Figure 5.22.

At SR1 = 0.4, Figure 5.21, significant amounts of volatile nitrogen remain to be oxidized to NO in the second stage. Since the system is globally fuel rich, the non-nitrogenous volatiles evolved early in the pyrolysis of the coal consume much of the oxygen before significant amounts of volatile nitrogen are evolved. The baseline NO profile is then suppressed. The remaining volatile nitrogen is evolved in an oxygen deficient environment and is subsequently oxidized to NO in the second stage. The plot at SR1 = 0.4 shows that the reduction of volatile nitrogen is more rapid than the reduction in the first stage baseline NO (170 ppm vs 70 ppm). Additional residence time at this very fuel-rich condition serves to enhance the depletion of the volatile nitrogen pool rather the first stage baseline NO to increase staging effectiveness.

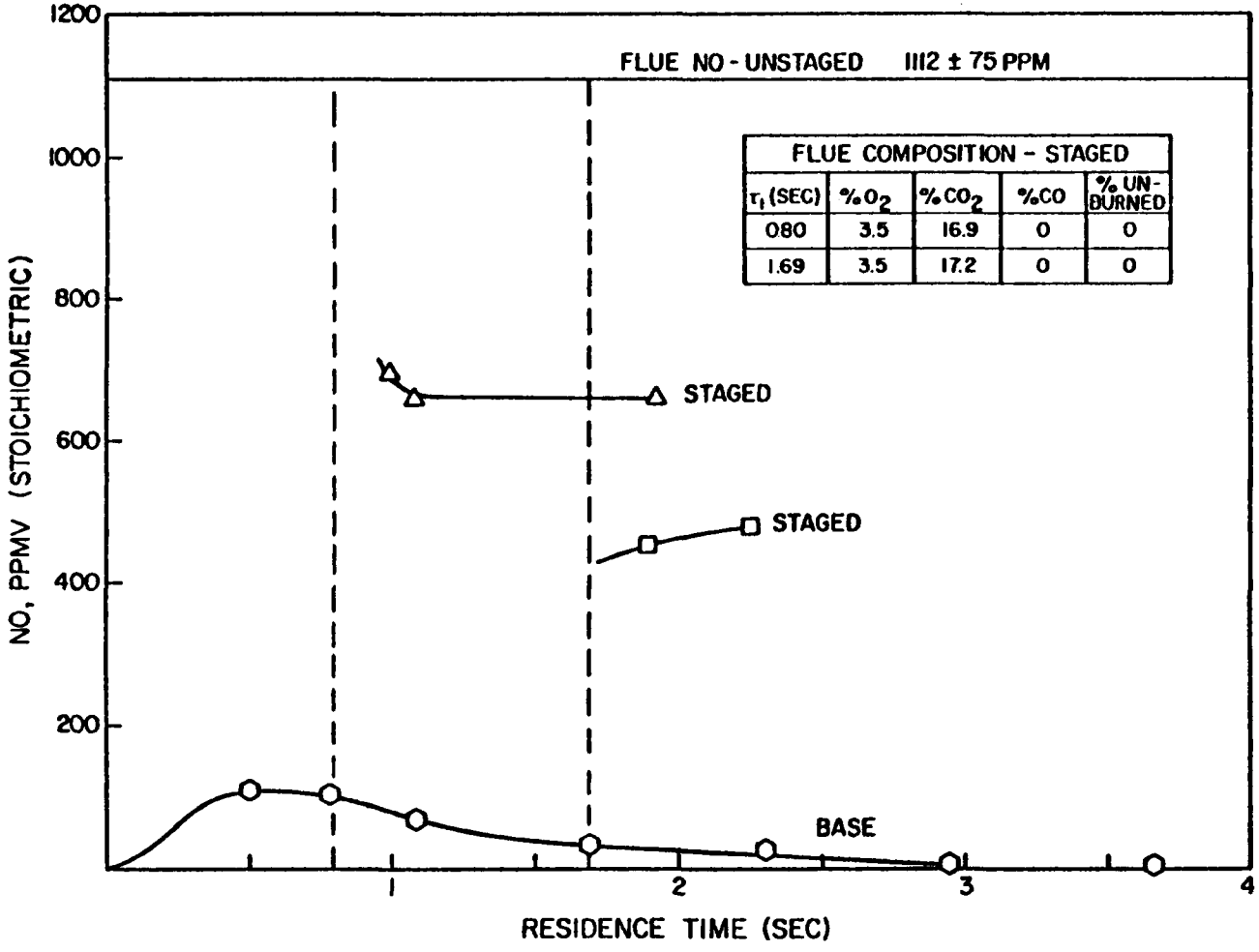

Figure 5.21. Staged Combustion Compositions
Montana-Powder River Coal, SR1 = 0.4, SR2 = 1.2.

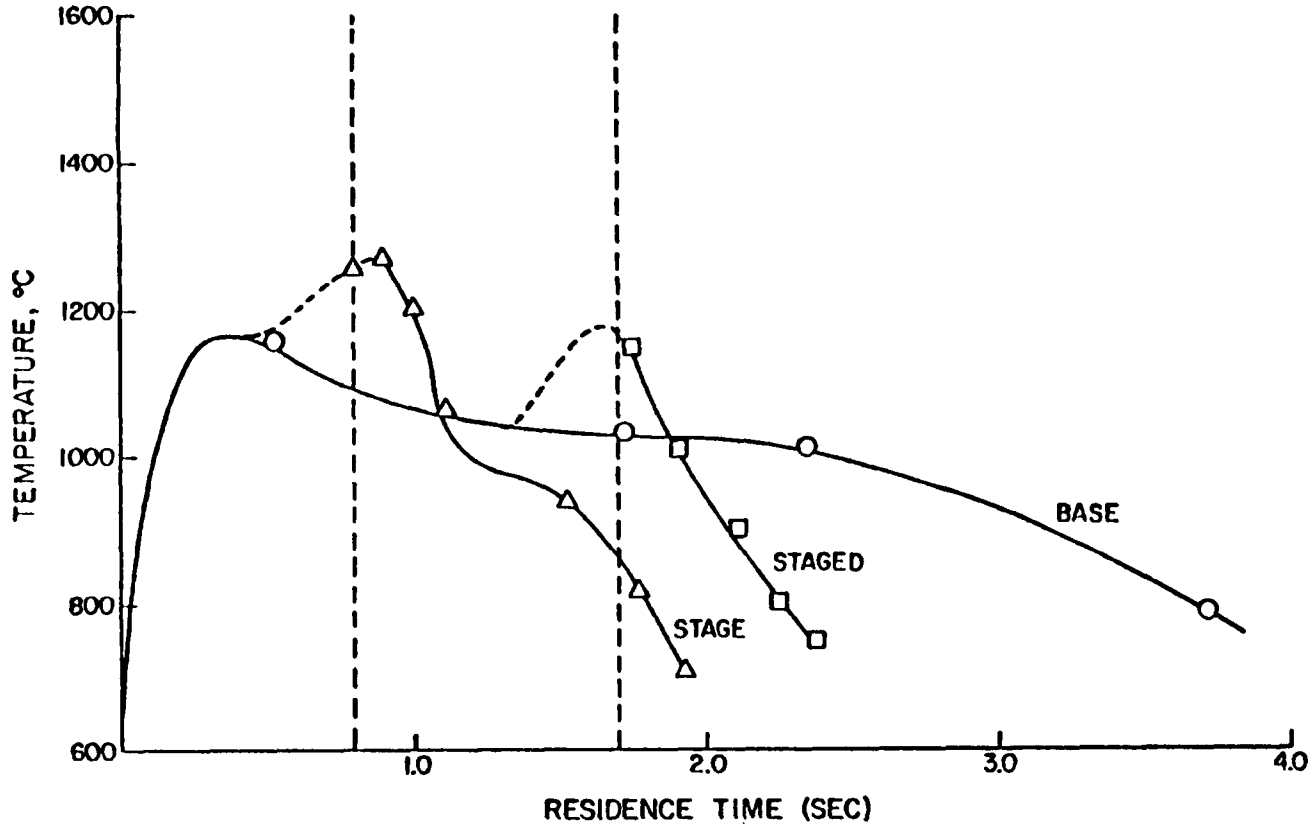

Figure 5.22. Baseline and Staged Temperature Profiles
Montana-Powder River Coal, Base SR = 0.4, Staged SR1 = 0.4, SR2 = 1.2.

In addition, the Montana coal is more effectively staged at SR1 = 0.8 than at SR1 = 0.4 at the residence times studied. This leads to the conclusion that at SR1 = 0.8, the volatile nitrogen has been evolved under thermal or stoichiometric conditions which have destroyed the volatile nitrogen before staging. At SR1 = 0.8, the volatile nitrogen has presumably formed N_2 plus substantial NO which can be effectively destroyed in the first stage, whereas at SR1 = 0.4, little NO has been formed. The volatile nitrogen pool is not as effectively reduced in the first stage at very fuel-rich conditions as is the NO under less fuel-rich conditions.

Fuel-lean conventional combustion of the Montana coal produces 1100 ppm NO at SR = 1.2, representing 27% of fuel nitrogen conversion. Staged combustion gives second stage fuel nitrogen conversion and staging effectiveness reported in Table 5.4.

5.5 Pittsburgh Number 8 Coal

The Pittsburgh #8 coal is the next most volatile (by proximate analysis) coal burned in this experiment. It is substantially more volatile than the Montana and contains significantly more sulfur (Table 3.1). One would expect the trend established for staging with the four previous coals to continue: that increasing volatility leads to increased volatile nitrogen carryover from the first to the second stage, especially under very fuel-rich conditions.

The baseline profile for the Pittsburgh coal at SR = 0.8, Figure 5.23, shows the effects of the high volatiles content on NO formation. The oxygen is apparently depleted well in advance of the appearance of the NO peak, as as consequence of the early evolution of large amounts of nitrogen-free volatiles. The volatiles content presumably suppresses NO formation by both scavenging oxygen and accelerating NO reduction.

TABLE 5.4

FUEL NITROGEN CONVERSION AND STAGING EFFECTIVENESS

MONTANA - POWDER RIVER COAL

SR1 (SR2 = 1.2)	τ_1, sec	Fuel N Conversion	Staging Effectiveness
0.8	0.36	13%	65%
	0.79	13	65
0.4	0.80	22	41
	1.71	16	57

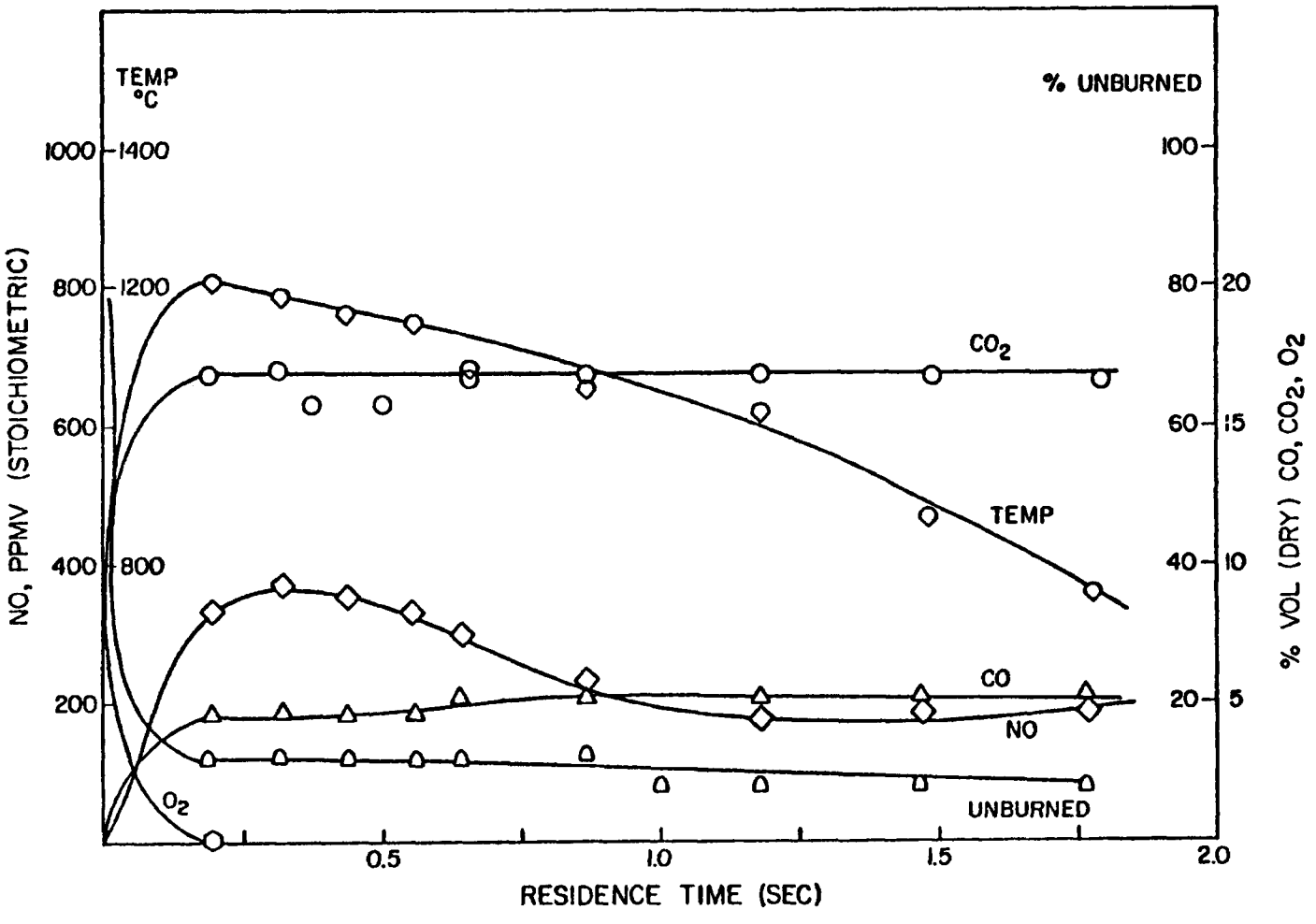

Figure 5.23. Baseline Substoichiometric Composition Profiles Pittsburgh No. 8 Coal, SR = 0.8.

The baseline profile at SR = 0.4, Figure 5.24 further reflects the effect of early volatiles in that the peak NO is vastly reduced to a level that is reminiscent of flue NO values for other coals.

The relative low levels of peak NO at both baseline conditions implies that much of the VN is released after significant combustibles have depleted the oxygen. If this were not the case, substantially more NO would be expected at the peak, since VN would have been released with oxygen present. Consequently, more VN carryover to the second stage at both stoichiometries is expected.

The effect of VN carryover is apparent in the staged runs at SR1 = 0.8, Figure 5.25, when the first stage residence time is 0.33 sec. but at longer first stage residence times very little volatile nitrogen is passed through. The injection of second stage air near the baseline peak shows that a great deal of volatile nitrogen remains in the first stage but is subsequently destroyed as first stage residence time increases. Virtually none remains at 0.65 seconds since the second stage flue NO approximates the baseline value (300 ppm) at the point of injection Apparently, the mechanism of VN reduction to N_2 is much more efficient than that of NO reduction in the fuel-rich first stage at this stoichiometry. The temperature profiles for these runs are shown in Figure 5.26.

The large amount of VN which exists near the baseline peak is a result of the large amount of non-nitrogenous volatiles evolved which consumes the available oxygen prior to nitrogenous volatiles evolution. VN is evolved later in an oxygen deficient fuel-rich environment so that a reduced amount of NO is formed in the first stage. The VN is eliminated quite rapidly, however, so that as residence time increases, substantial improvement in second stage flue NO emissions is achieved.

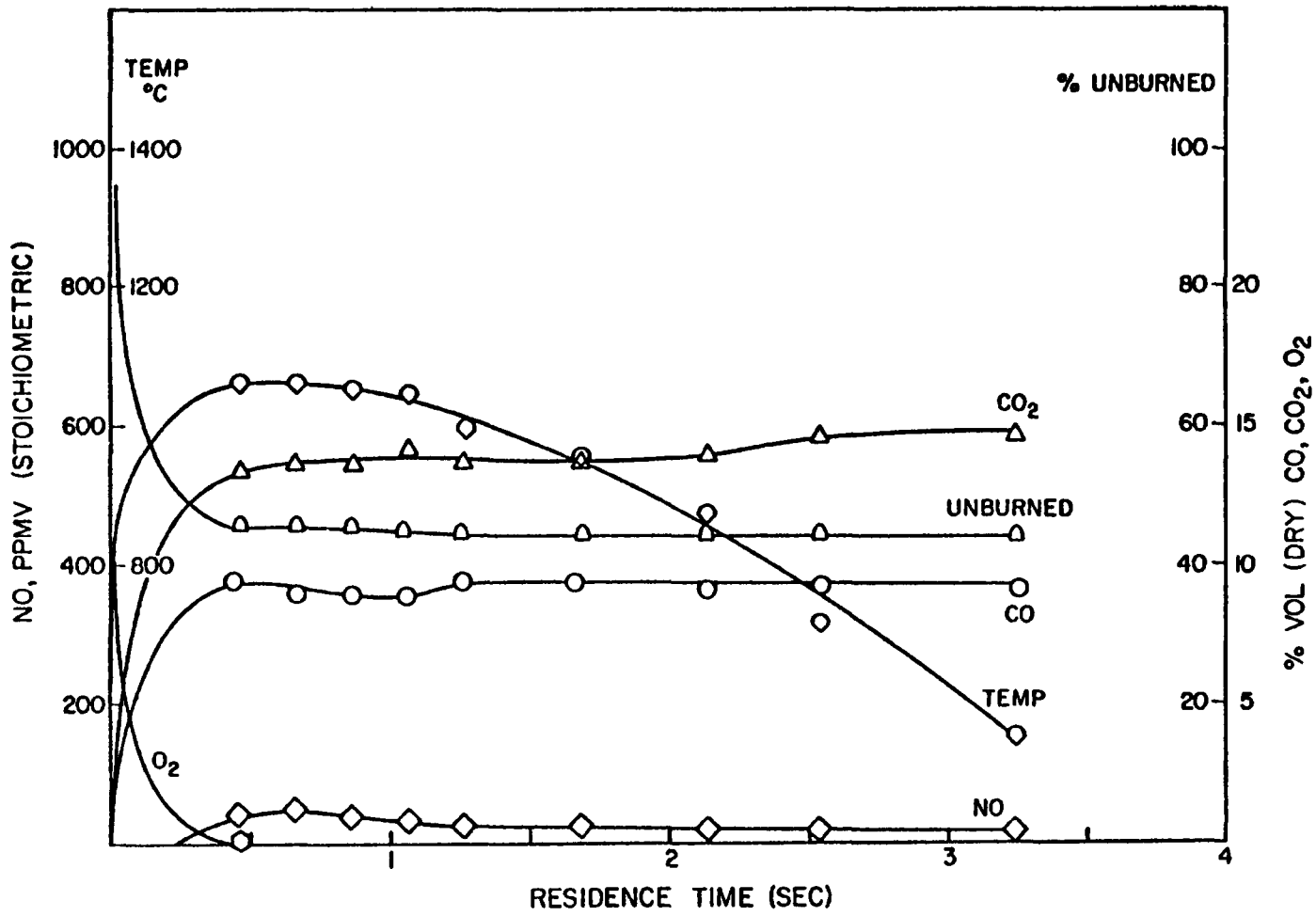

Figure 5.24. Baseline Substoichiometric Composition Profiles Pittsburgh No. 8 Coal, SR = 0.4.

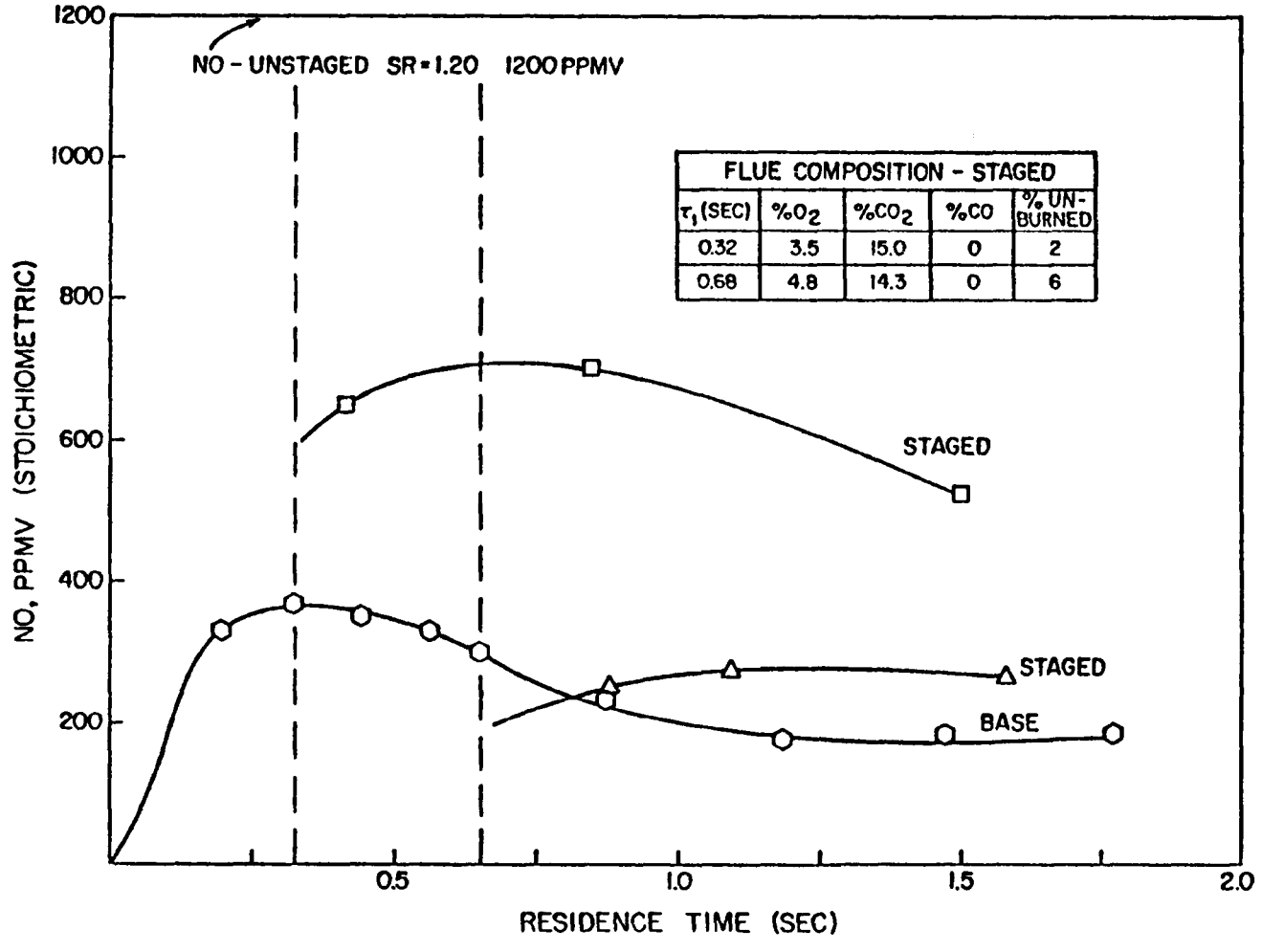

Figure 5.25. Staged Combustion Compositions
Pittsburgh No. 8 Coal, SR1 = 0.8, SR2 = 1.2.

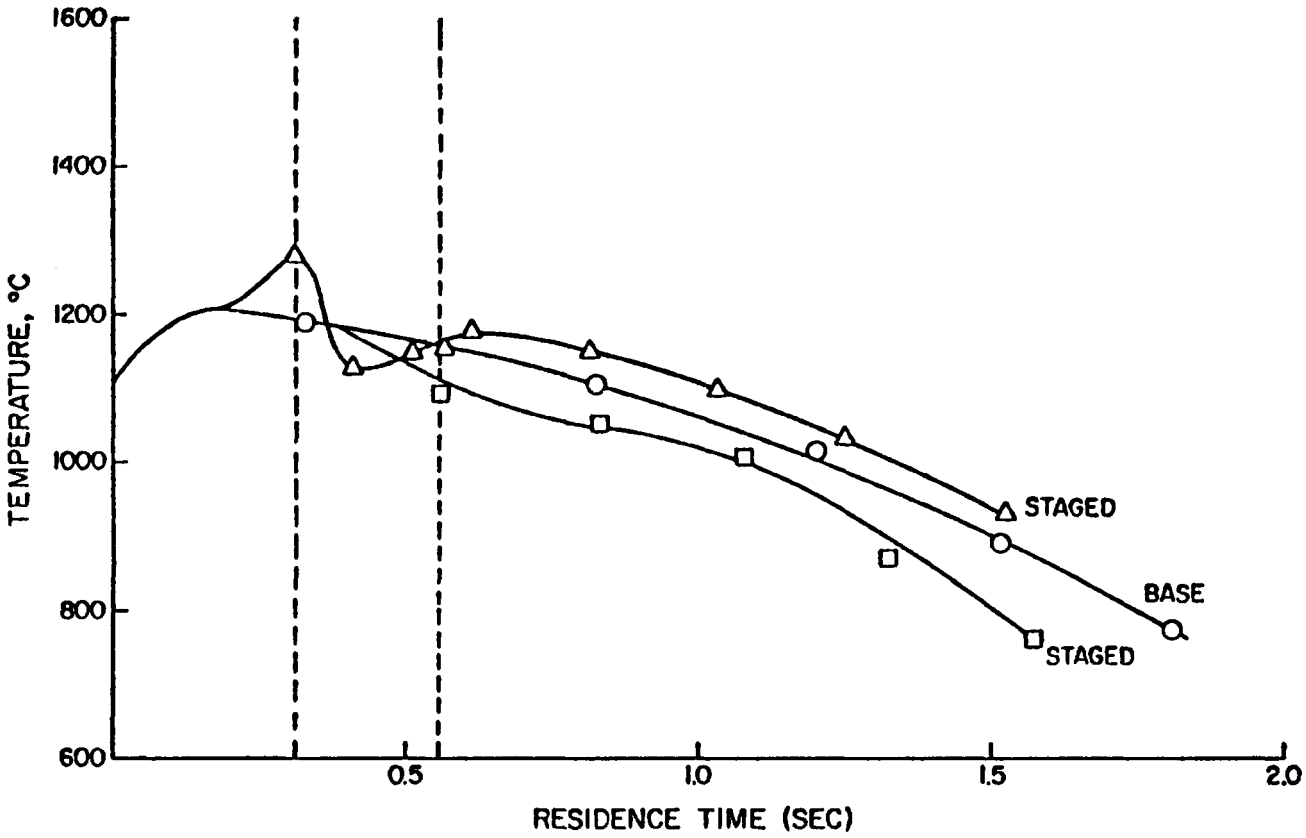

Figure 5.26. Baseline and Staged Temperature Profiles
Pittsburgh No. 8 Coal
Base SR = 0.8, Staged SR1 = 0.8, SR2 = 1.2.

That the mechanisms for NO and VN elimination are quite effective with this coal is indicated in the staged runs at SR1 = 0.4, Figure 5.27. The temperature profiles for these runs are shown in Figure 5.28. The baseline NO profile is suppressed, presumably since the early non-nitrogenous volatiles consume the oxygen before large amounts of VN are evolved. VN destruction in the first stage is also more effective under extreme fuel-rich conditions since the second stage NO is about the same (240 ppm) at SR1 = 0.4 as at SR1 = 0.8 provided enough time is allowed for destruction of the VN pool prior to staging.

The best staging condition for Pittsburgh #8 is SR1 = 0.8 and first stage residence time of the order of 0.65 seconds. This gives enough time for NO and VN reduction in the first stage so that little additional NO is formed in the second. While this could also be achieved at SR1 = 0.4, near-stoichiometric first stage conditions enhance the combustion efficiency via higher first stage temperatures (Figures 5.26 and 5.28).

Unstaged fuel-lean combustion of the Pittsburgh coal gives 1200 ppm of emitted NO amounting to 50% of fuel N conversion. With the exception of the FMC char, this is the highest fuel N conversion encountered with the fuels used and is the highest found for the coals. The staged fuel nitrogen conversion and staging effectiveness for the Pittsburgh coal is given in Table 5.5.

5.6 Colorado Coal

The most volatile coal, based on the proximate analysis (Table 3.1), studied in this experiment is the Colorado although the ASTM Volatile Matter is not substantilly different from that of the Pittsburgh #8 (38.9% vs. 37.0%).

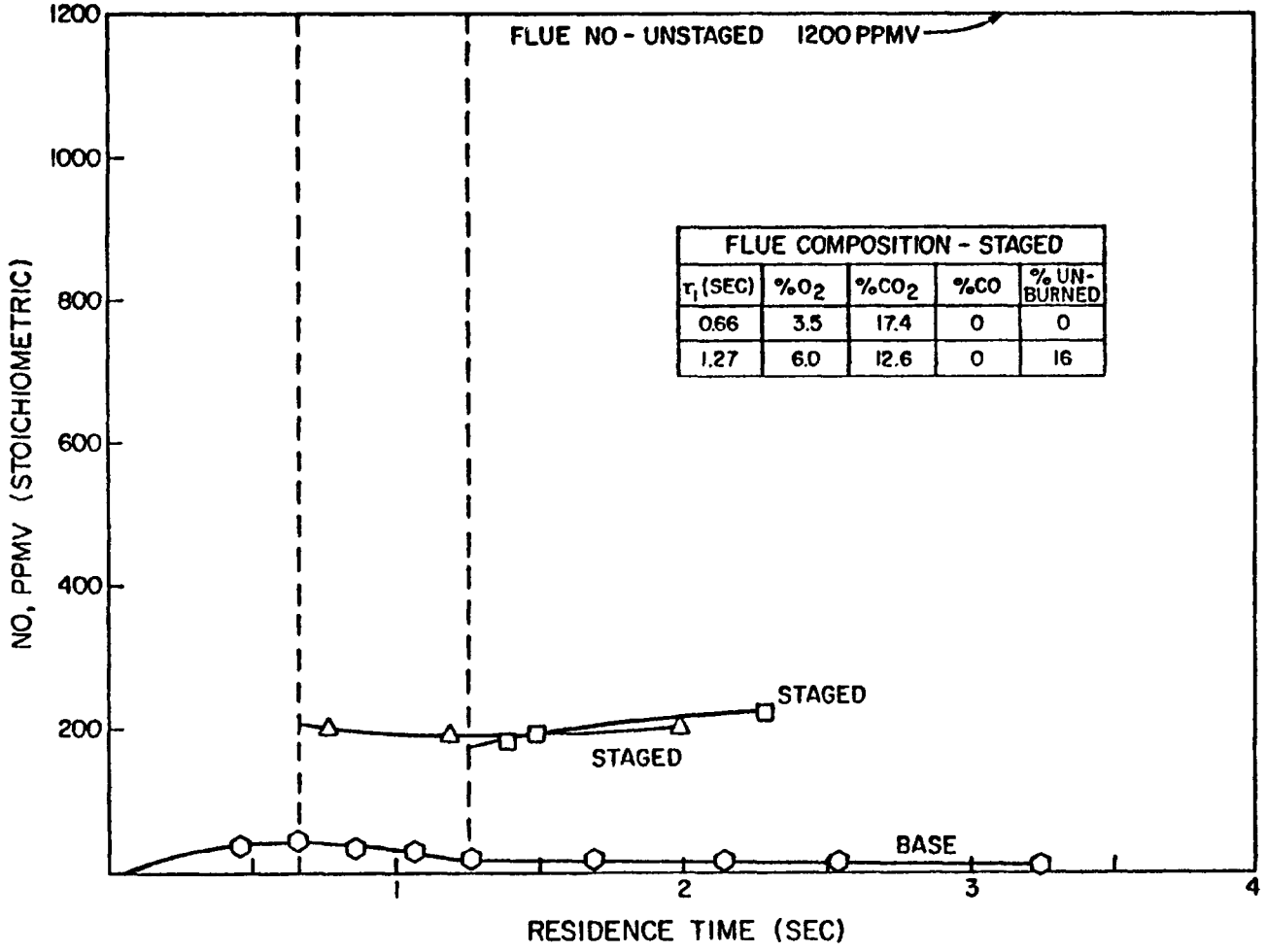

Figure 5.27. Staged Combustion Compositions
Pittsburgh No. 8 Coal
SR1 = 0.4, SR2 = 1.2.

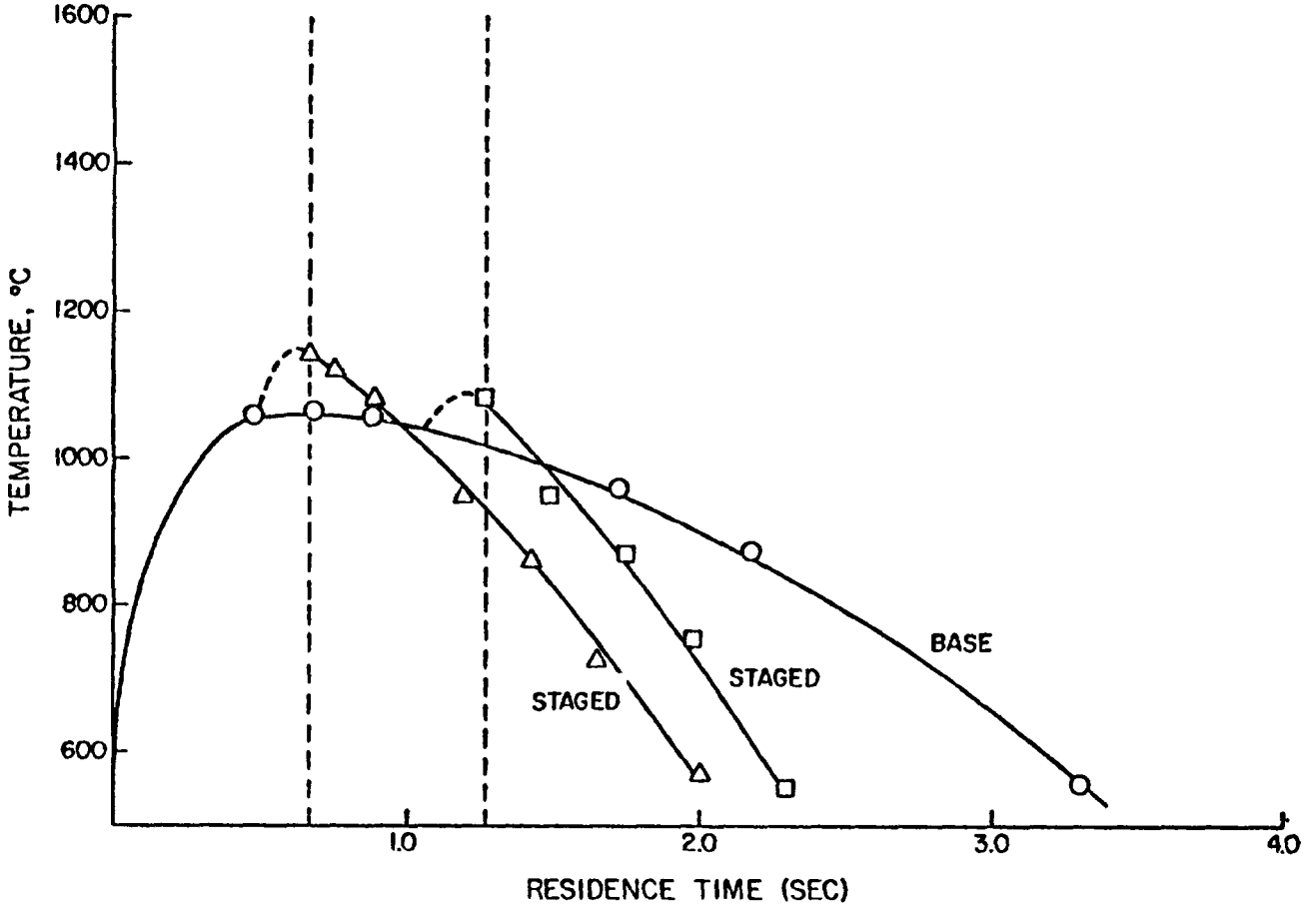

Figure 5.28. Baseline and Staged Combustion Compositions
Pittsburgh No. 8 Coal
Base SR = 0.4, Staged SR1 = 0.4, SR2 = 1.2.

TABLE 5.5

FUEL NITROGEN CONVERSION AND STAGING EFFECTIVENESS

PITTSBURGH #8 COAL

SR1 (SR2 = 1.2)	τ_1, sec	Fuel N Conversion	Staging Effectiveness
0.8	0.33	6	47
	0.65	13	74
0.4	0.65	10	80
	1.26	11	78

The nitrogen volatiles release of the Colorado coal is much different from that from the Pittsburgh coal as can be inferred from the baseline plot, Figure 5.29. At SR1 = 0.8, the baseline NO profile for the Colorado is more than twice as great as the Pittsburgh coal (Figures 5.25 and 5.27) at the same residence time and more closely resembles the lignite profile (Figures 5.9 and 5.12) under the same conditions. Evidently, the VN is evolved from the Colorado coal somewhat earlier, in the presence of more oxygen than is the case with the physically similar Pittsburgh #8.

At SR = 0.4, Figure 5.30, however, the Colorado begins to behave similarly to the less volatile Pittsburgh although it is evident that VA is evolved earlier here, also, since the peak NO value is higher. The peak NO occurs in the presence of oxygen as indicated, although the data might be interpreted differently by others.

The staged combustion runs are described in Figure 5.31 at SR1 = 0.8. The associated temperature profiles are shown in Figure 5.32. After staging at SR1 = 0.8, Figure 5.31, the Colorado coal behaves differently than the other coals. The second stage NO decreases to less than the baseline values whereas all other second stage NO measurements either increased or remained essentially constant after staging at the same first stage stoichiometry. This behavior was observed by Wendt, Lee and Pershing (1978) for the Western Kentucky coal as well. The least that these results indicate is that the VN pool has been entirely converted to non-oxidizable compounds prior to the first staging position. Alternatively, NO reaction with VN and second stage oxygen might be occurring.

The staged combustion runs for SR1 = 0.4 are shown in Figure 5.33 and the associated temperatures are shown in Figure 5.34. The behavior of the Colorado coal when staged at SR1 = 0.4 is more along the lines

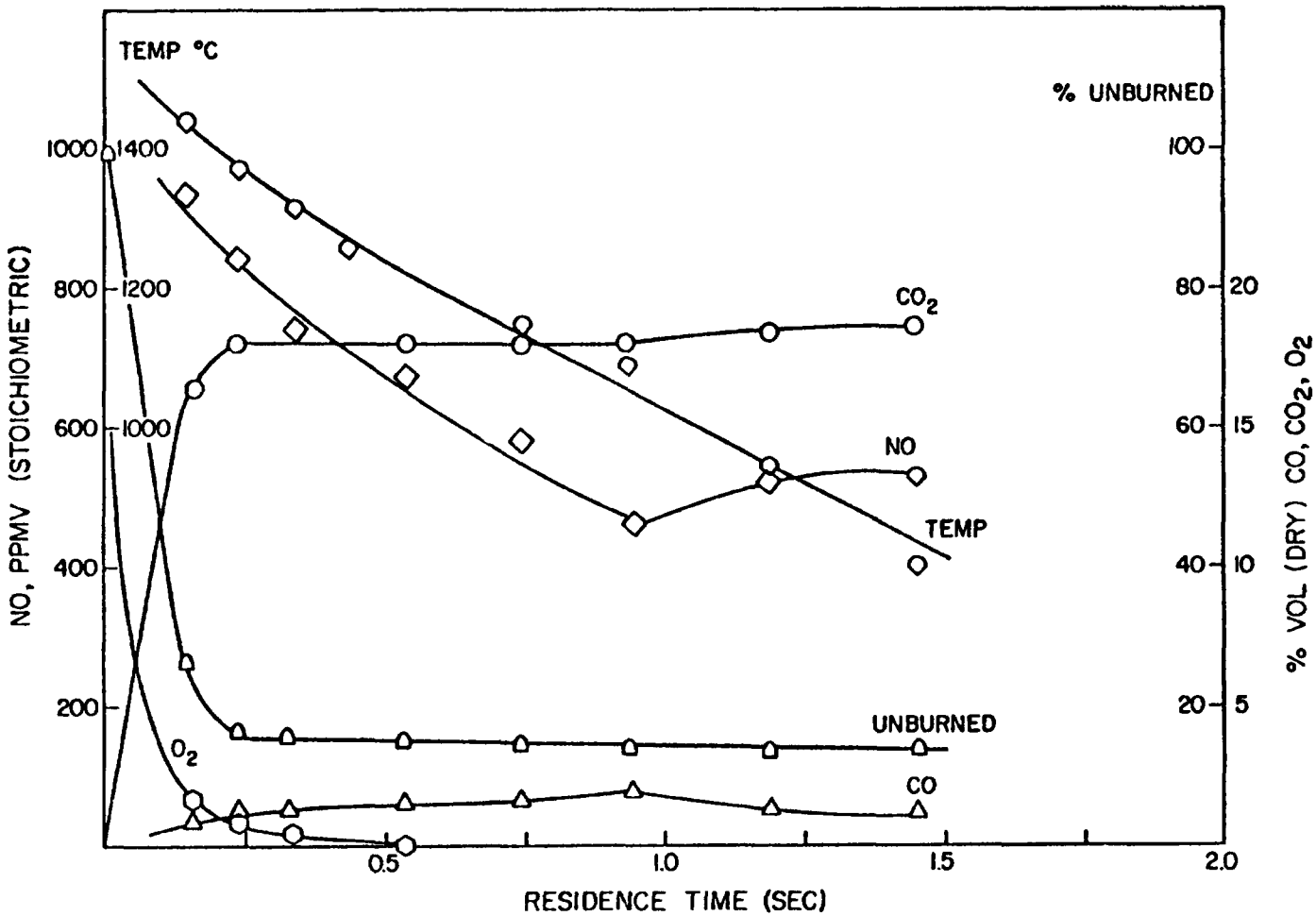

Figure 5.29. Baseline Substoichiometric Composition Profiles Colorado Coal SR = 0.8.

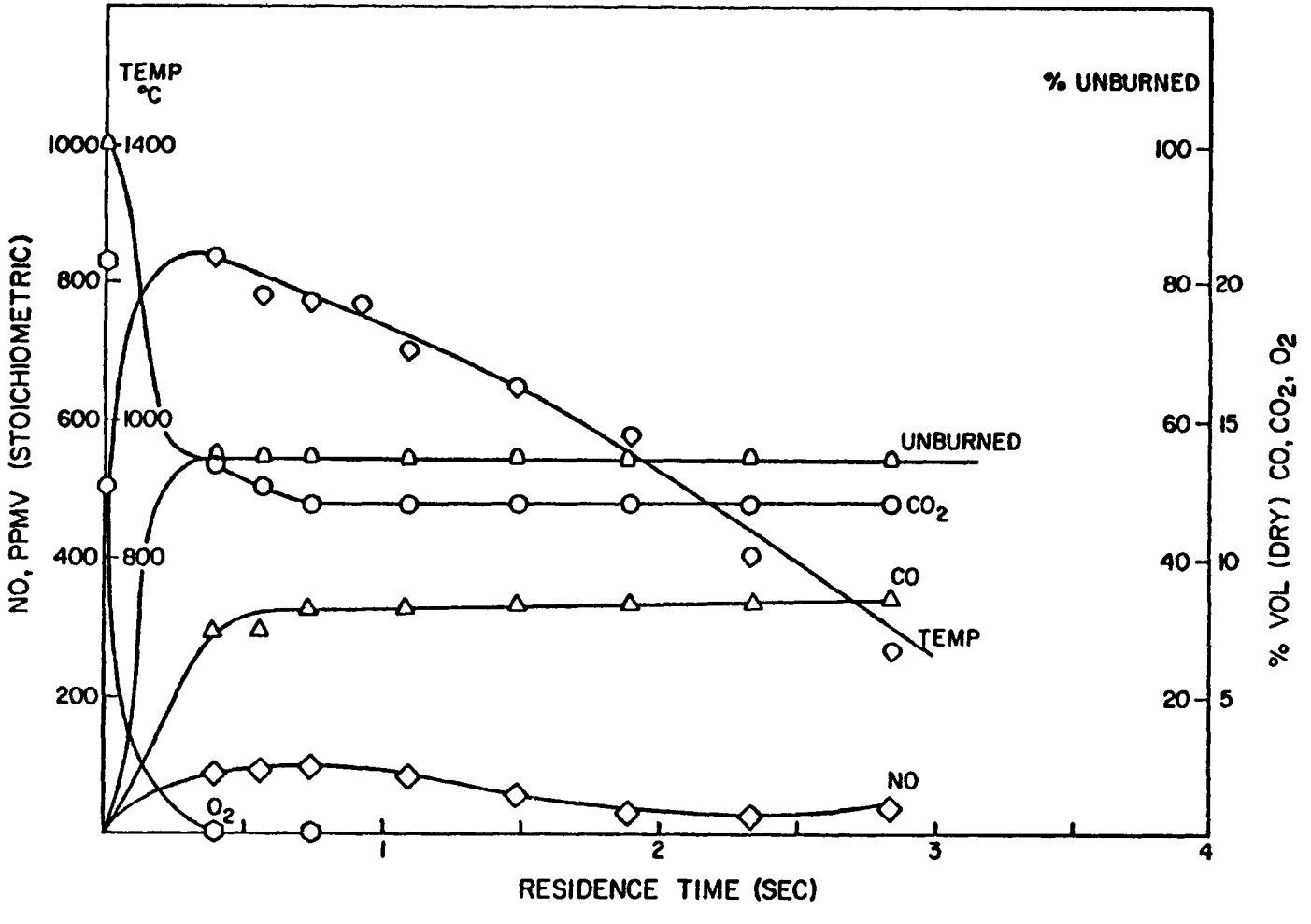

Figure 5.30. Baseline Substoichiometric Composition Profiles Colorado Coal SR = 0.4.

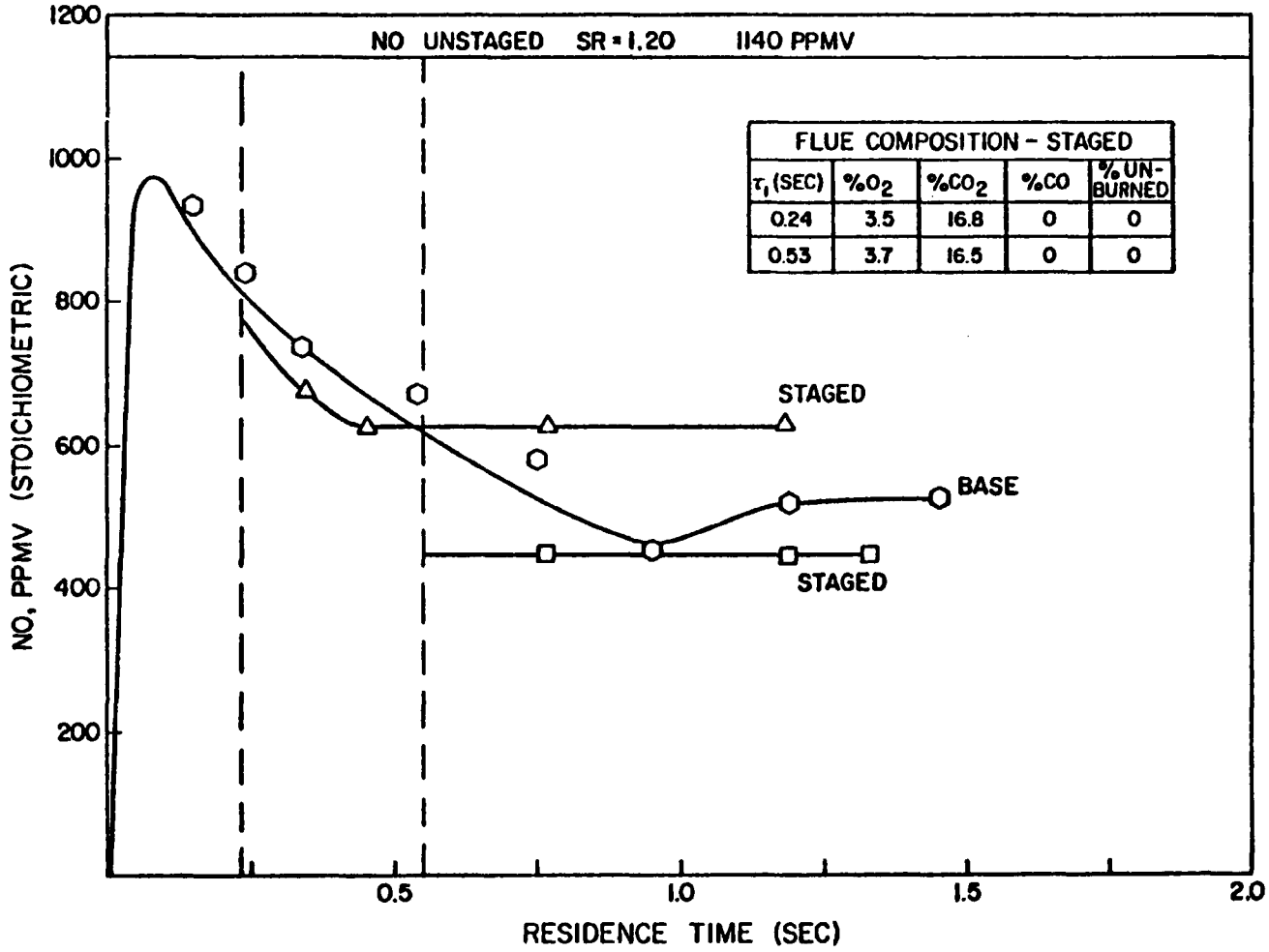

Figure 5.31. Staged Combustion Compositions Colorado Coal, SR1 = 0.8, SR2 = 1.2.

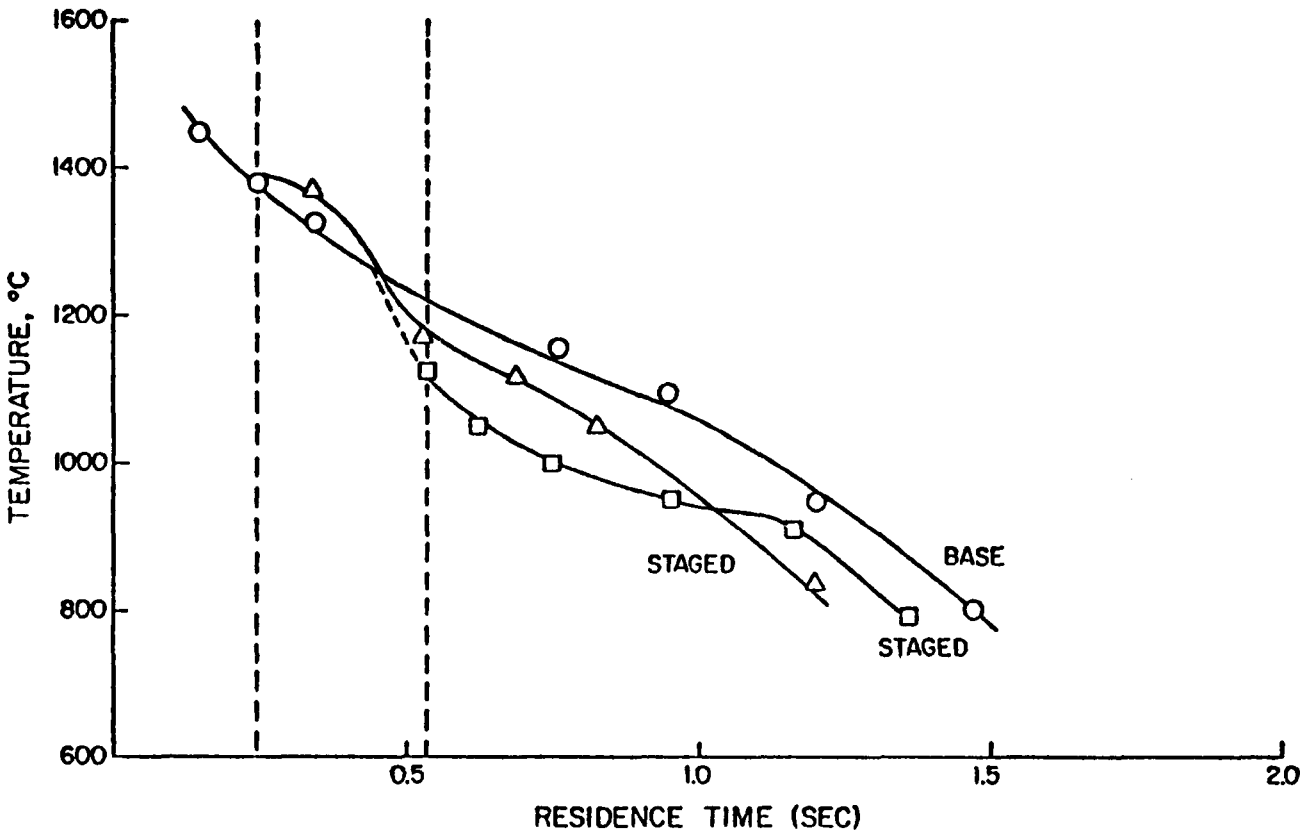

Figure 5.32. Baseline and Staged Temperature Profiles
Colorado Coal
Base SR = 0.8, Staged SR1 = 0.4, SR2 = 1.2.

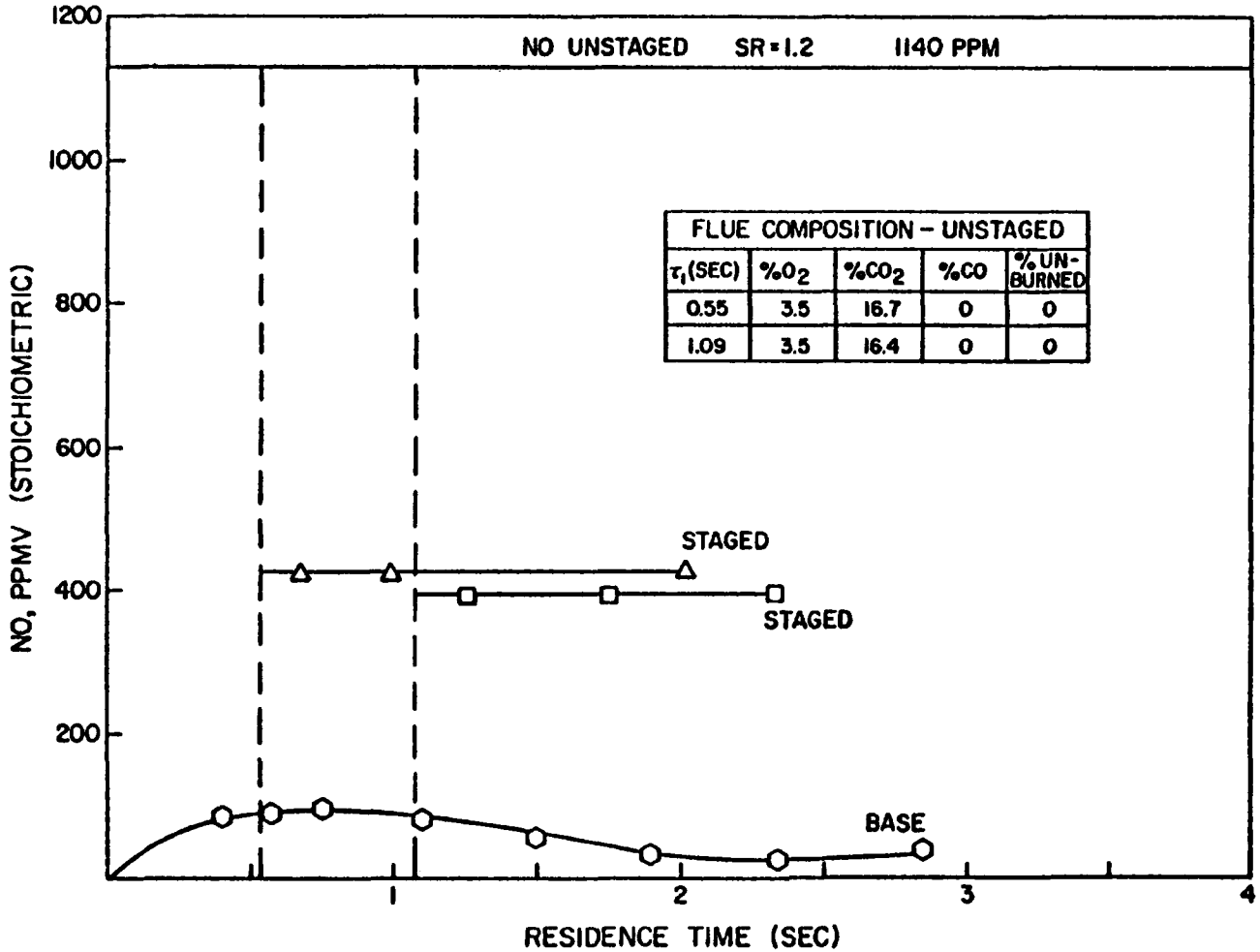

Figure 5.33. Staged Combustion Compositions
Colorado Coal, SR1 = 0.4, SR2 = 1.2.

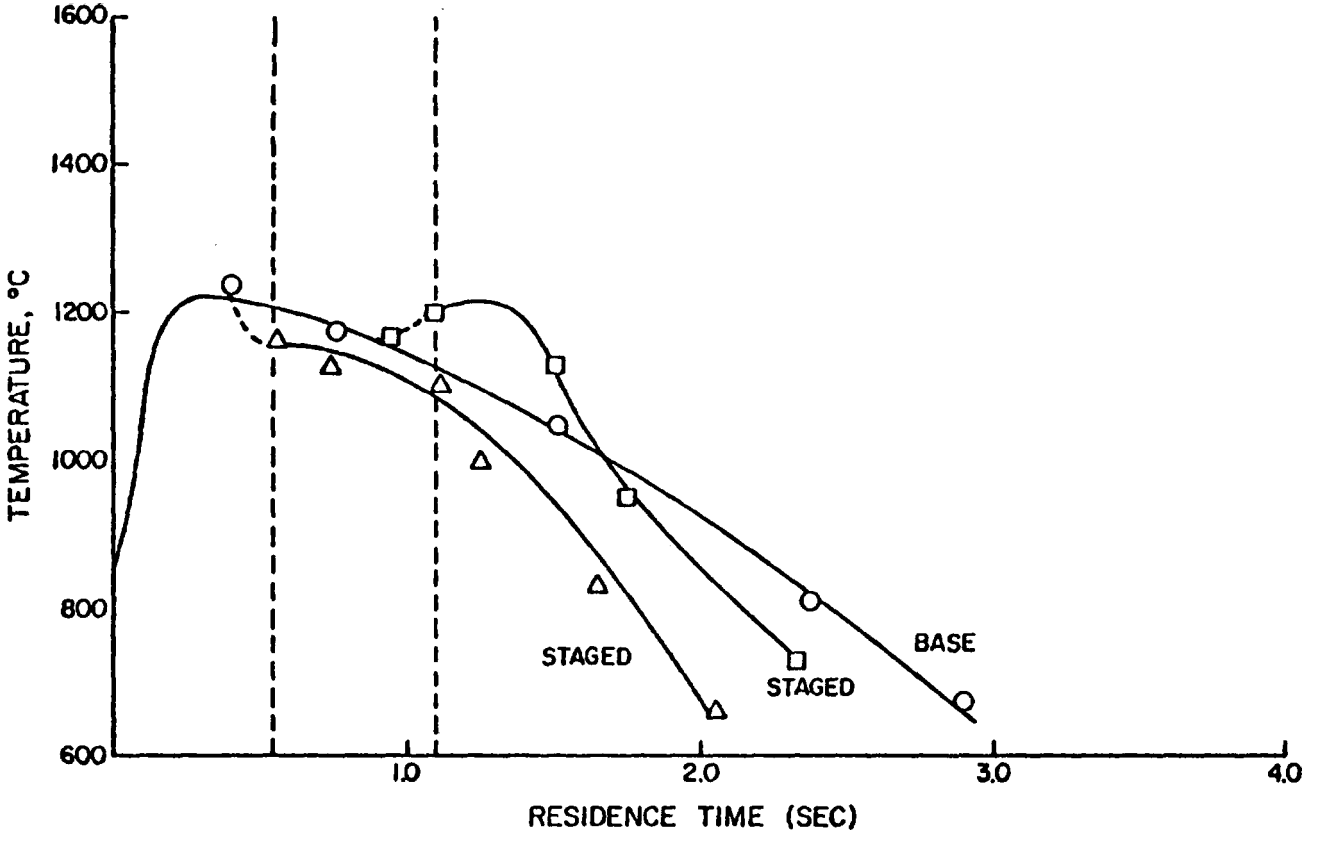

Figure 5.34. Baseline and Staged Temperature Profiles
Colorado Coal, Base SR = 0.4, Staged SR1 = 0.4, SR2 = 1.2.

established for the previous coals. In Figure 5.33 at very fuel-rich first stage conditions, some VN escapes oxidation to NO when oxygen is depleted by rapid evolution of non-nitrogenous combustible gases. In this case, much of the VN has reacted to form N_2 before staging although a substantial amount remains to form NO when second stage air is introduced. The VN remaining appears to be relatively inert to destruction since an increase in first stage residence time is ineffective in promoting its reduction.

As was the case with the Pittsburgh #8 coal, the better staging condition is SR1 = 0.8 with about 0.6 seconds residence time to give the first stage NO sufficient time to disappear before the injection of second stage air. Staging effectiveness at SR1 = 0.4 is limited by the slow destruction of the VN pool in the first stage.

The Colorado coal gives 1140 ppm of emitted NO, 40% fuel N conversion, from conventional combustion at SR = 1.2. The fuel nitrogen conversion and staging effectiveness for the Colorado coal are given in Table 5.6.

5.7 Effect of Temperature in the First Stage:

The previous data pertained to the influence of coal composition and stoichiometry on NO profile. Temperatures were measured, and showed some variation form coal to coal. In this section of the report the focus is on the influence of temperature on the NO profile of one coal-Western Kentucky. Temperature profiles were altered by changing the firing rate. A maximum firing rate of 8 lb/h gave a residence time of about 1 s in the combustor at SR = 0.8. A minimum firing rate of 2.7 lb/h gave a residence time approximately three times that. Because the combustor contained a

TABLE 5.6

FUEL N CONVERSION AND STAGING EFFECTIVENESS

COLORADO COAL

SR1 (SR2 = 1.2)	τ_1, sec	Fuel N Conversion	Staging Effectiveness
0.8	0.23	24%	41%
	0.55	17	49
0.4	0.53	16	60
	1.07	15	63

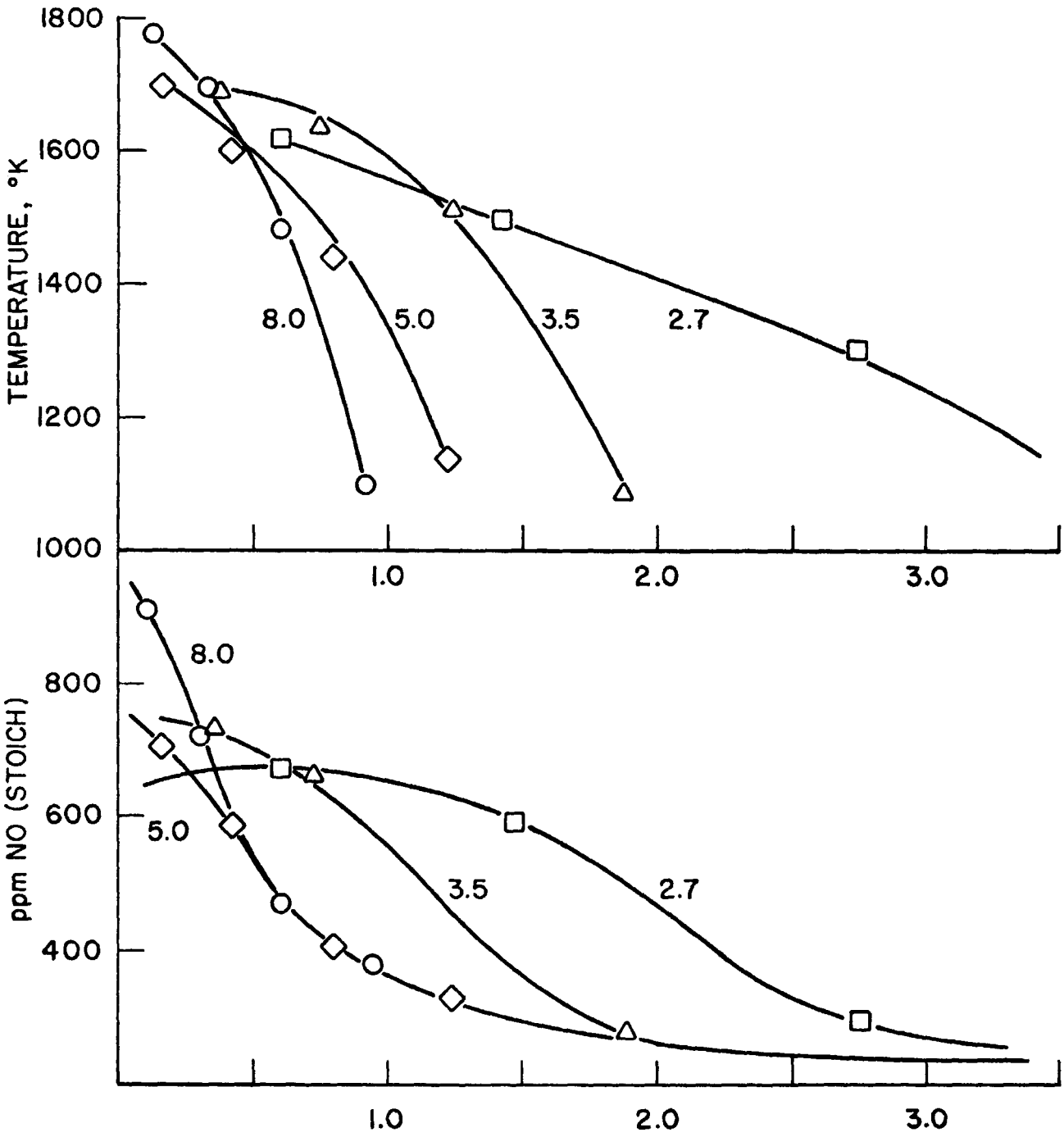

Figure 5.35: Effect of Temperature History on NO. Western Kentucky Coal. Numbers Refer to Feed Rate in lb/hr.

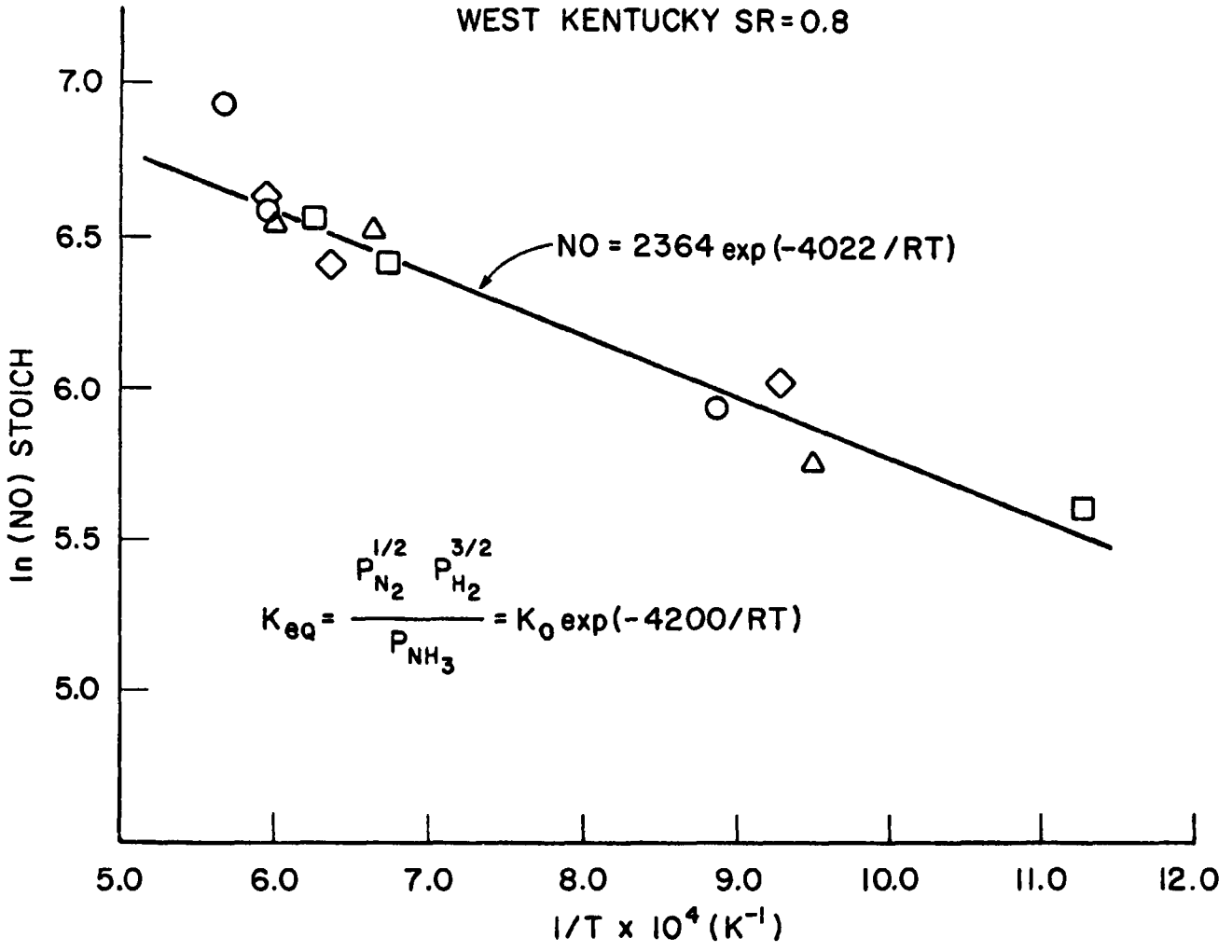

Figure 5.36: Effect of Temperature on NO

high thermal mass, some heat was being transferred from the walls to the flue gas at the low firing rate conditions. In each case, the dependence of temperature on residence time was drastically altered. In general, the temperature measurements show that the lower firing rates allowed the flue gas to remain hotter longer as shown on Figure 5.35. It might therefore be anticipated that NO reduction would be promoted at the low firing rate if the rate of NO reduction should increase with temperature. The equilibrium NO under theses fuel rich conditions was well below 1 ppm. The NO profiles (Figure 5.35), however, shows that, as temperature is increased the rate of NO destruction does not increase, but rather the NO measured increases. The surprising result is that the actual level of NO (not the rate of destruction) correlates well with temperature. This is shown in Figure 5-36, in which log NO is plotted against 1/T. A straight line is obtained. The lower the temperature, the less NO leaves the first stage. This result requires further validation, and if true, could have significant repercussions on the use of thermal programming to increase staging effectiveness.

6.0 CORRELATION DEVELOPMENT

6.1 Use of Correlations

The foregoing data clearly demonstrates that much still remains to be discovered before the NO_x abatement behavior from any one coal can be predicted with any certainity. The empirical correlations presented in this section of the report are merely to show what coal and combustion parameters are statistically relevant in determining the peak NO formed under baseline conditions, and the flue NO formed after staging. Because details of the processes involved are not understood at this time, it would be very unwise to place undue significance on the correlations presented below, and they clearly cannot be used for scale up criteria.

6.2 Correlations of Baseline Data

Empirical correlations of the peak baseline NO concentration and the peak NO expressed as percentage of fuel nitrogen conversion were obtained with a stepwise multiple linear correlation program (White, 1978). The resulting equations are:

$$\ln \text{PEKNO} = 2.43 \ln \text{SR1} + 7.49 \ln \text{NITRO} - 10.34 \ln \text{HYDRO} + 5.34 \ln \text{VOLWT} + 1.99 \ln \text{ASHDR} + 22.38 \quad (6.1)$$

$$\ln \%\text{CONV} = 0.0181 \frac{1}{\text{NITRO}} - 1.31 \frac{1}{\text{SR1}} + 3.52 \quad (6.2)$$

where SR1 = Baseline stoichiometric ratio

NITRO = N/C molar ratio in coal

HYDRO = H/C molar ratio in coal

VOLWT = ASTM proximate volatiles, % wt

ASHDR = Dry basis ash, % wt

PEKNO = Baseline peak NO, ppm stoichiometric

%CONV = Baseline peak NO as % of fuel nitrogen conversion

Plots of the measured versus predicted values are shown in Figures 6.1 for peak NO and 6.2 for percentage conversion of fuel nitrogen.

Other empirical parameters such as the temperature at the baseline peak NO and molar ratios to carbon of sulfur and oxygen were not significant. A listing of the regression statistics and confidence limits on the coefficients in Equations 6.1 and 6.2 are given in Table 6.1.

These equations are limited to the coals and experimetal conditions herein and have no more than phenomenological significance. However, the formula for peak baseline NO indicates the dependencies on stoichiometry and nitrogen content of the coal that are expected. The effect of volatiles in this correlation perhaps indicates that the NO is formed from the nitrogen contained in the early volatiles, as reasonable conclusion since volatiles evolved late in fuel-rich pyrolysis will have little chance for oxidation to NO as the oxygen is depleted.

Hydrogen is inherently associated with volatiles so that the negative effect on NO is not easily justified. One possible explanation is that the hydrogen remaining in fuel-rich areas does reduce NO by Myerson-type reactions. The more initial hydrogen in the coal, the more will remain for reducing reactions as the oxygen is destroyed locally.

The dependence on ash is very weak, with an F ratio of 2.0. However, that ash content affects peak NO positively is uncertain. Experimental evidence suggests that ash should influence NO reduction, not formation, so that in this case, the ash content probably relates to some other feature of the NO formation process.

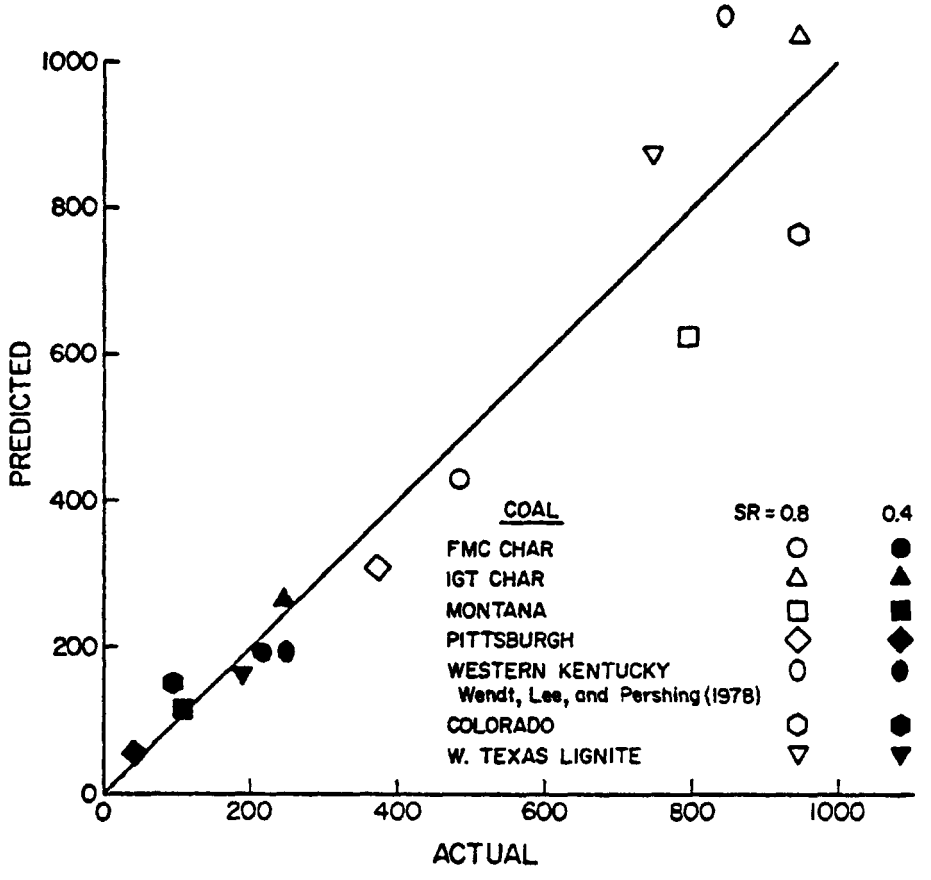

Figure 6.1 First Stage Peak NO, Equation 6.1, Actual vs. Predicted, ppm(stoich).

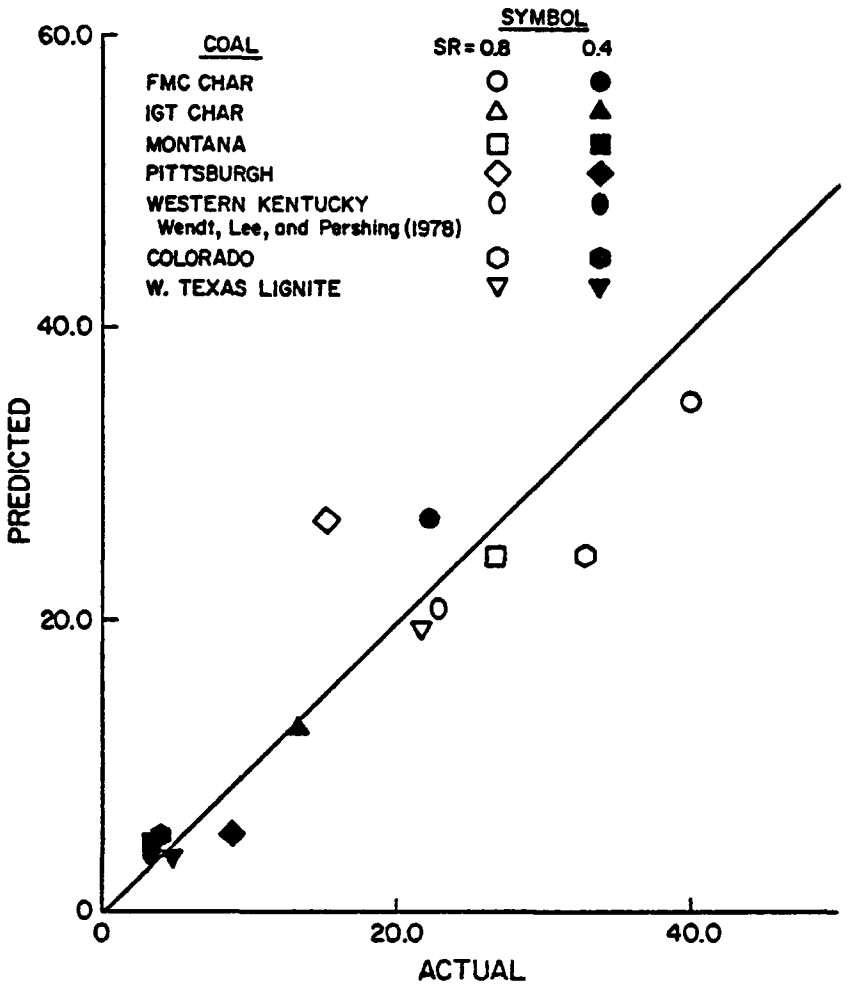

Figure 6.2 First Stage Peak Fuel Nitrogen Conversion, Equation 6.2 Actual vs. Predicted, %.

TABLE 6.1

STATISTICAL SUMMARY OF REGRESSIONS

Equation	F Ratio (Regression)	r^2 (Regression)	Independent Variables Coefficient ± Confidence Limits (95%)*				
5.1	101	0.96	1/SR	NITRO	HYDRO	VOLWT	ASHDR
			-2.43 ± 0.25	7.49 ± 1.75	-10.34 ± 1.46	5.34 ± 1.89	1.99 ± 0.70
5.2	150	0.92	1/SR	1/NITRO			
			-1.31 ± 0.17	0.0181 ± 0.0034			
5.3	11	0.69	TIMEZ	NITRO	H/N	SULFR	ASHDR
			-145 ± 60	517 ± 223	-741 ± 404	-215 ± 140	-199 ± 138
5.4	7	0.51	%CONV	η**	ASHDR-NITRO**	1/T2	
			0.0185 ± 0.011	2.56 ± 2.4	-636 ± 756	-3415 ± 2300	

*Basis t-distribution with N_1, N_2 degrees of freedom; N_1=Number of independent variables, N_2=29-N_1
**Coefficient possibly not different from zero.

The correlation of percentage conversion of fuel nitrogen at the baseline peak NO is significant in that only two parameters, SR1 and nitrogen content, are required to give a high correlation. Equation 6.2 reflects the generally accepted viewpoint for homogeneous systems (Fenimore, 1977) that conversion of fuel nitrogen to NO decreases as fuel nitrogen concentration increases. That conversion of fuel nitrogen should depend strongly on global oxygen stoichiometry is expected.

6.3 Correlations of Staging Results

The results of the staged combustion runs were correlated with the physical properties of the coal and experimental conditions to attempt to shed additional light on the data. The following are regressions of the second stage NO (flue value) and second stage NO as percentage conversion of fuel nitrogen.

$$\text{2NDNO} = -145.5 \ln \text{TIME 2} + 517.0 \ln \text{NITRO} - 740.7 \ln \text{HYDRO} - 215.5 \ln \text{SULFR} - 199.3 \ln \text{ASHDR} + 4523 \qquad 6.3$$

$$\ln \text{SSCON} = -3415 \left(\frac{1}{\text{TEMP2}}\right)^2 + 0.0185 \,\%\text{CONV} - 636 \,\text{ASHDRY} \times \text{NITRO} - 2.56 \,\eta - 0.03 \qquad 6.4$$

where

2NDNO = second stage fuel NO, ppm STOICH

SSCON = second stage NO as fractional conversion of fuel nitrogen

TIME 2 = residence time at the second stage conjection point (first stage residence time)

NITRO = N/C molar ratio in coal

HYDRO = H/C molar ratio in coal

SULFR = S/C molar ratio in coal

η = H/H_2O molar ratio in coal

ASHDR = percent ash calculated on a water-free basis

TEMP2 = temperature at the second stage injection point

%CONV = percentage conversion of fuel nitrogen at the baseline peak

The actual versus predicted values of these correlations are plotted in Figures 6.3 (2NDNO), 6.4 (SSCON). The statistics for the correlations and confidence limits on the coefficient are shown in Table 6.1.

As was the case for the regressions for the first stage experimental results, these equations apply only to the experimental conditions and coals reported herein. Further, the predictive abilities of these expressions are limited as evidenced by the scatter in Figures 6.3 and 6.4. It is interesting that these purely empirical equations do correctly predict the trends in the data on the basis of *a priori* physical and operating parameters without resort to mechanistic kinetic expressions.

In general, second stage NO (Equation 6.3) is a function of first stage residence time; albeit, more or less strongly dependent depending on the type of coal. It is reasonable that increased fuel nitrogen should increase second stage NO, especially at very fuel-rich first stage conditions which lead to increased VN carryover to the second stage. The negative dependence of second stage NO on the coal hydrogen content, as in the regression for first stage peak NO, possibly implies that hydrogen or some mechanism involving a hydrogen derivative is responsible for reducing baseline NO. The negative dependence of NO on the coal sulfur content in the fuel-lean second stage may have some significance in the case of a

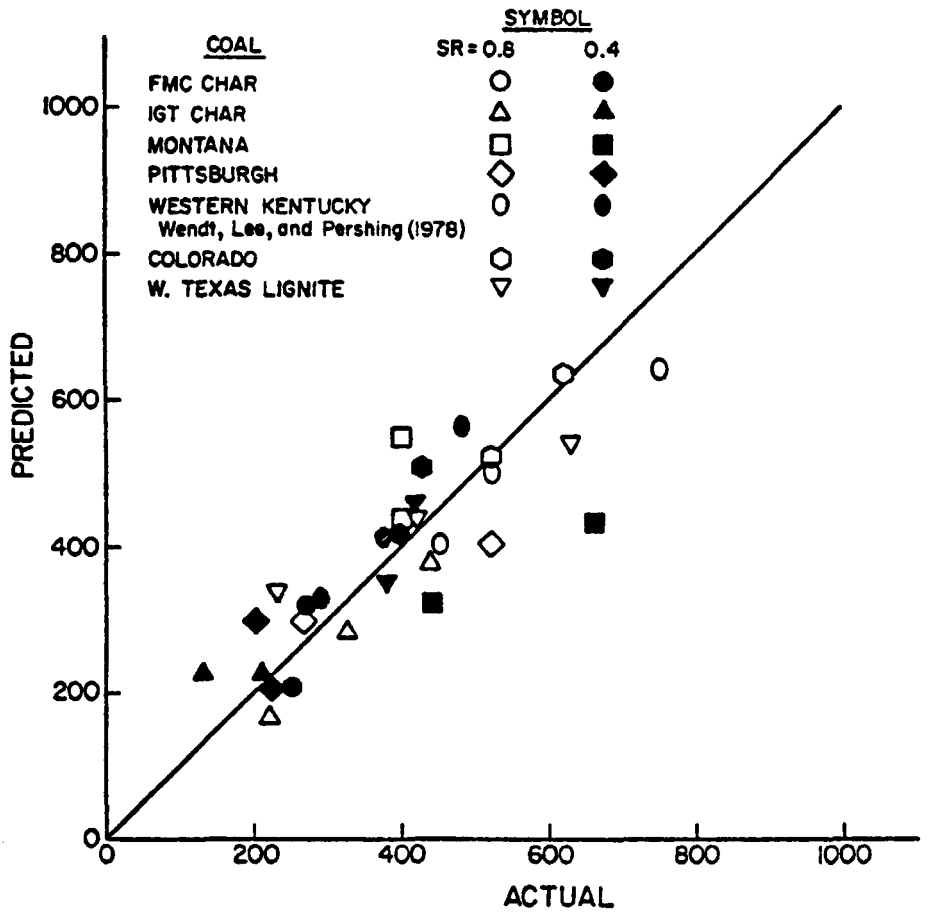

Figure 6.3 Second Stage NO, Equation 6.3
Actual vs. Predicted, PPM (Stoich.).

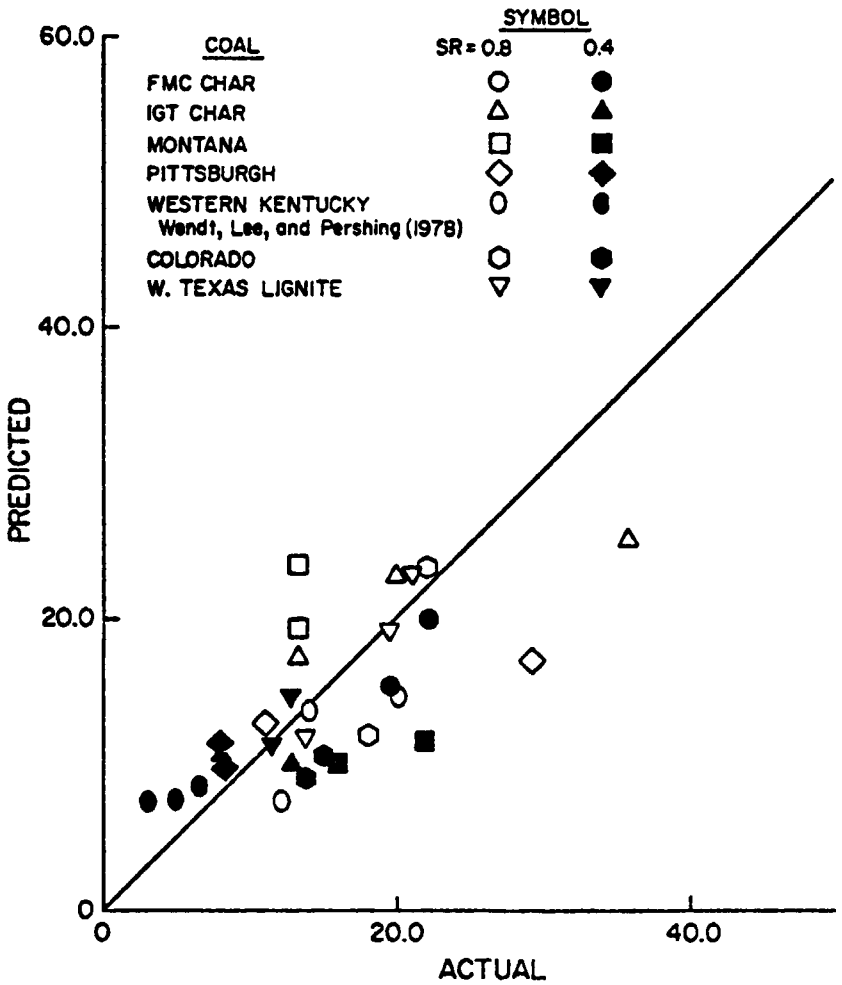

Figure 6.4 Second Stage Fuel Nitrogen Conversion, Equation 6.4 Actual vs. Predicted, %.

desulfurized fuel burned under staged conditions. The interactions of SO_x and NO_x will undoubtably be pursued in heterogeneous systems as it has in homogeneous systems (DeSoete, 1975; Morcomb, 1977).

The regression equation for fractional conversion of fuel nitrogen in the second stage (Equation 6.4) contains parameters, the product of ash and nitrogen contents, the second staging point temperature and the hydrogen to water ratio for which no satisfactory justification can be proposed. That second stage fuel nitrogen conversion should depend on first stage peak fuel nitrogen conversion to NO is statistically weak as indicated by the wide confidence limits on the coefficient (Table 6.1). The dependence could, in fact, be nonexistent. The temperature dependence in this equation probably reflects the true kinetics of net NO formation in the second stage.

The correlation coefficients for these equations and those for the first stage peak NO and fuel nitrogen conversion show that additional work is justified in pursuing empirical predictive equations of these types in the absence of predictive kinetic models for staged combustion. These regressions can be used to determine, at a first approximation, the parameters that might be important in the mechanisms of NO formation reduction in a specific type of combustion configuration, for example. More detailed analytical information on the types of VN compounds present in the first stage (amine or cyanide, for example) or the amount of fuel nitrogen and non-nitrogenous combustibles evolved during controlled pyrolysis experiments would also prove useful in predictive empirical models for staged combustion insofar as these relate to the behavior of the fuel during the initial time in the fuel-rich first stage when NO formation and VN reduction is occurring.

It is significant that staging effectiveness could not be correlated with the physical properties of the fuels or experimental conditions. This is indicative that the kinetics of the processes involved must be considered in any model formulation.

6.4 FMC Char Correlation

The FMC Char NO profiles (Figure 6.5) at both SR = 0.8 and SR = 0.4 can be correlated well with a simple heterogeneous reaction scheme:

$$R_{NO} = 3.3 \times 10^{7} \exp\left(-\frac{54500}{RT}\right) P_{O_2}^{0.4} C_N - 7.7 \times 10^{4} \exp\left(-\frac{47000}{RT}\right) X_{NO}^{0.6} W_{ASH} \quad \left(\frac{\text{moles}}{\text{cc sec}}\right) \qquad 6.5$$

where

P_{O_2} = local partial pressure of oxygen (atm)

C_N = moles N in char/(volume of reactor) (assumed to be proportional to char N surface/unit volume) $\left(\frac{\text{moles}}{\text{cm}^3}\right)$

X_{NO} = mole fraction NO

W_{ASH} = gm ash/(cm^3 reactor) (assumed to provide the time invariant area for NO reduction and assumed to be proportional to surface area/unit volume) (g/cm^3)

The formation reaction activation energy is higher than that obtained by Hamor, 1973, for coal char combustion, since the data show that NO is formed more slowly than O_2 is consumed. The reduction of NO is less than first order in NO, also with an appreciable activation energy. The variable W_{ASH} appears merely to account for the variable fuel loading at the two stoichiometric ratios.

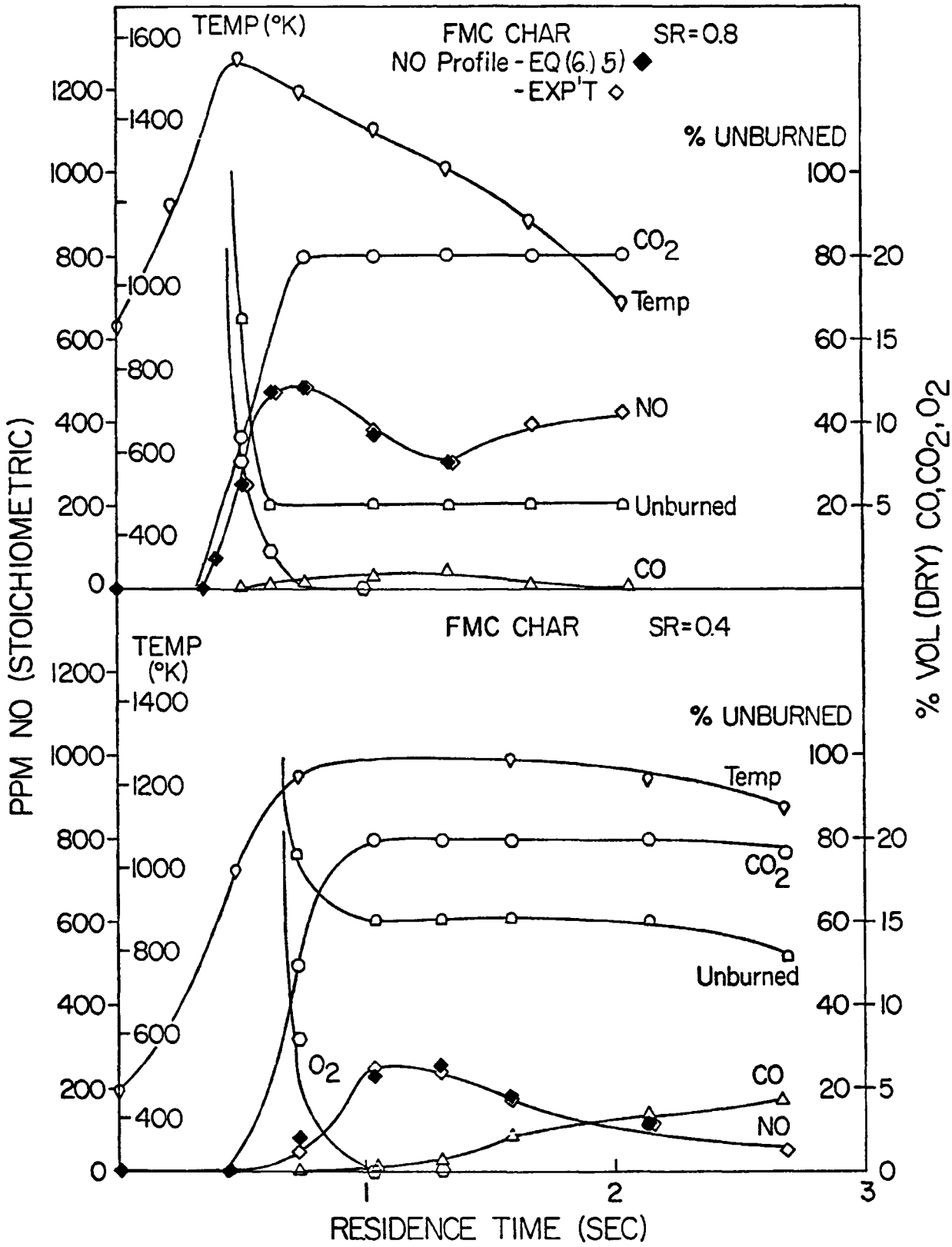

Fig. 6.5. Time Resolved Species Profiles: FMC Char
Top: SR = 0.8; Bottom: SR = 0.4

If it is assumed that the rate of NO reduction is dependent on the measured CO concentration one can fit the char data on Figure 6.5 by the expression

$$R_{NO} = 1.486 \times 10^{7} \exp\left(-\frac{53{,}000}{RT}\right) P^{0.4} C_N - 1.89 \times 10^{7} \exp\left(-\frac{46870}{RT}\right) X_{NO}^{0.7} P_{CO}^{0.6} W_{ASH} \qquad 6.6$$

This equation gives as good a fit to the char data as does Equation (6.5). This indicates a potential pitfall in the use of empirical correlations such as these, since there will be other expressions that fit the data equally well. However, it is interesting to note that both Equations (6.5) and (6.6) have essentially similar activation energies, and reaction orders with respect to O_2 and NO.

7.0 REFERENCES

Axworthy, A. E. "Chemistry and Kinetics of Fuel Nitrogen Conversion to Nitric Oxide," AIChE Symposium Series, No. 148, 71, 1957.

Axworthy, A. E., G. R. Schneider and V. H. Dayan. "Chemical Reactions in the Conversion of Fuel Nitrogen to NO_x," EPA 600/2-76-039, NTIS, Springfield, Virginia, 1976.

Bird, R. B., W. E. Stewart and Edwin N. Lightfoot. Transport Phenomena, John Wiley and Sons, Inc., New York, 1960.

Blair, D. W., J. O. L. Wendt and W. Bartok. "Evoluation of Nitrogen and Other Species during Controlled Pyrolysis of Coal," Sixteenth Symposium (International) on Combustion, The Combustion Institute, Pittsburgh, 1977.

Brackett, C. E. and J. A. Barsin. "The Dual Register Pulverized Coal Burner; A NO_x Control Device," Proceedings of the NO_x Control Technology Seminar, EPRI Report SR-39, Electric Power Research Institute, Palo Alto, California, 1976.

Brown, R. A., H. B. Mason, D. W. Pershing and J. O. L. Wendt. "Investigation of First and Second Stage Variables on Control of NO_x Emissions using Staged Combustion in a Pulverized Coal Wall-Fired Furnace," Paper presented at the 83rd National Meeting, AIChe, Houston, Texas, March, 1977.

Brown, R. A., H. B. Mason and P. Neubauer. "Investigation of Staging Parameters for NO_x Control in Both Wall- and Tangentially-Fired Biolers",Proceedings of the Second Stationary Source Combustion Symposium, EPTS-600/7-77-073C, NTIS, Springfield, Virginia, 1973.

Cortes-Chavez, Rogelio Miguel. "A Computer Program for the Calculation of Complex Chemical Equilibrium," M.S. Thesis, University of Arizona, 1976.

DeSoete, G. G. "Heterogeneous Reduction of NO on Surfaces," presented at EPA Fundamental Contractors' Meeting, Newport Beach, June, 1978.

Edwards, H. W. "Interaction of Nitric Oxide with Graphite," AIChE Symposium Series 68, 126, 1972.

Field, M. A., D. W. Gill, B. B. Morgan and P. G. W. Hawkesley. Combustion of Pulverized Coal, The British Coal Utilization Research Association, Leatherhead, 1967.

Gray, W. A., I. K. Kilham, and R. Müller. Heat Transfer from Flames, Elek Science, London, 1976.

Hamor, R. J., I. W. Smith and R. J. Tyler, Comb. Flame 21 p. 153-162 (1973).

Hottel, H. C. and A. F. Sarofim. Radiative Transfer, McGraw-Hill, New York, 1967.

Howard, J. "Mechanisms of Ignition and Combustion in Flames of Pulverized Bituminous Coal," Ph.D. Dissertation, The Pennsylvania State University, 1965.

Howard, J. B. and R. H. Essenhigh. "Pyrolysis of Coal Particles in Pulverized Fuel Flames," Ind. Eng. Chem. Process Design and Development, 6, 1, 1976.

Land, T. "Suction Pyrometry," Instruments and Automation, 29, 7, 1956.

Lee, J. W. Personal Communication, 1977.

Lyon, R. K. and J. P. Longwell. "Selective, Non-Catalytic Reduction of NO_x by NH_3," Proceedings of the NO_x Control Technology Seminar EPRI Report SR-39, Electric Power Research Institute, Palo Alto, California, 1976.

Morcomb, J. T. "Interactions of Fuel Sulfur and Fuel Nitrogen in Fuel-Rich Flames," M.S. Thesis, The University of Arizona, 1977.

Muzio, L. J., J. K. Arand and D. P. Teixeira. "Gas Phase Decomposition of Nitric Oxide in Combustion Products," Sixteenth Symposium (International) on Combustion, The Combustion Institute, Pittsburgh, 1977.

Myerson, A. L. "The Reduction of Nitric Oxide in Simulated Combustion Effluents by Hydrocarbon-Oxygen Mixtures," Fifteenth Symposium (International) on Combustion, The Combustion Institute, Pittsburgh, 1975.

Perry, R. H. and C. H. Chilton, Eds. Chemical Engineers Handbook, Fifth Edition, McGraw-Hall Book Company, New York, 1973.

Pershing, D. W. "Nitrogen Oxide Formation in Pulverized Coal Flames," Ph.D. Dissertation, University of Arizona, 1976.

Pershing, D. W. and J. O. L. Wendt. "Pulverized Coal Combustion: The Influence of Flame Temperature and Coal Composition on Thermal and Fuel NO_x," Sixteenth Symposium (International) on Combustion, The Combustion Institute, Pittsburgh, 1977.

Pohl, J. H. and A. F. Sarofim. "Devolatilization and Oxidation of Coal Nitrogen," Sixteenth Symposium (International) on Combustion, The Combustion Institute, Pittsburgh, 1977.

Smith, J. M. and H. C. Van Ness. Introduction to Chemical Engineering Thermodynamics, Third Edition, McGraw-Hill Book Company, New York, 1975.

Warshawsky, I. "Pyrometry of High Velocity Gases," Sixth Symposium (International) on Combustion, The Combustion Institute, Pittsburgh, 1957.

Wendt, J. O. L., J. W. Lee and D. W. Pershing. "Pollutant Control through Staged Combustion of Pulverized Coal," DOE Report FE-1817-4, University of Arizona, 1978.

Wendt, J. O. L., C. V. Sternling and M. A. Motovich. "Reduction of Sulfur Trioxide and Nitrogen Oxides by Secondary Fuel Injection," Fourteenth Symposium (International) on Combustion, The Combustion Institute, Pittsburgh, 1973.

West, W. E., Jr. and J. W. Westwater. "Radiation-Conduction Corrections for Temperature Measurements in Hot Gases," Industrial and Engineering Chemistry 45, 1953.

White, J. W. Personal Communication, 1978.

APPENDIX A

MATERIAL BALANCES AND HEAT BALANCES

Stoichiometry of Coal Combustion--Fuel-Lean Flames

For one mole of carbon in the coal feed to the furnace, the stoichiometry (neglecting the minor contribution of nitrogen and sulfur and on an ash-free basis)

$$CH_hO_o[H_2O]_w + \gamma Z(O_2 + 3.76\ N_2) \longrightarrow$$
$$yH_2O + aCO_2 + bCO + (1-\alpha)\ C + (\gamma Z - \alpha - \tfrac{h}{4} + \tfrac{O}{2})\ O_2 + 3.76\ \gamma Z\ N_2 \qquad \text{A.1}$$

where $Z = 1 - \frac{o}{2} + \frac{h}{4}$ stoichiometric oxygen

$y = w + \frac{h}{2}$ potential water

$\gamma =$ stoichiometric ratio

$\alpha =$ carbon conversion

A carbon balance gives

$$\alpha = a + b$$

and, on a dry basis

$$X_{CO_2} = \frac{a}{4.76\gamma Z - \frac{h+O}{4}\frac{}{2}} = \frac{a}{FG_D}$$

where $FG_D \equiv$ dry flue gas

$$X_{CO} = \frac{b}{FG_D}$$

$$X_{O_2} = \frac{\gamma Z(\alpha+\delta)}{FG_D}$$

where $\delta = \frac{h}{4} - \frac{O}{2}$, the noncarbon oxygen requirement

The burned carbon is, by carbon balance

$$\alpha_{CO_2} = FG_D\ (X_{CO} + X_{CO_2}) \qquad A.2$$

and, by oxygen balance

$$\alpha_{O_2} = \gamma Z - \delta - FG_D\ X_{O_2} \qquad A.3$$

so that the unburned carbon is $(1-\alpha)$.

Equating the carbon conversions by oxygen and carbon balances gives

$$\gamma_c = \frac{\delta\ \left[1 - (X_{CO} + X_{CO_2} + X_{O_2})\right]}{Z\ \left[1 - 4.76(X_{CO}+X_{CO_2}+X_{O_2}\right]} \qquad A.4$$

If the carbon conversion can be assummed to be complete

$$\gamma_{O_2} = \frac{1 + \delta\ (1 - X_{O_2})}{Z\ (1 - 4.76\ X_{O_2})} \qquad A.5$$

$$= \frac{.21}{.21 - X_{O_2}} \quad \text{if } \delta \text{ is small}$$

if carbon burnout is complete,

$$\gamma_{C^1} = \frac{1}{4.76Z}\ \left[\frac{1}{X_{CO} + X_{CO_2}} + \delta\right] \qquad A.6$$

$$= \frac{0.21}{X_{CO_2}} \quad \text{if } \delta \text{ is small}$$

The wet product to feed ratio is

$$\left(\frac{P}{F}\right)_W = 1 + \frac{W + \frac{h}{4}}{4.76\ \gamma Z} \qquad A.7$$

The volumetric flow rate on a wet basis is

$$Q_W = SA \cdot \gamma \cdot (P/F)_W \cdot \frac{T}{T_o} \qquad A.8$$

The reported NO concentration must be on a basis which conserves mass so that meaningful comparisons among data sets can be made. The

The "stoichrometric NO" is

$$NO_{ST} \quad NO_{measured} \ \frac{FG_D}{FG_{DO}} = NO_m \ SCRF$$

where SCRF is the stoichiometric ratio correction factor and FG_{DO} is the dry flue gas at stoichiometric conditons

$$SCRF = \frac{4.76\ \gamma Z - \delta}{4.76Z - \delta} \sim \gamma \text{ if } \delta \text{ is small}$$

Stoichiometry of Coal Combustion--Fuel-Rich Flames

For one mole of carbon in the coal,

$$CH_hO_o[H_2O]_w + \gamma\ Z\ (O_2 + 3.76N_2) =$$

$$C_{(1-\alpha\gamma)} + \alpha(a\ CO_2 + b\ CO) + dO_2$$

$$+y\left[(1-\eta)H_2O + \eta\ H_2\right] + 3.76\ \gamma Z\ N_2$$

where $\gamma \leq 1$

by a carbon balance,

$$\gamma = a + b \qquad \text{A.10}$$

The dry flue gas is

$$FG_D = \frac{\gamma\left[4.76Z + \alpha\right] + \frac{3}{2}\mu y + \frac{0}{2}}{1 + \frac{X_{CO}}{2} + X_{CO_2}} \qquad \text{A.11}$$

since

$$X_{CO_2} = \frac{a\alpha}{FG_D}$$

$$X_{CO} = \frac{b\alpha}{FG_D} \qquad \text{A.12}$$

$$X_{O_2} = \frac{d}{FG_D}$$

equating the stoichiometric moles of flue gas to (FG_D)

$$\alpha_C = \frac{X_{CO} + X_{CO_2}}{1 - X_{CO} + X_{CO_2} + X_{O_2}} \left(\frac{\eta y}{\gamma} + 3.76Z\right) \qquad \text{A.13}$$

The unburned carbon is then 1-α.

From an oxygen balance

$$\alpha_o = \frac{GZ(X_{CO} + X_{CO_2})/(1 - \frac{X_{CO}}{2})}{G\left(\frac{X_{CO_2} + X_{O_2} + X_{CO}/2}{1 - \frac{X_{CO}}{2}}\right) + \frac{h}{4}(1-\eta) - \frac{w}{2}\eta - \frac{0}{2}} \qquad \text{A.14}$$

$$G = 4.76\gamma Z + \frac{3}{2}\eta y - \frac{h}{4}, \text{ the stoichrometric dry flue gas.} \qquad \text{A.15}$$

The dry flue gas becomes

$$FG_D = \frac{G}{1 - \frac{X_{CO}}{2}} \sim 4.76\gamma Z \text{ if } h, o, \eta, X_{CO} \ll 1 \qquad \text{A.16}$$

The dry product to feed ratio is

$$(P/F)_D = \frac{FG_D}{4.76\gamma Z} \sim 1 \text{ if } h, o, \eta, X_{CO} \ll 1 \qquad \text{A.17}$$

and

$$SCRF = \frac{G}{G_O}\left(\frac{1}{1 - \frac{X_{CO}}{2}}\right) \sim \gamma \text{ if } h, o, \eta, X_{CO} \ll 1 \qquad \text{A.18}$$

The wet product to fuel ratio is

$$(P/F)_w = \frac{FG_w}{4.76\gamma Z} \sim 1 \text{ if } h, o, \eta, X_{CO} \ll 1 \qquad \text{A.19}$$

$$FG_w = FG_D + (1-\eta)y$$

The volumetric flow rate in the furnace is

$$Q_w = SA\gamma \left(\frac{P}{F}\right)_w \frac{T}{T_o} \qquad \text{A.20}$$

Residence Time

The differential residence time for a plug flow combustor is given by

$$d\tau = \frac{dv}{Qw}$$

or $$\Delta\tau = \int_{L_1}^{L_2} \frac{dv}{Qw}$$

L_1, L_2 are axial distances in the furnace.

Since

$$dv = \frac{\pi d^2}{4} dL$$

$$\Delta\tau = \frac{\pi d^2}{4} \int_{L_1}^{L_2} \frac{dL}{Qw}$$

$$= \frac{\pi d^2 T_o}{4SA\gamma} \int_{L_1}^{L_2} \frac{dL}{(P/F)_w T(L)} \qquad \text{A.21}$$

$$\simeq \frac{\pi d^2 T_o}{4SA\gamma} \int_{L_1}^{L_2} \frac{dL}{T(L)} \quad \text{if } h, o, n, X_{CO} \ll 1$$

Equation A.21 can be evaluated with any convenient quadrature. The trapezoid rule gives sufficient accuracy since the integrand is only slightly nonlinear in most cases (see Chapter 4).

Furnace Enthalpy Balances--Stoichiometric Combustion

Based on stoichiometric combustion and assumming that 15% of the stoichiometric air is used as primary air, neglecting the carbon heat capacity, $\alpha = 1$, the heat release during stoichiometric combustion is

$$q_o = \Delta H^o_{298} + \int_{T_{in}}^{T_{out}} \left\{ C_{P_{CO_2}} + y\, C_{P_{H_2O}} + 3.76Z\, C_{P_{N_2}} \right\} dT$$

$$- 4.05\, Z \int_{298}^{T_{in}} C_{P_{air}}\, dT$$

Using ideal gas heat capacities (Smith and Van Ness, 1975, p. 121)

$$
\begin{aligned}
{}_{o} = {} & \Delta H^{o}_{298} - 3934 - 2285y + 768Z \\
& + (10.5Z + 7.30y + 25.68Z)\, T_{out} \\
& + (1.05 + 1.23y + 1.69Z)\, T_{o}^{2} \times 10^{-3} \\
& + \left(27.92\, T_{in} + 1.8 \times 10^{-3}\, T_{in}^{2} + \frac{7.28 \times 10^{-4}}{T_{in}}\right)
\end{aligned}
\qquad \text{A.22}
$$

where ΔH_{o}^{298} is the heat of combustion of the coal, cal/gmolC in coal

T_i = secondary air inlet temperature, K

T_o = flue gas outlet temperature, K

Furnace Enthalpy Balance--Fuel-Rich

Neglecting the dissociation of water ($\eta = 0$), and assumming the carbon conversion effectiveness, α; stoichiometric ratio γ, and the moles of CO formed are known, the stoichiometric heat balance requires adjustment for the reaction

$$bCO_2 \longrightarrow bCO + \frac{b}{2} O_2, \quad \Delta H^{o}_{298} = + 68.317 \frac{KCAL}{MOL}$$

$$\Delta H^{o}_{T} = \alpha b \left\{ \Delta H^{o}_{298} + \int_{T_i}^{T_o} \left(C_{P_{CO}} - C_{P_{CO_2}} - \frac{C_{P_{O_2}}}{2}\right) dT \right\}$$

so that

$$
\begin{aligned}
q_r = {} & q_o \alpha\gamma + \alpha B \left\{ 70{,}093 - \left(3.60 T_o + 0.56 \times 10^{-3}\, T_o^{2} \right.\right. \\
& \left.\left. + \frac{1.95 \times 10^{5}}{T_o}\right) \right\} + (1-\alpha\gamma)\, W \left\{ 8216 + 7.3\, T_o + 1.23 \times 10^{-3}\, T_o^{2} \right\}
\end{aligned}
\qquad \text{A.23}
$$

[=] Kcal/mol

where the last term accounts for the coal moisture which is vaporized and heated in any event.

Furnace Enthalpy Balance--Fuel-Lean

The fuel-lean heat balance, $\gamma>1$, is the sum of the stoichiomatric heat balance plus the effect of additional secondary air added

$$\eta_L = \eta_o - (\gamma-1)\left\{6.90\ (T_o-T_i) + 0.45\ (T_o^2 - T_i^2) + 0.18 \times 10^5\ \left(\frac{1}{T_o} - \frac{1}{T_i}\right)\right\} \qquad \text{A.24}$$

APPENDIX B

EQUILIBRIUM COMPOSITION OF PULVERIZED COAL COMBUSTION PRODUCTS

The graphs presented in this section are the results of calculations of the thermodynamic equilibrium compositions of the products of combustion of the coals used in this experiment. They are included primarily for reference. It should be noted that the calculated values of the water dissociation parameter, η, presented in the following graphs as a function of true gas temperature and parameterized in the stoichiometric ratio, must be used in the material balance calculations in Appendix A.

These results were obtained with the University of Arizona's thermodynamic equilibrium program CHEMEQ (Cortes-Chavez, 1976). This program utilizes the method of steepest descent to minimize the system Gibb's free energy given the temperature, pressure, and an initial composition of up to 35 elements and compounds.

Figures B.1-B.7 show the results of the calculations. The equilibrium NO is only shown for values in excess of 1 ppmv.

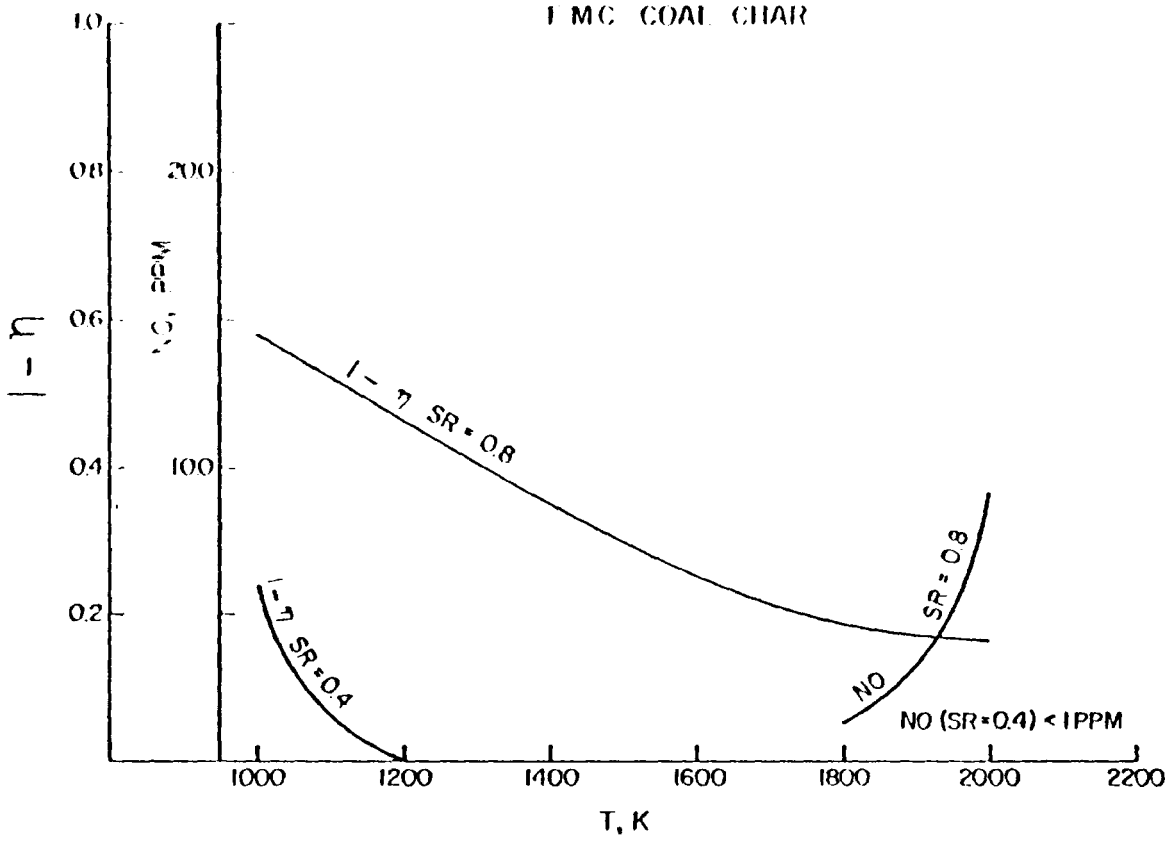

Figure B.1. Equilibrium NO and Fraction of Undissociated Water (1-η) FMC Coal Char; SR = 0.8 and 0.4.

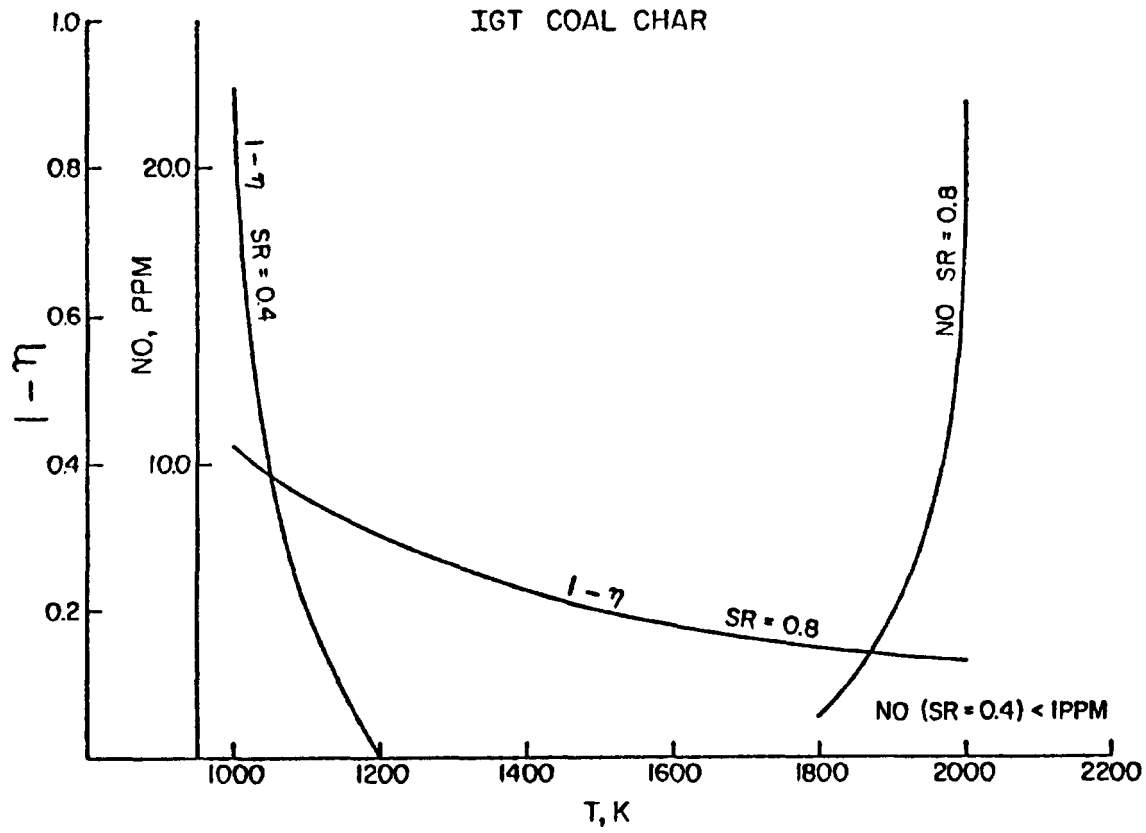

Figure B.2. Equilibrium NO and Fraction of Undissociated Water (1-η) IGT Coal Char; SR = 0.8 and 0.4.

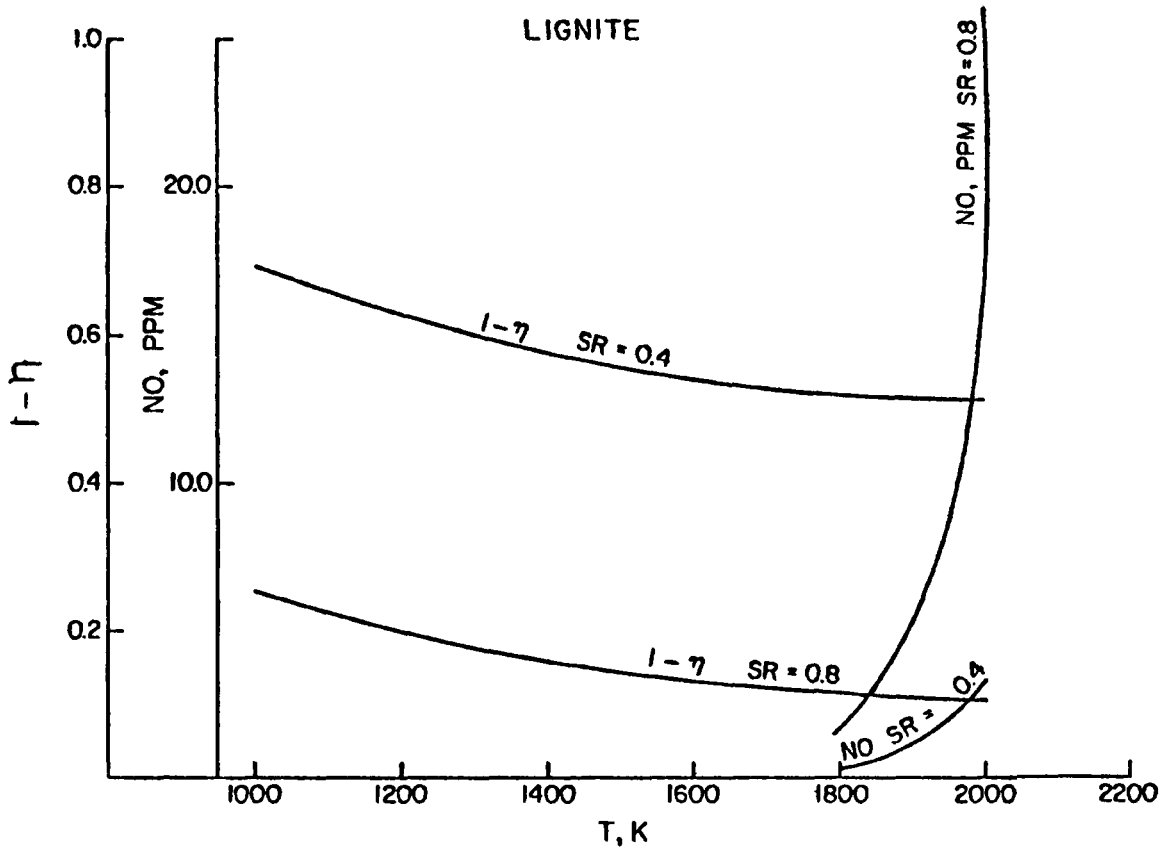

Figure B.3. Equilibrium NO and Fraction of Undissociated Water (1-η) Lignite Coal; SR = 0.8 and 0.4.

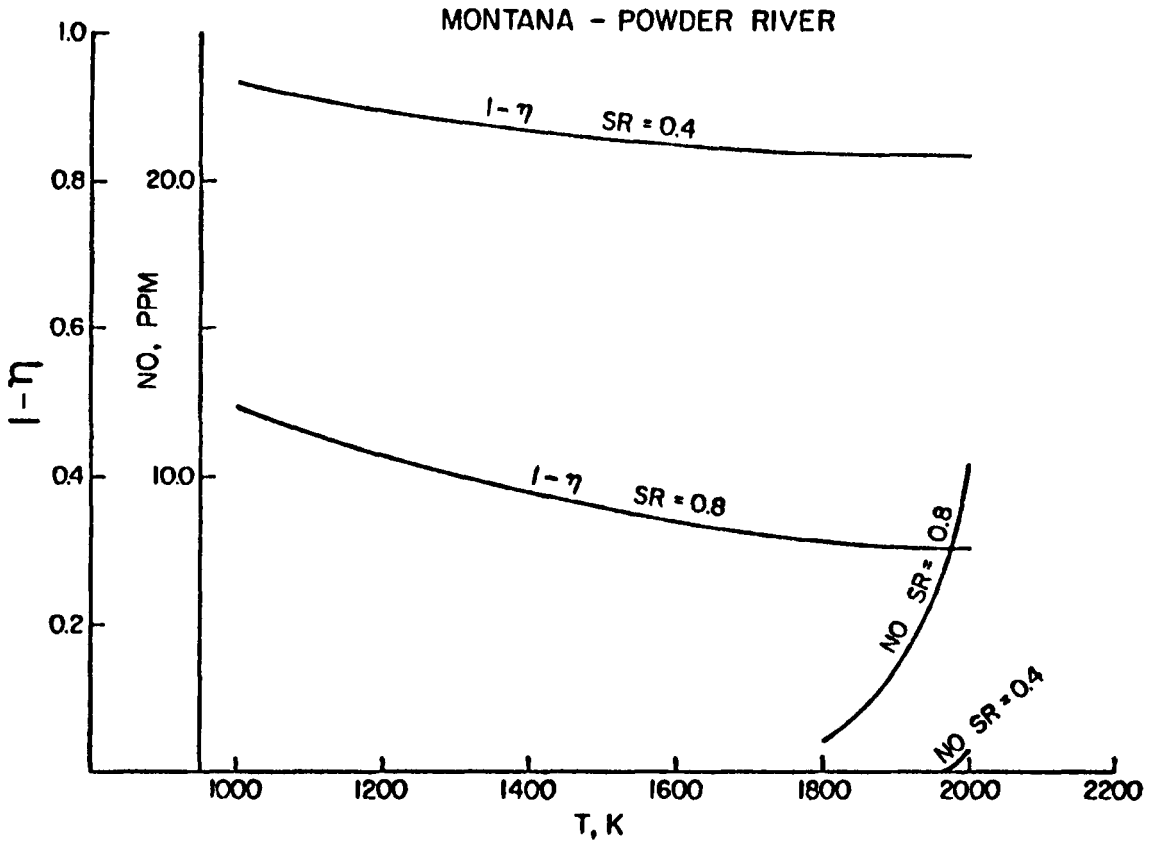

Figure B.4. Equilibrium NO and Fraction of Undissociated Water (1-η) Montana-Powder River Coal; SR = 0.8 and 0.4.

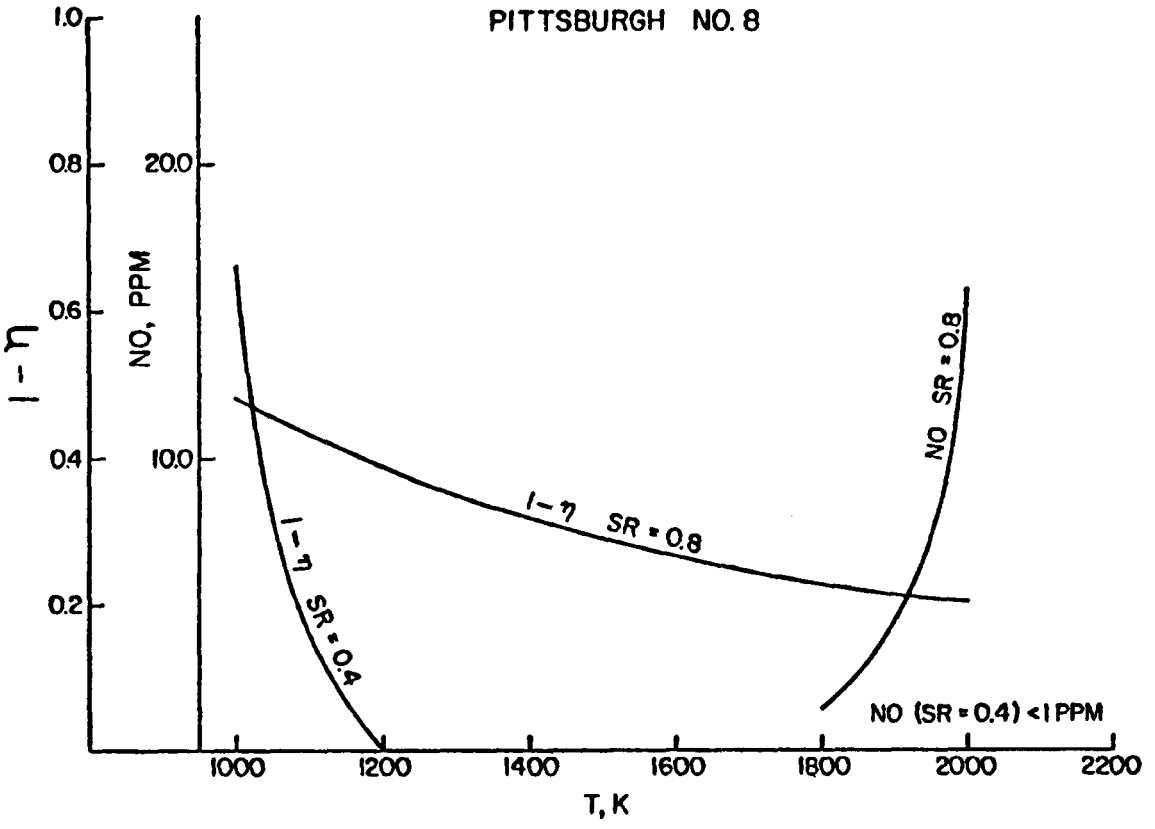

Figure B.5. Equilibrium NO and Fraction of Undissociated Water (1-η) Pittsburgh No. 8 Coal; SR = 0.8 and 0.4.

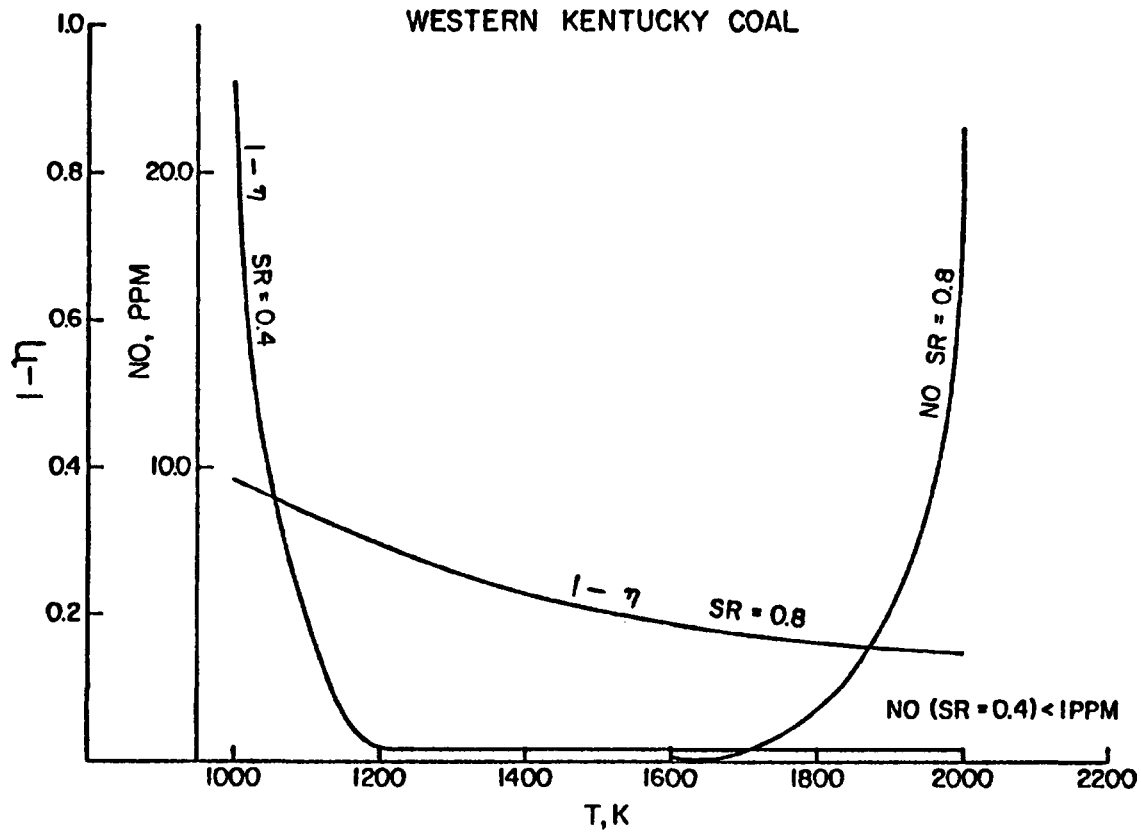

Figure B.6. Equilibrium NO and Fraction of Undissociated Water (1-η) Western Kentucky Coal; SR = 0.8 and 0.4.

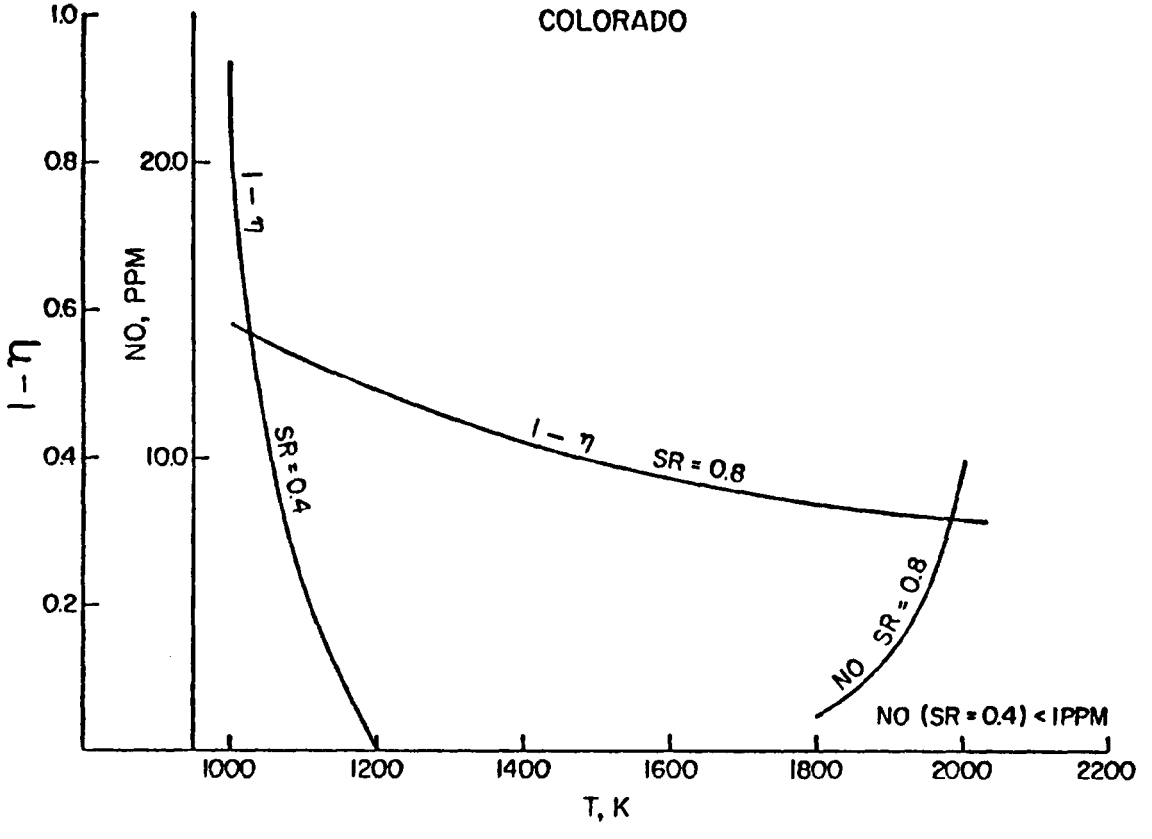

Figure B.7. Equilibrium NO and Fraction of Undissociated Water (1-η) Colorado Coal; SR = 0.8 and 0.4.

APPENDIX C

SAMPLE PROBE STUDY

Summary

The operation of the water spray probe was studied in a fuel rich (SR = 0.8) pulverized Western Kentucky coal flame.

Analysis of the measured concentrations of NO, CO, and CO_2 under conditions of varying spray (quench) water and gas sampling flow rates shows that significant variations in measured concentrations can be expected depending on the sampling conditions.

The major controlling parameter appears to be the quench water to sample gas ratio. Most variation in measured concentrations occur at low values of the water to gas ratio. As the ratio is increased, more or less asymptotic values of gas concentrations are observed with three-fold variations of the gas sampling rate as long as the water to gas ratio is in excess of 10. Most of the observed variations are attributed to poor quench water/gas mixing.

The calculated equilibrium recoveries of sampled gases show that insignificant amounts of NO, CO and CO_2 and H_xS are lost to the spray water. NH_3 and SO_2 recoveries are strongly affected by the water to gas ratio. At current sampling conditions, the majority of these two compounds is lost. If the ionic affects of ammonia and the acid gases in water are considered, the recovery of the reacting species, especially CO_2 is expected to be substantially lower.

Test Procedure

The probe was positioned at 64 cm in the furnace to maximize the sampled gas temperature and eliminate the possibility of drawing oxygen into the probe. The system was allowed to equilibrate before the analysis was started to minimize possible transient temperature effects on the sampled gas.

Temperatures were measured with type K thermocouples and corrected according to established methods. The corrected gas temperatures in the vicinity of the sample probe tip was 1400° K..

The furnace was set at fuel rich SR = 0.8 with Western Kentucky Coal as fuel to investigate the effect of quench water rate and gas sampling rate on the measured concentrations of NO, CO and CO_2.

Experimental Conditions

The study was run with Western Kentucky Coal at fuel rich SR = 0.8. A probe position of 64 cm was used since there is no oxygen present and the temperature is high enough that kinetic effects of sampling variation are maximized. Other pertinent experimental data are shown in Table C-1

The minimum gas sampling rate which can be used is that required to supply the analytical system. As measured by the wet test meter, the minimum rate is 0.30 SCFM. The maximum rate is set by the capacity of the knockout drum compressor at about 1.3 SCFM.

The water rate can be varied continuously from zero flow to a maximum of 7,8 gal/s as limited by the capacity of the two parallel rotameters used in the test.

Table C-1

Sampling Probe Experimental Conditions

Fuel: Western Kentucky Coal @ 4.87 lb/hr

Primary Air @ 77°F	1.87 SCFM
Secondary Air @ 533°K preheat	5.59 SCFM
Total Air @ 473°K	7.46 SCFM

Temperature at 64 cm 1400°K

SR = 0.8 basis 9.32 SCFM stoichiometric air

The probe testing was done by varying both the gas and water rate over the full range of both flows. The quench water flow was not shut off entirely, however, at the low end of its range to prevent plugging the probe tip and spray holes.

NO Measurements

The resulting variation of the measured NO is plotted as a function of water flow rate and parametrically in gas flow rate in Figure C-1.

Several points (on this graph) are worth describing. First, the data become more or less a function of spray water only at rates above 4 gal/s. This seems to indicate that gas quenching, or spray formation and gas/liquid contacting are satisfactory at this level.

At lower water rates, the measured NO is a strong function of gas sampling rate. Presumably this is a result of poor gas/liquid contact and poor convective cooling on the probe walls at low gas flows. This effect is diminished as the gas flow increases.

The NO data are replotted as a function of the water to gas mass ratio in Figure C-2. It is clear from this graph that the measured NO is asymptotic at high values of this ratio. It is also evident that the ratio controls the measured NO except at the lowest gas flow rates. This is as expected if gas/liquid contacting is good, since the temperature, and enthalpy of the quenched mixture depend solely on the water to gas ratio imposed on the system. The deviation at the lowest gas flow rate is due to poor gas/liquid contacting, which allows NO reduction reactions to continue after quenching.

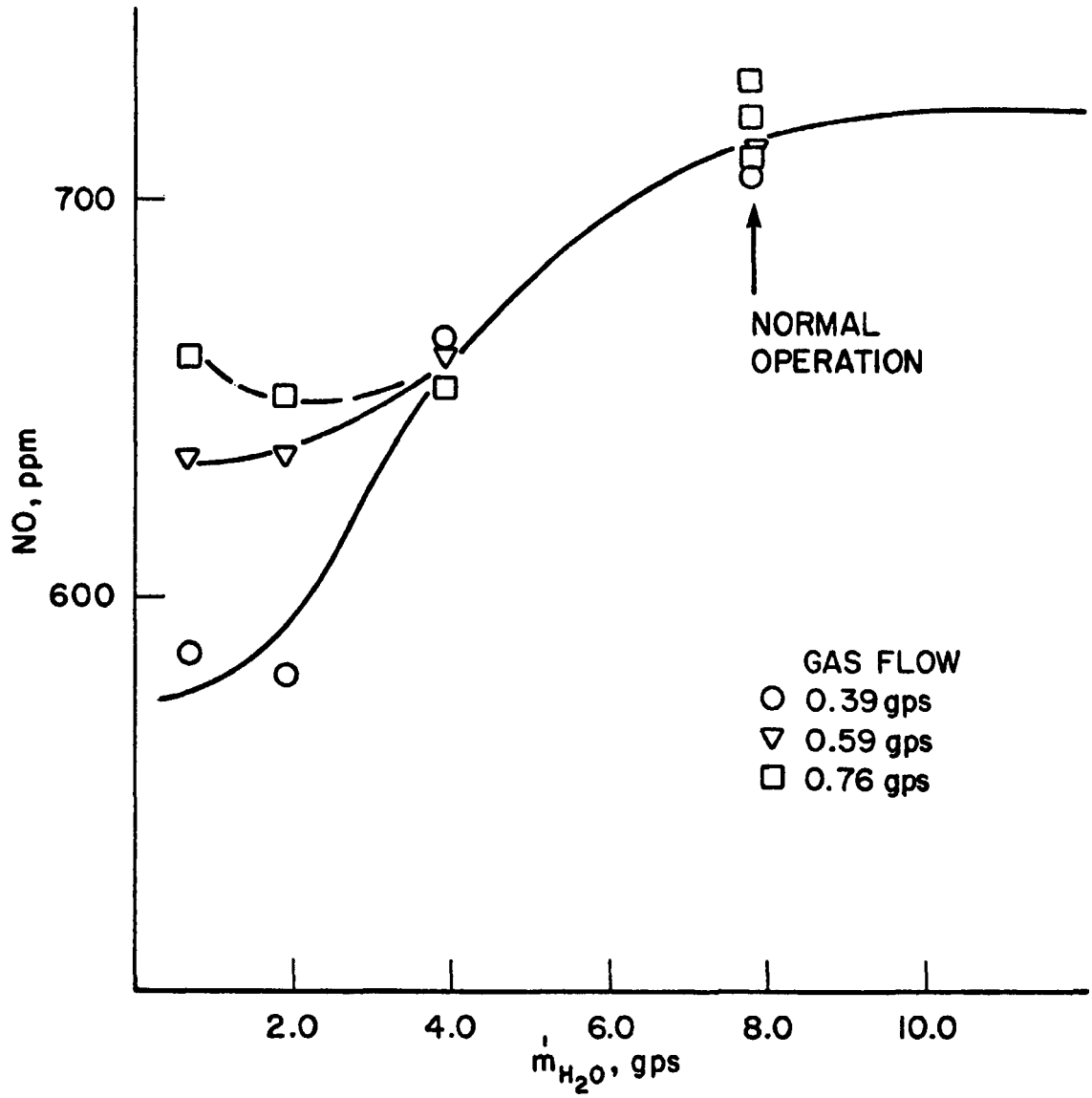

Figure C-1: NO (measured) vs. Quench Water Flow

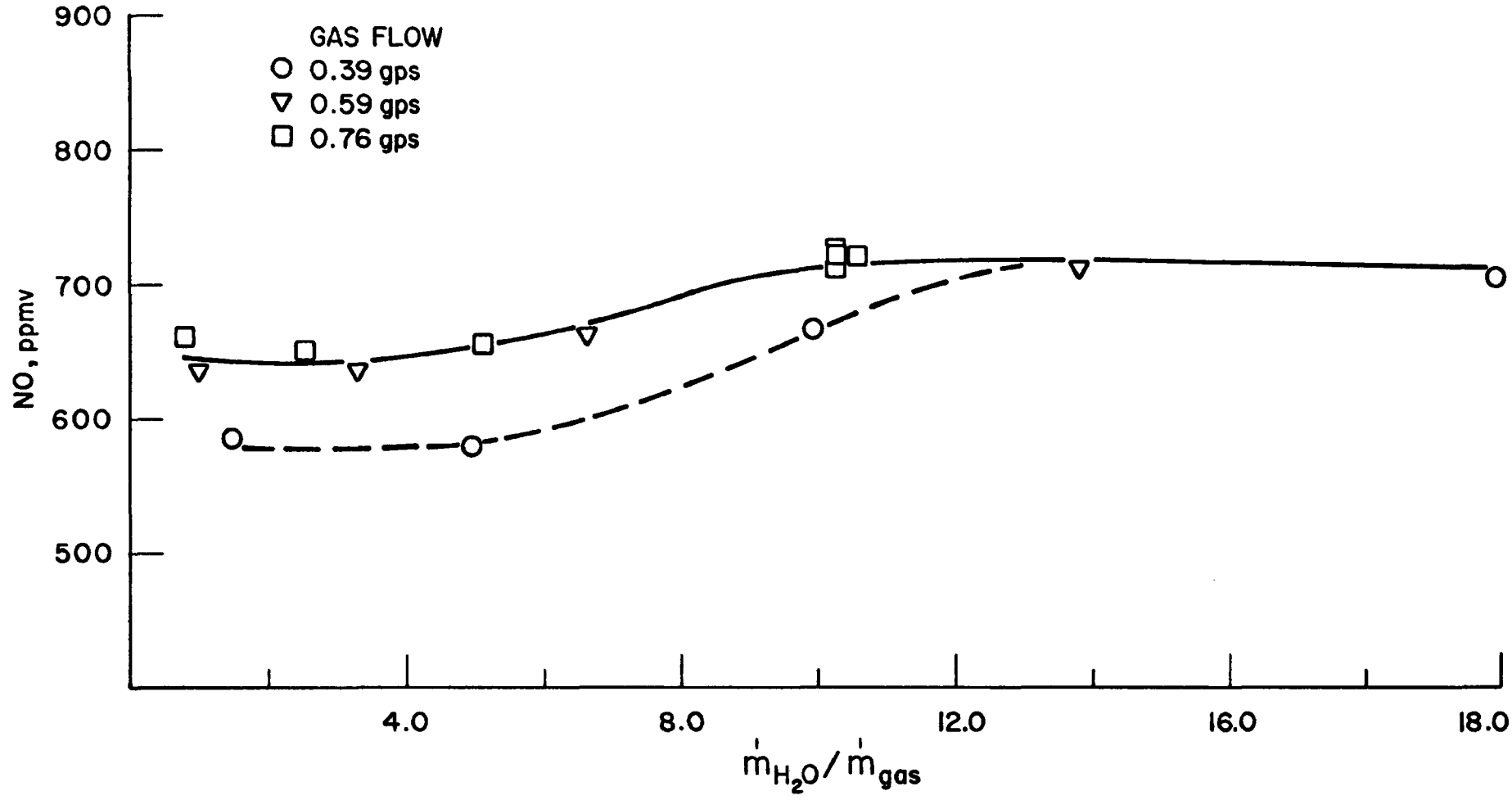

Figure C-2: NO (Measured) Vs. Water to Gas Mass Ratio

Carbon Oxides

The measured CO and CO_2 concentrations are showr in Figures C-3 and C-4.The measured concentrations of both gases decline to asymptotic values as the water to gas ratio is increased. Presumably, at low quench water rates, cooling is slow enough and the char is hot enough that the water gas reactions can contribute to carbon conversion.

The carbon conversion, the total of CO and CO_2, is plotted in Figure C-5.Although there is considerable scatter, the carbon conversion appears to be asymptotic at high water to gas ratios also.

Quenched Sample Temperatures

The temperature found by a simple enthalpy balance on the system, presuming that mixing is instantaneous, is shown in Figure C-6. If water/gas contacting is perfect, the amount of water required to give adequate cooling to just the 351° F dew point of the quenched mixture is only 44% of the gas mass flow. In normal operation of the probe, the temperature of the quenched gas should be about 330° K at water/gas mass ratio of 8.0. A much reduced water flow will give adequate gas quenching if contacting is good. The new side-entry probes will be designed to take advantage of the moderate dew point of the system to minimize or eliminate water dropout and soluble gas losses, by operating the probes above the dew point to give adequate cooling with out introducing massive quantities of water.

Soluble Gas Losses in Spray Water

The equilibrium solubility losses of the gases NO, CO, CO_2, H_2S, SO_2 amd NH_3 have been estimated and plotted in Figure C-7, as a function of the water to gas mass ratio. The recovery ratio for each was calculated

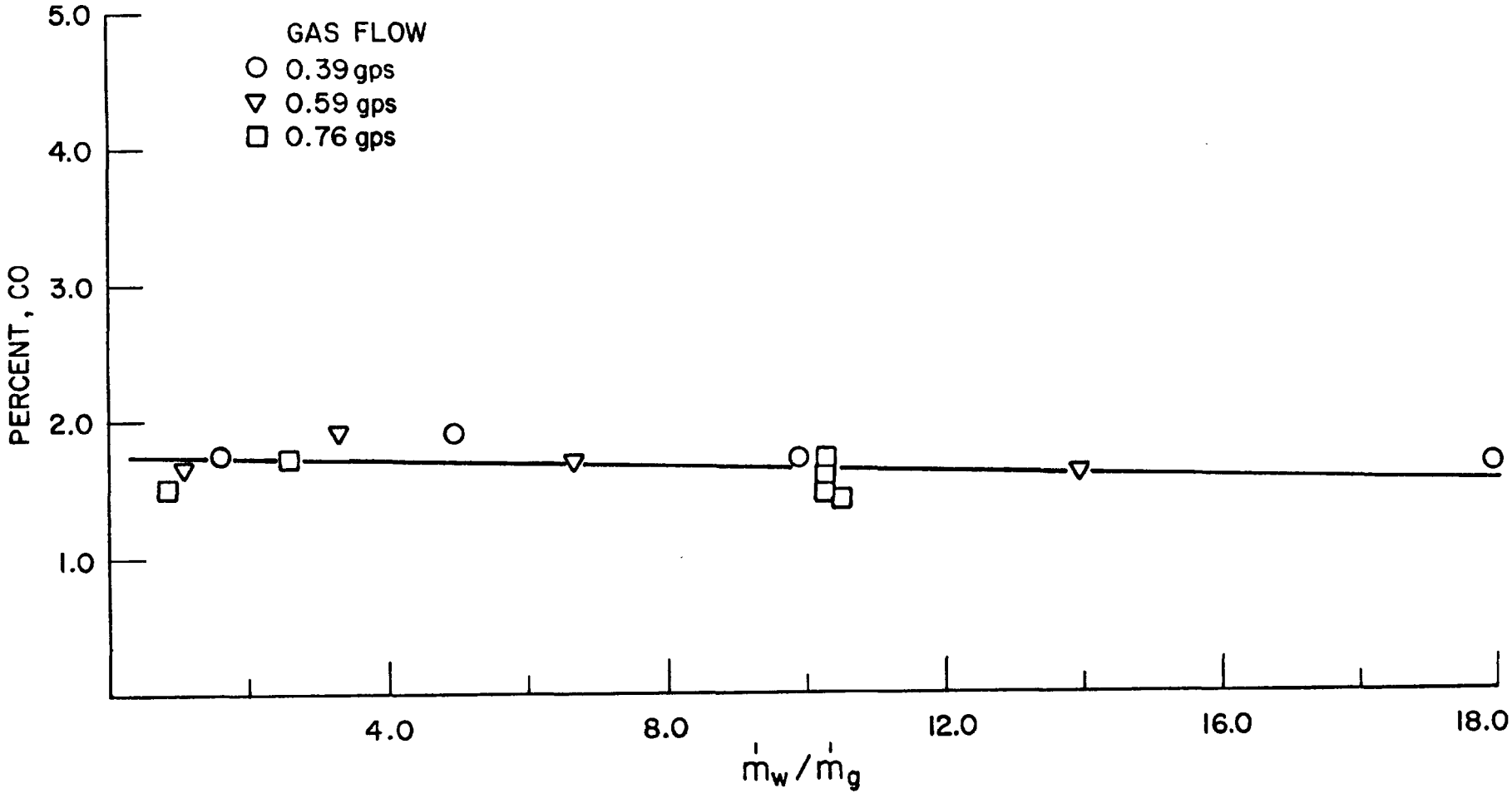

Figure C-3: CO Versus Water to Gas Mass Ratio

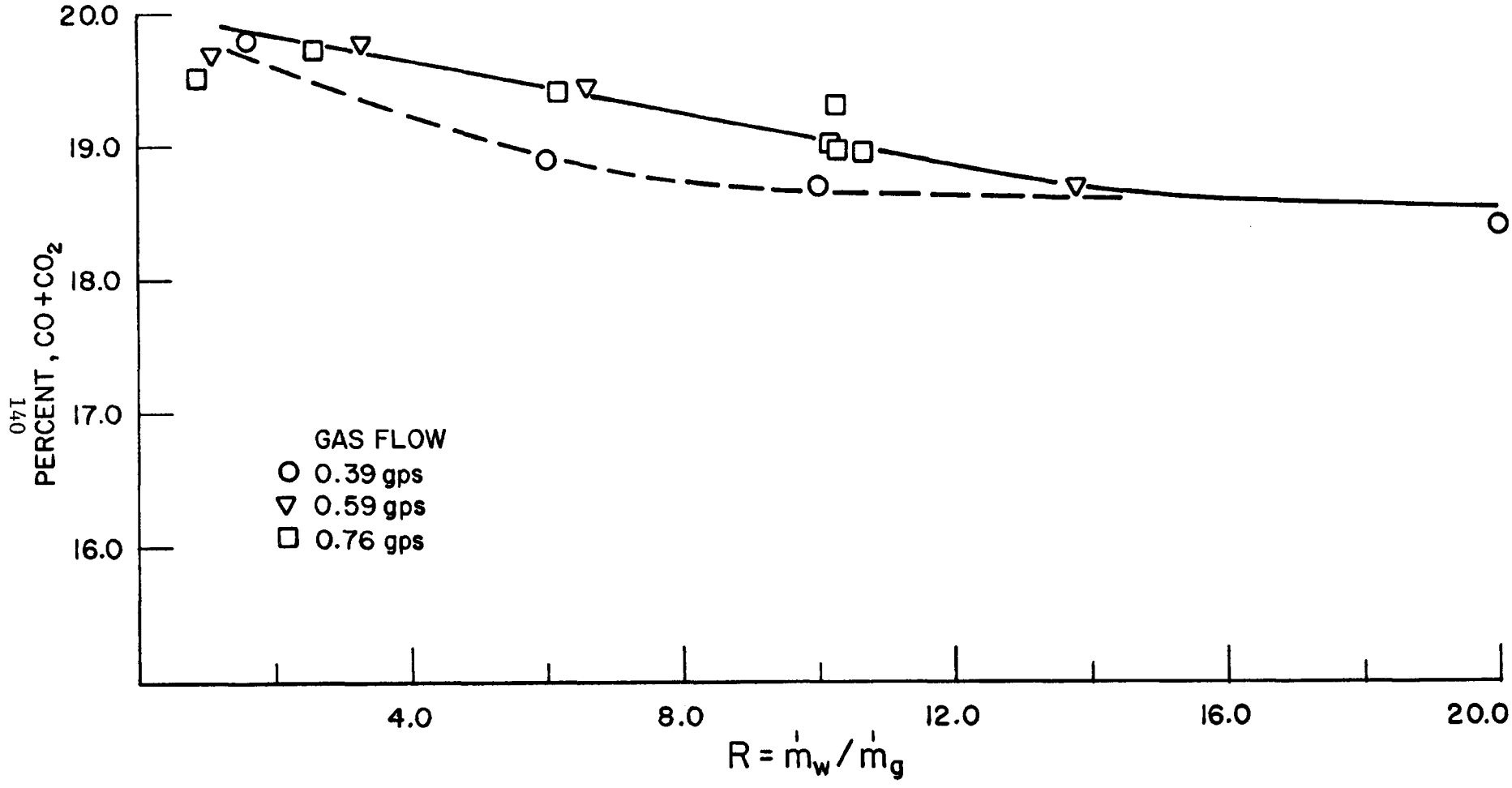

Figure C-4: CO_2 vs Water to Gas Mass Ratio

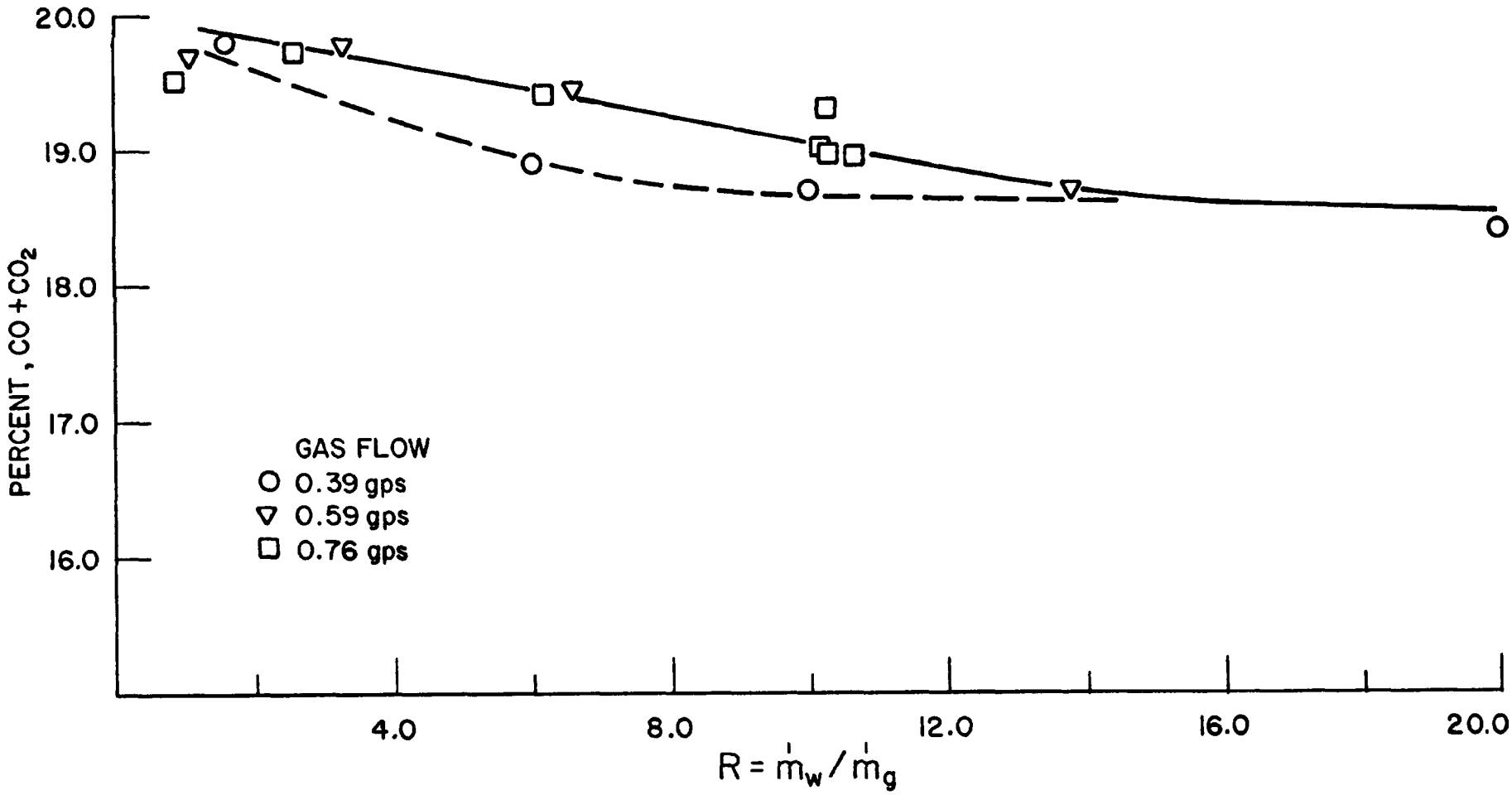

Figure C-5: Total Carbon Oxides vs Water to Gas Mass Ratio

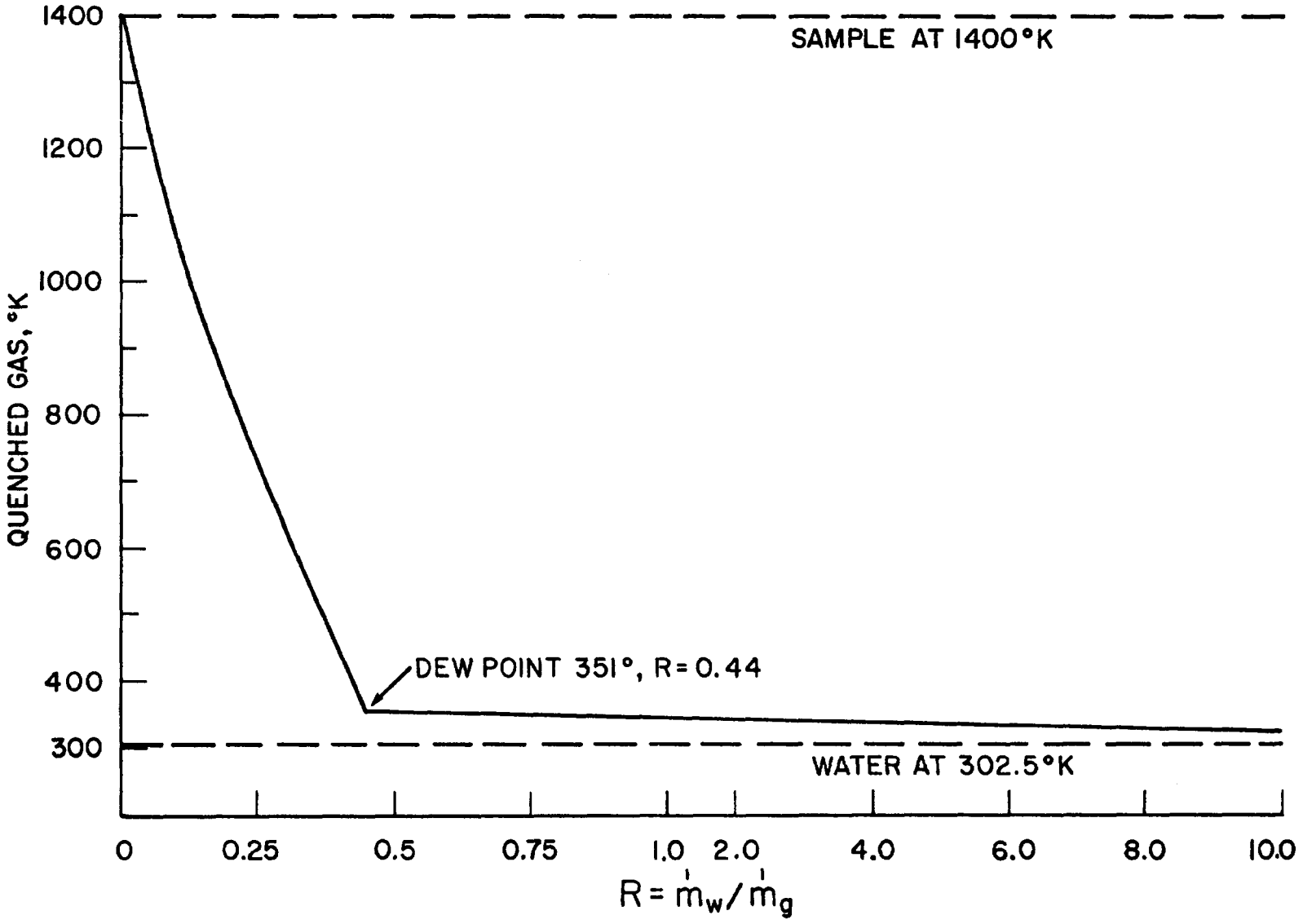

Figure C-6: Quenched Sample Temperature Vs. Water to Gas Mass Ratio

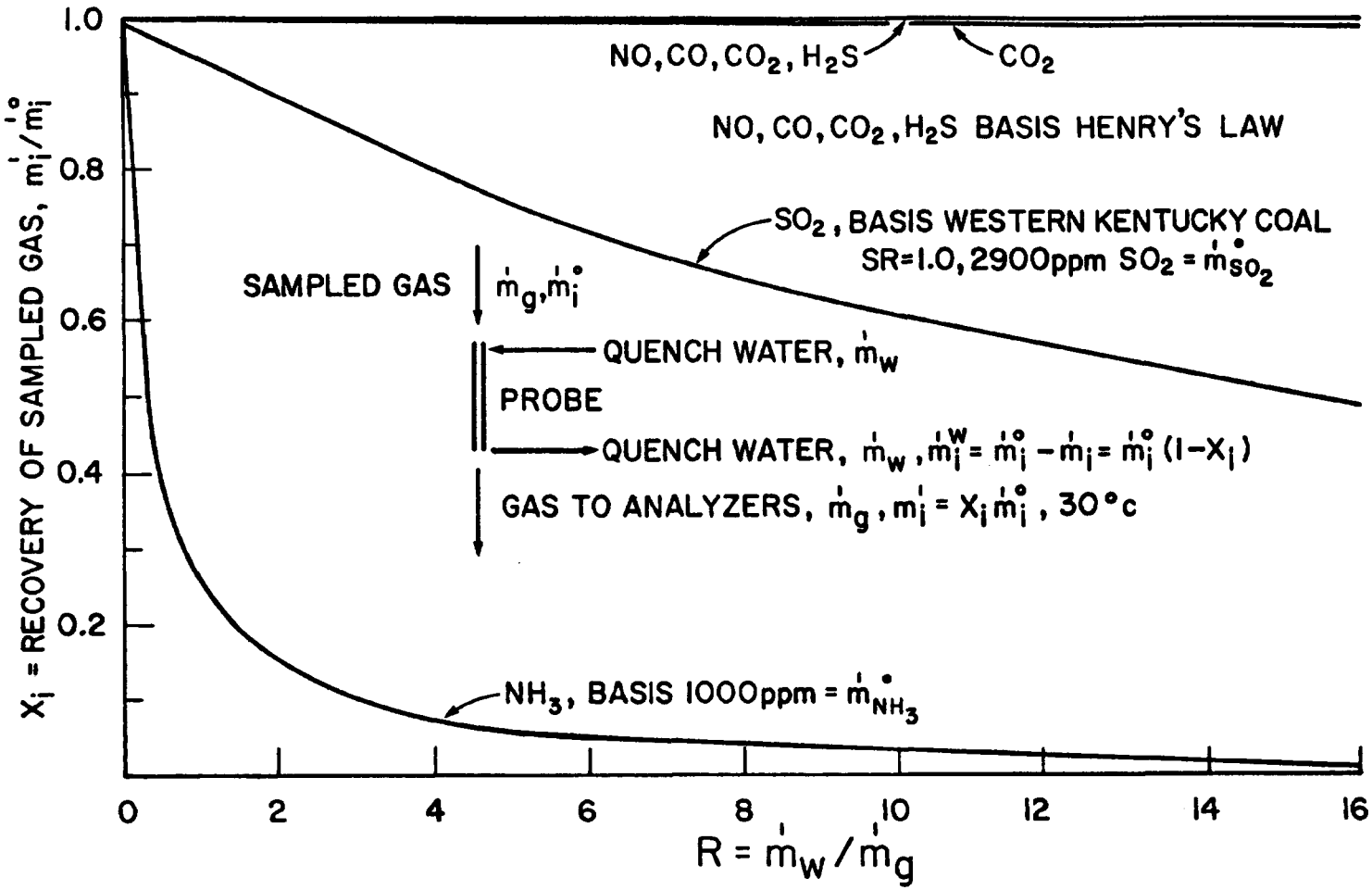

Figure C-7: Recovery of Sampled Gas Versus Quenching Ratio.

on the basis that it was absorbed in a single equilibrium staged in pure water. No itneraction among the acid gases and ammonia have been considered. Such interactions are expected to greatly increase the solubilities of H_2S, CO_2, SO_2 and NH_3 compared to the limiting case examined here.

As far as NO, CO, H_2S and CO_2 are concerned, the absorption into water is minimal. Ammonia and SO_2 absorption are not negligible. The recovery of these gases is so poor that either complete absorption into water or "dry" sampling should be considered if these are to be analyzed efficiently.

Isokinetic Conditions

The gas sampling rates reported in this study are far in excess of the isokinetic sampling rate required at the velocity of the sampled gas. However, the normal sampling rate is about twice the rate required to intercept the sampled gas within the sample probe outside diameter. Sampling conditions and isokinetic conditions are tabulated in Table C-2.

The effect of drawing the sample at greater than the isokinetic rate will be to mix the gas drawn axially and radially into the probe. Radial variation is not as bad as axial variations since the furnace flow and gas composition is relatively one-dimensional axial variations will tend to raise the NO profile as gas from low residence time regions mixes with gas having a lower NO value. The effect of the non-isokinetic sampling is being studied and will be reported at a later date.

Conclusions

These results indicate that the quench water to sampled gas ratio is the major controlling parameter in determining the accuracy of gas composition measurements. The normal operating conditions will give

Table C-2

Sampling Rates

	g/mol/min	g/min	SCFM
Isokinetic Rate @ 1440°K, as N_2 (basis 3/8" probe I.D.)	5.0×10^{-4}	1.39×10^{-2}	4.17×10^{-4}
Probe Interception Rate (basis 2" probe O.D.)	1.410	400	1.18
Actual Sampling Rate	1.63	456	1.30

Furnace Velocity = 122 cm/s

asymptotic concentration measurements. Since the sampling conditions are super-isokinetic, some deviation from the true gas concentration are expected. The magnitude of the error is being estimated and will be reported at a later date.

The temperature of the quenched sample, calculated by enthalpy balance, shows that the amount of quench water to required to cool the sample is much less than we currently use. Good gas/water contacting is required to reduce the actual water rate to the calculated levels.

Equilibrium calculations show that the absorptions of NO, CO, CO_2, and H_2S are negligible if ionic effects are ignored. NH_3 and SO_3 absorption is great at all water rates. Dry sampling or complete water absorption must be used to analyze these two compounds.

APPENDIX D

THE EFFECT OF FLY ASH ON VOLATILE FUEL NITROGEN CONVERSION TO NO.

Summary

A premixed natural gas/ammonia flame was used to investigate the conversion of volatile fuel nitrogen to NO as a function of the global stoichiometric ratio. All gas phase NO, CO, and CO_2 measurements were made of the furnace flue with the water spray probe.

Ammonia conversion to NO was 90-93% under fuel-lean conditions. Conversion decreased as the system became more fuel-rich to a minimum of about 4% at a stoichiometric ratio of 0.4.

The experiment was repeated with about 0.016 g/cm^3 (basis stoichiometric air, 70° F) fly ash from Four Corners coal. This is somewhat higher than the ash concentration expected from coal flames.

Under fuel-lean conditions, ammonia conversion to NO was 90%. Under fuel-rich conditions, conversion decreased more rapidly with decreasing stoichiometric ratio with fly ash than in the ash-free case. For example, at SR = 0.8, ammonia conversion was 50% of that in the ash-free case. At SR = 0.4 there is almost negligible ammonia conversion to NO.

Methane conversion to CO_2 is marginally less, and conversion to CO is marginally greater in the presence of ash. Total methane conversion to CO and CO_2 is constant in the presence of ash except at very fuel rich conditions where ash enhances total fuel conversion to CO and CO_2.

Experimental Conditions

The furnace was fired at approximately 54 MBTU/hr with natural gas as the fuel. 1.5% wt (basis fuel) of ammonia was added to the air. The natural gas, ammonia and air were mixed prior to combustion.

The Four Corners fly ash was supplied by Dr. S. A. Hoenig of the E. E. Department. Its chemical composition and particle size distribution are not known. Dr. Hoenig believes that it has virtually no carbon or nitrogen residue or any extraneous dirt. It appearance it is a fluffy, finely divided off-white powder.

The ash was fed from the coal feeder which was recalibrated accordingly. About 15% of the total stoichiometric air was used as transport air, similar to the operation when burning coal. The total ash feed was 1 lb/hr which is 0.015 g/cm^3 in the flue gas under stoichiometric conditions (70° F). This is about the concentration of ash in a coal char flame and is at the low limit of the coal feeder's ability to feed the ash reproducably.

All of the gas phase compositions were measured with the water spray probe according to standardized procedures. The stoichiometric ratio is reported on the basis of measured gas and air flows.

Experimental Results

The effect of ash on the conversion of ammonia to NO is shown in Figure D-1. Conversion is 90-93% under fuel-lean conditions. Conversion declines, as expected, as the system becomes more fuel-rich. The decline is less rapid at extreme fuel-rich conditions.

The effect of the added fly ash is significant in the fuel rich flames. NO formation is 50% of the ash-free NO at SR = 0.8 and 20% at SR = 0.07. As the system becomes extremely fuel-rich, NO formation is suppressed to a negligible level at SR = 0.4.

The ash has minor effects on the conversion of methane to CO and CO_2. As shown in Figure D-2, under fuel rich conditions the ash slightly suppresses methane conversion to CO_2.

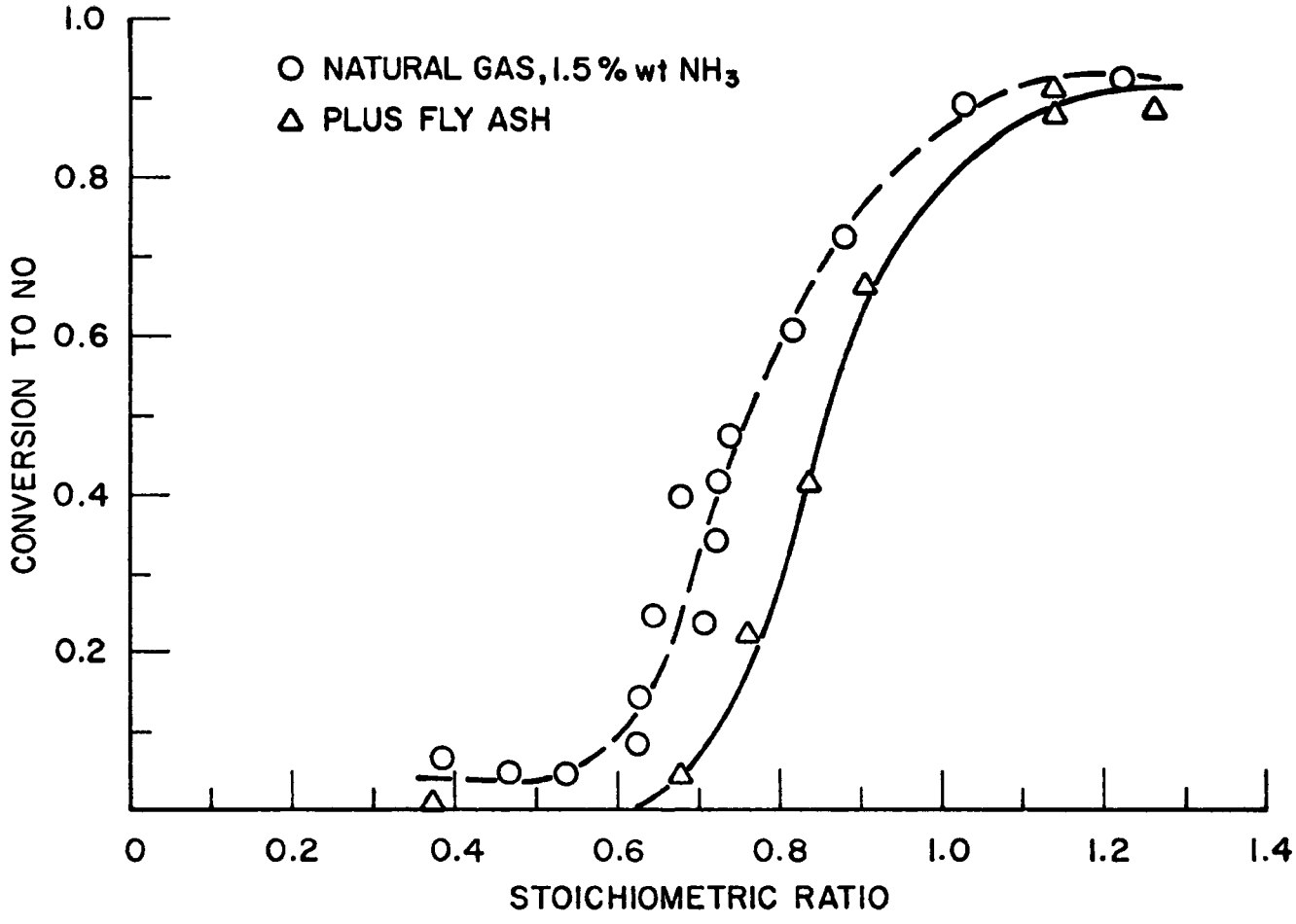

Figure D-1: Ammonia Conversion to NO

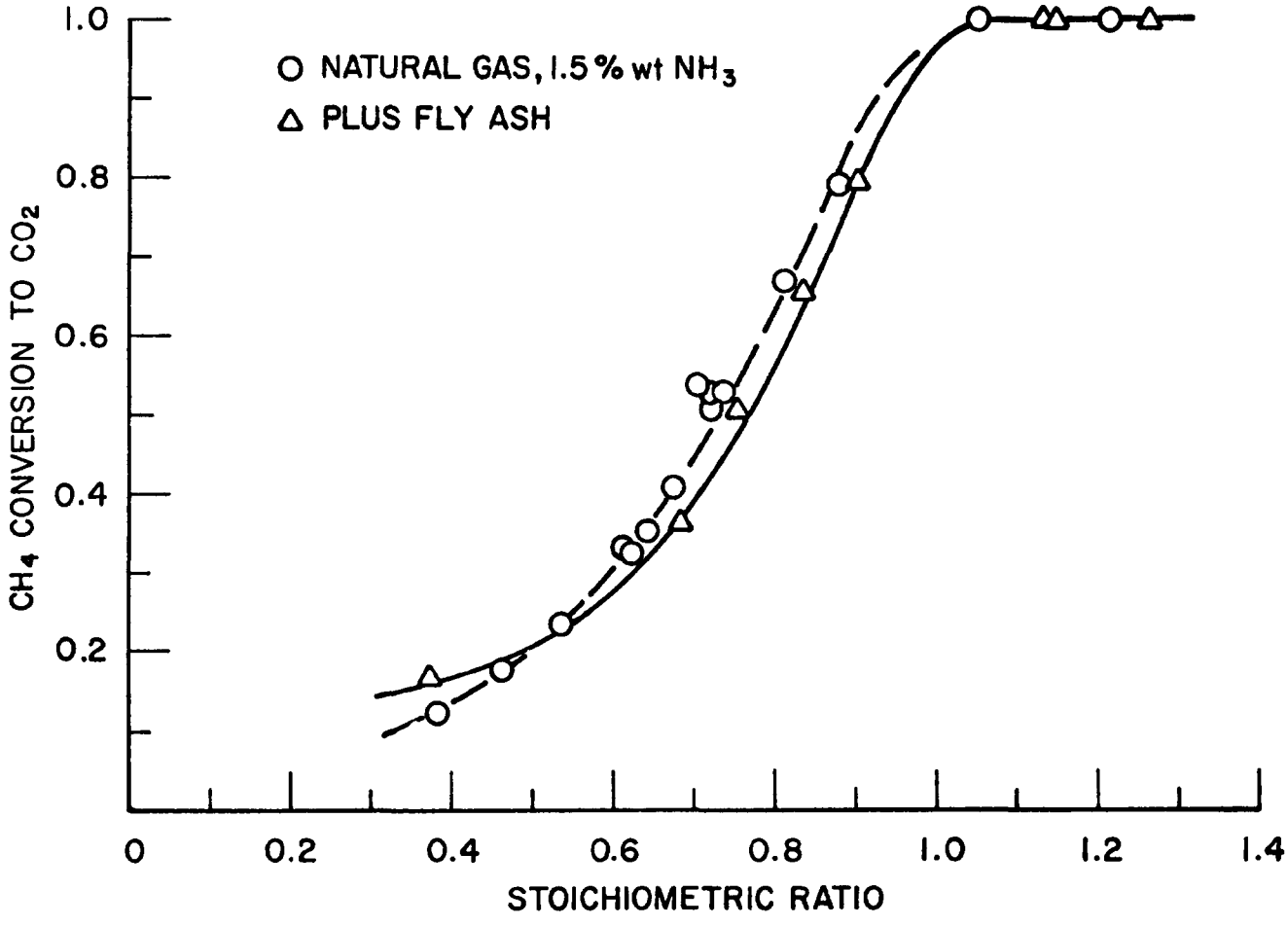

Figure D-2: Methane Conversion to CO_2

The conversion of the fuel to CO is shown in Figure D-3 enhances conversion to CO especially at very fuel rich stoichiometries, represented by the single experimental point. Whether the enhancement at SR = 0.4 can be reproduced is somewhat questionable, but the overall effect of ash on CO is obviously real.

The total fuel conversion (to CO and CO_2) is shown in Figure D-4. With the exception of the single point at SR = 0.4 for the ash-added case, the total conversion of the fuel is not affected by the ash.

The experimental evidence is somewhat meager and in the absence of direct volatile nitrogen species measurements at the flue, not much can be said about the mechanistic effects of ash. It should be noted that ash may well have a significant influence on the temperature decay in the furnace because of enhanced radiation. Temperatures were not measured in this study, thus adding additional uncertainty.

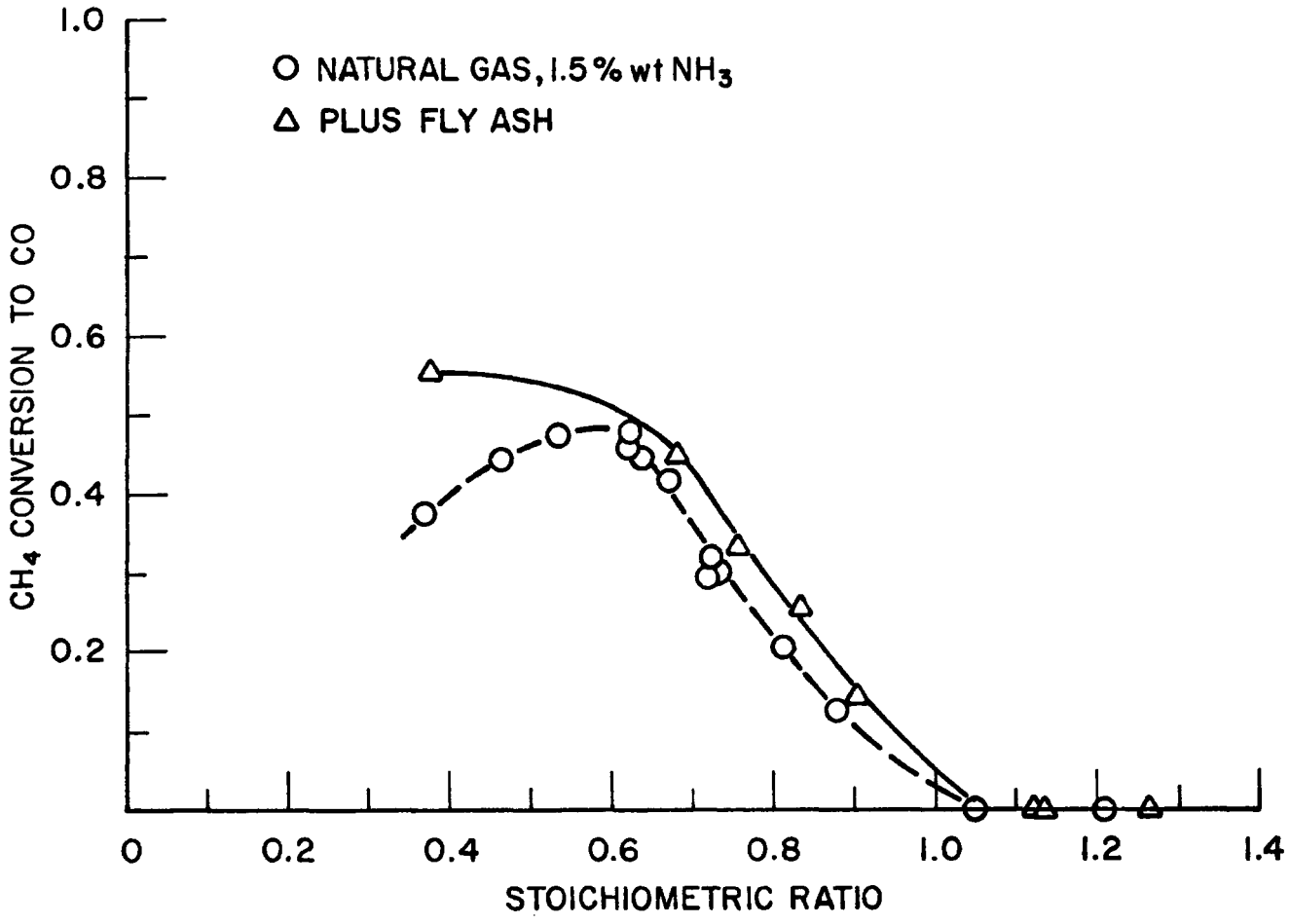

Figure D-3: Methane Conversion to CO

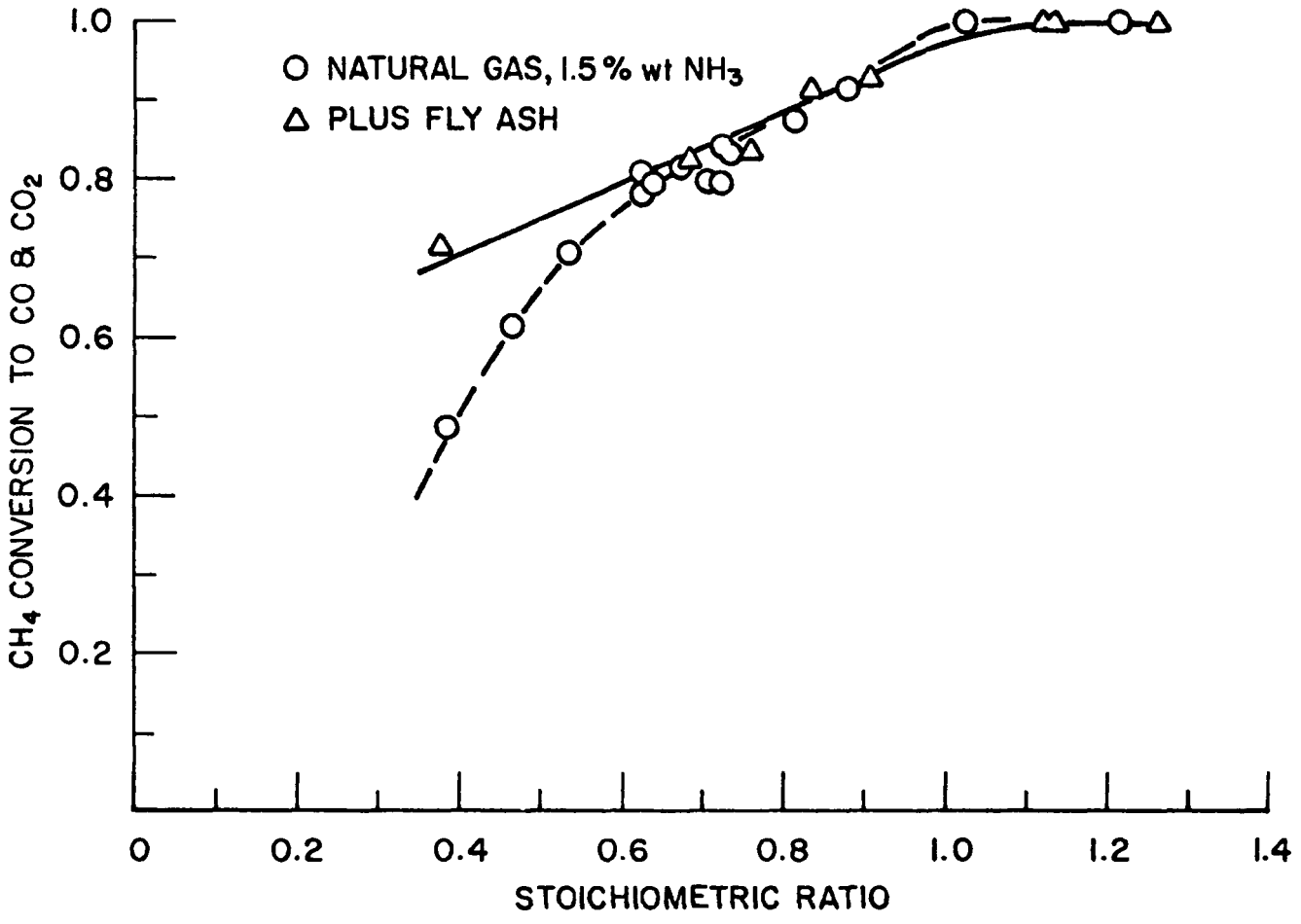

Figure D-4: Methane Conversion to CO and CO_2

U.S. GOVERNMENT PRINTING OFFICE: 1980—640-258/1703